STABILITY AND CONTROL ISSUES ASSOCIATED WITH LIGHTLY LOADED ROTORS AUTOROTATING IN HIGH ADVANCE RATIO FLIGHT

A Dissertation
Presented to
The Academic Faculty

by

James Michael Rigsby

In Partial Fulfillment
Of the Requirements for the Degree
Doctor of Philosophy in the
School of Aerospace Engineering

Georgia Institute of Technology
December 2008

STABILITY AND CONTROL ISSUES ASSOCIATED WITH LIGHTLY LOADED ROTORS AUTOROTATING IN HIGH ADVANCE RATIO FLIGHT

Approved by:

Professor J.V.R. Prasad, Advisor
School of Aerospace
Engineering
Georgia Institute of Technology

Professor Dewey H. Hodges
School of Aerospace
Engineering
Georgia Institute of Technology

Professor Daniel P. Schrage
School of Aerospace
Engineering
Georgia Institute of Technology

Professor L.N. Sankar
School of Aerospace
Engineering
Georgia Institute of Technology

Professor David A. Peters
Department of Mechanical, Aerospace
and Structural Engineering
Washington University, St. Louis

Date Approved: October 14, 2008

ACKNOWLEDGEMENTS

I would like to acknowledge my sincerest appreciation to Professor J.V.R. Prasad for his mentorship, incredible patience, and guidance during my time at the Georgia Institute of Technology. I would also like to thank Professor Daniel Schrage and Professor Lakshmi Sankar as well. It was within this circle of influence that I developed my appreciation for rotorcraft engineering, undoubtedly one of the most interesting, challenging, and multidisciplinary fields in all of aerospace engineering. In addition, I thank Professor Dewey Hodges and Professor David Peters for their guidance and participation in the review and evaluation of this work.

I also thank the students who were finishing as I was just beginning: Chen Chang, Geoffrey Jeram, Suraj Unnikrishnan, Illkay Yavrucuk, and many others. Special thanks to Manuj Dhingra, whose friendship, assistance, and patience opened my eyes to the wider world of computing and who was always there to resolve my major computing crises with a few magical lines of code.

I thank all of my friends at Georgia Tech for their help and support. Those friends include, but are not limited to: Mandy Goltsch, B.Y. Min, Alex Moodie, Kyle Collins, Troy Schank, and Jongki Moon, Ersel Olcer, and Suresh Kannon. Also, I offer a special thanks to Dr. Hong Xin, for friendship and fantastic software support.

Finally, I thank my family, without whose love and support, none of this would have been possible. My wife Xiaohong, my parents, my sister and brother-in-law, all encouraged me and provided steadfast support. I dedicate this work to them.

TABLE OF CONTENTS

LIST OF TABLES

LIST OF FIGURES

LIST OF SYMBOLS AND ABBREVIATIONS

Symbols

C_ς	Lead-lag damper constant [ft-lbf-s/rad]
C_ς^*	Non-dimensional lead-lag damping parameter, $C_\varsigma / I_b \Omega$
I_b	Blade second moment of inertia with respect to flap or lag hinge
K_β	Rotor blade flap hinge spring constant
L, M, N	Body frame roll, pitch, and yaw moments
M_x , M_y	Rolling and pitching hub moments
Q	Rotor Torque
X, Y, Z	Body frame axes
i_s	Rotor shaft incidence to free stream velocity
p, q, r	Angular velocity components in body axis system
u, v, w	Velocity components in the body axis system
Δ	Increment or change
Ω	Rotor angular velocity
β	Rotor blade flap angle
β_{ss}	Rotor blade flap angle in steady state
$\delta_{[]}$	Pilot control inputs
γ	Lock number
μ	Advance ratio
$\phi \quad \theta \quad \psi$	Euler angles
ν	Non-dimensional flapping frequency
ς	Non-dimensional lead-lag frequency

Subscripts

a	aileron
el	elevator
coll	Collective control
lat	Lateral control
lon	Longitudinal control
max	Maximum
pedals	Yaw control
p, q, r	Partial derivatives with respect to angular velocity components
u, v, w	Partial derivatives with respect to velocity components
x, y	Rolling and pitching axes
Ω	Partial derivative with respect to rotor speed
0	Initial condition or rotor coning mode
1c	First harmonic cosine component
1s	First harmonic sine component

Abbreviations

ACP	Aerodynamic computation points
BEM	Blade element model
CCTD	CarterCopter Technology Demonstrator
CFD	Computational fluid dynamics
CSD	Computational structural dynamics
FTM	Floquet transition matrix
MFT	Matrix Floquet theory
NACA	National Advisory Committee for Aeronautics

NASA	National Aeronautical and Space Administration
Rev	Rotor revolution
RIA	Runway independent aircraft
RVR	Reverse velocity rotor
SCP	Structural computation points
System ID	System identification analysis
VTOL/STOL	Vertical takeoff and landing/ short takeoff and landing

SUMMARY

Interest in high speed rotorcraft has directed attention toward the slowed-rotor, high advance ratio compound autogyro concept as evidenced by the current DARPA Heliplane project. The behavior of partially unloaded rotors, autorotating at high advance ratio is not well understood and numerous technical issues must be resolved before the vehicle can be realized. Autorotation in helicopters usually indicates an emergency loss of power. For the concept vehicle autorotation is the normal working state of the rotor. The necessity for a reduction in rotor speed with increasing flight speed results in high advance ratio operation where the retreating side of the rotor is dominated by the reverse flow region. Further, rotor speed changes also affect the rotor dynamics and the associated hub moments generated by cyclic flapping. The result is rotor characteristics that vary widely depending on advance ratio. In the present work, rotor behavior is characterized in terms of issues relevant to the control system conceptual design and the rotor impact on the intrinsic vehicle flight dynamics characteristics. A series of trim, stability, and control analyses, based on features inherent in the concept vehicle, are performed. Trends are identified through parametric variation of rotor operating conditions, augmented by inclusion of the sensitivities to blade mass and blade stiffness properties.

In this research, non-linear models, including the rotor speed degree of freedom, were created and analyzed with FLIGHTLAB^{TM} rotorcraft modeling software. Performance analysis for rotors trimmed to autorotate with zero average hub pitching and rolling moments indicates reduced rotor thrust is achieved primarily through rotor speed reduction at lower shaft incidence angle, and imposing hub moment trim constraints results in a thrust increment sign reversal with collective pitch angle above

advance ratio $\mu \sim 1.0$. Swashplate control perturbations from trim indicate an increase in control sensitivities with advance ratio, and advance ratio dependent control cross coupling. Hub moment response to rotor disturbances results in transients where rotor damping is reduced due to low Lock number blades and reduced rotor angular velocity. Experimentally identified frequency response shows dominant low frequency modes with advance ratio dependent damping and the frequencies are on the order of typical airframe modes. Rotor speed response to swashplate control perturbations from trim results in non-linear behavior that is advance ratio dependent, and which stems from cyclic flapping behavior at high advance ratio. Rotor control strategies were developed including the use of variable shaft incidence to achieve rotor speed control with hub moment suppression achieved through cyclic control. Flight dynamics characteristics resulting from the coupling of the rotor and airframe were predicted in flight using a baseline airframe with conventional fixed-wing controls, representative of the current interest in the concept vehicle. Results predicted by linearization of the non-linear models were compared with system identification results using the non-linear simulation as surrogate flight test data. Low frequency rotor response is shown to couple with the vehicle motion for short period and roll mode response to airframe control inputs. The rotor speed mode is shown to couple with short period and long period vehicle modes as the rotor torque balance is sensitive to vehicle speed and attitude changes.

CHAPTER 1

INTRODUCTION

1.1 Overview

Increased speed and altitude capability are desirable for the survivability of military vehicles and the cost efficiency of civilian aircraft [1]. The slowed-rotor, high advance ratio compound autogyro has received attention as a potential configuration to meet these needs while retaining the equally desirable V/STOL capability. Several current research efforts are evidence of the current interest. The DARPA sponsored Heliplane Demonstrator Aircraft (HDA), being developed by Groen Brothers Aviation of Salt Lake City, Utah is one such project. The publically stated program objectives are to achieve a 400 mph cruise speed with an unrefueled range of 1,000 miles [2]. This speed objective is considerably beyond the capabilities of current helicopters, and the range objective suggests high altitude capability for efficient turbine engine operation. Carter Aviation Technologies of Wichita Falls, Texas is also engaged in the development of high advance ratio rotorcraft, claiming to be the "first and only aircraft to achieve $\mu = 1.0$", while during a flight test of the CarterCopter Technology Demonstrator the rotor speed was reduced to 107 rpm at a flight speed of 170 mph for 1.5 seconds [3].

Before a safe, practical high-speed design (~400 mph) can be realized however many technical issues must be resolved. The behavior of partially unloaded rotors, autorotating at high advance ratio is not well understood and numerous technical issues must be resolved before the vehicle can be realized. The inherent features contained in the concept description allude to the most critical technical issues. Autorotation itself is well understood since the predecessors to helicopters were autogyros, but the features

of high advance ratio, reduced and variable rotor speed, and compounding introduce a multitude of complexities. In high advance ratio operation the retreating side of the rotor is dominated by the reverse flow region, which is a complex aerodynamic environment. The effect of the reverse flow region is often neglected in helicopter analytical work, but likely represents a significant consideration for the concept vehicle. Further, along with an increase in flight speed, a reduction in rotor speed is required to avoid sonic conditions on the advancing blade which would lead to increased drag, structural loads, vibration, etc. These rotor speed changes affect the rotor dynamics and the associated hub moments generated by cyclic flapping. Compounding results from the addition of redundant lifting and thrusting devices such as wings and auxiliary propulsion. The addition of a wing allows the task of lift generation to be transferred from the rotor to the more aerodynamically efficient wing. The rotor will still produce some lift however in order to remain in autorotation. The addition of auxiliary propulsion assumes the task of thrust generation for forward propulsion, with the rotor adding to the vehicle drag when the thrust vector is pointed aft. When these aspects are considered collectively, the implications for controlling the lightly-loaded rotor autorotating in high advance ratio flight and the impact of the rotor on the intrinsic vehicle flight dynamics characteristics are obfuscated.

1.2 Literature Review

Previous research efforts were surveyed to ascertain the extent to which the existing knowledge base could be utilized to clarify the rotor behavior and its impact on vehicle flight dynamics. A review of the relevant literature shows that it generally falls into several broad categories related to certain aspects of the concept vehicle. The characteristics of autogyros and autorotating rotors are well documented as the

predecessors to modern helicopters. A large amount of the early research related to rotor behavior was based on autogyros and this work contributes to the understanding of autorotating rotors, albeit at relatively low flight speeds. Compound helicopters have been analyzed and built by many of the major helicopter manufacturers as research vehicles, but none are currently in production. The research does however contribute to understanding of the lift sharing between the rotor and wing, which relates to the inherent concept vehicle feature of partially unloading the rotor. Rotors operating at high advance ratio have been investigated in a variety of wind-tunnel experiments and analytical studies. This work highlights the significance of the reverse flow region at high advance ratio as well as slowed-rotor dynamics, although autorotational constraints are not a prominent feature. Several experimental vehicles have been built and two of the most notable compound autogyros were the Fairey Rotodyne and the McDonnell Aircraft XV-1 Convertiplane.

1.2.1 The Fairey Rotodyne

The Fairey Aviation Company Limited was a British aircraft manufacturer that demonstrated, with its Fairey Rotodyne, a compound autogyro capable of cruising at 160 knots [4]. The Rotodyne flew as a reaction drive helicopter for takeoff and landing, and then transitioned to an autogyro flight mode by reducing rotor power and increasing propeller pitch for forward propulsion. At around 110 knots, reaction drive fuel was turned off, and the auxiliary compressors were declutched. At this point the collective was set to about 3 degrees and the rotor settled into autorotation. Figure 1 from reference [4] shows the Rotodyne near hover.

Figure 1: The Fairey Rotodyne, from ref [4]

The Rotodyne made its first flight on November 6th, 1957, and made its first full transition to autogyro flight April 10th, 1958. Political and financial constraints eventually led to the program cancellation in 1962. The project did however demonstrate the management of a partially unloaded autorotating rotor up to an advance ratio of $\mu \sim 0.6$ [4].

The Rotodyne controls were similar to a helicopter at low speed, except with yaw control provide by differential propeller thrust. In autogyro flight, cyclic control provided pitching and rolling moments, with the rudder providing yaw moments. Propulsion control was probably the most unique aspect, with the need to switch between powered, and un-powered rotor. Reference [4] provides an overview of the propulsion control scheme. Vehicle stability and control assessments are mentioned in reference [4] as "so far being made mainly by the pilots", with no other reference or explanation.

1.2.2 The McDonnell Aircraft XV-1 Convertiplane

The McDonnell Aircraft XV-1 Convertiplane was a U.S. Army and Air Force sponsored research project in the 1950's [5]. The XV-1, shown in Figure 2, flew in three distinct flight modes: helicopter mode, autogyro mode, and airplane mode [5].

Figure 2: The McDonnell Aircraft XV-1 Convertiplane, from reference [5].

During transition to autogyro mode the collective was set to a fixed value of about six degrees while the tip jet fuel was turned off and the propeller clutched in. Finally in transition to airplane mode (125 knots and higher) the pilot used a manual lever to lock the rotor gimbal to the control stem and disengage the pilot longitudinal stick from the rotor. Simultaneously the collective was lowered to zero degrees. At this point the rotor speed was controlled by a fly ball governor that adjusted the control stem fore and aft as needed [5]. During flight testing the XV-1 achieved a maximum flight speed of 174 knots and advance ratio in excess of 0.9. The XV-1 rotor hub was a unique design by Kurt Hohenemser, who was the Chief Engineer at the McDonnell Aircraft, Helicopter Division at the time. The design is explained in detail in references [5] and [6]. That

design allowed the rotor to retain the desirable speed stability and pitch damping characteristics, but also provide positive angle of attack static stability using a large delta-3 arrangement with pitch-coning hinges [6].

The longitudinal stability and control characteristics of the XV-1 were investigated in the Ames 40 by 80 foot wind tunnel, and reported by Hickey in 1956 [7]. The tests were conducted for the autogyro and airplane flight modes, covering speeds from 75 to 150 knots [7]. The tests included determination of the static speed stability, static angle of attack stability, and to a lesser degree, the longitudinal dynamic stability. The full-scale tests included rotor-on and rotor-off configurations, and powered and un-powered propeller configurations. The tests were conducted at the most rearward center of gravity position, and concluded that the XV-1 exhibited positive speed stability throughout the range tested and negative angle of attack stability in autogyro mode at the rearward center of gravity position. Other important results included an investigation of the downwash at the horizontal tail and interference effects between the hub and pylon [7].

1.2.3 High Advance Ratio Wind-Tunnel Experiments

Rotors operating at high advance ratio have been investigated by a number of researchers. Jenkins and Sweet [8] [9] investigated a 15-foot diameter, two-bladed teetering rotor in the Langley full-scale tunnel for tip speed ratios from 0.65 to 1.45. This data was used to compare with theoretical calculations to indicate the predictability of the results [9]. The test procedure called for trimming the tip-path plane normal to the shaft for each test point. The results of the test reveal an interesting point. Jenkins noted that near an advance ratio of 1.0, there was a control reversal, in that a "combination of collective and cyclic pitch which produces a positive thrust increment at

conventional tip speed ratios now produces a negative thrust increment" [9]. Jenkins further suggested that this "reversal could be quite disconcerting to a pilot … with manual control of the rotor". This reversal is the combined result of re-trimming the rotor to maintain constant rotor attitude, which is "desired to maintain rotor-fuselage clearance" [9].

In 1968, McCloud, Biggers, and Stroub [10] investigated five full-scale rotors in the 40 by 80 foot wind tunnel at the NASA Ames Research Center. They tested two articulated rotors and three teetering rotors. The two articulated rotors were identical except for twist, 0 degrees and -8 degrees linear twist respectively. The teetering rotors consisted of one 48 ft and 34 ft diameter rotor, along with a 48 ft diameter rotor with tapered-thickness blades. The results were presented without discussion, but were meant to provide design guidance for high speed rotorcraft. Data was presented for advance ratios up to 1.05.

Fairchild Republic Company, under contract with the Naval Air Systems Command, performed a series of tests at NASA's Ames Research Center on a $1/7^{th}$ scale model of the *Reverse Velocity Rotor* (RVR) concept [11]. The RVR rotor was designed to operate at high advance ratio by using reversible airfoils capable of producing lift in the reverse flow region. Two-per-rev control was also a feature of the RVR concept, but substantial results were presented with the two-per-rev control disengaged for comparison purposes. The RVR rotor was a four-bladed articulated rotor with coincident flap and lag hinges at 6.5 percent of the blade radius and a delta-3 hinge angle of 26.5 degrees [11]. Results were obtained for advance ratios from 0.3 to 2.4. The test procedure was to adjust the longitudinal and lateral cyclic controls at each test point to achieve zero flapping. A primary purpose of the test was the determination of the structural loads, however a series of control inputs were made to examine the dynamic stability of the rotor. No rigorous flapping stability analysis was performed, but

the time histories of flapping behavior after the control inputs showed a damped response up to an advance ratio of at least 2.0. The tests results showed the same apparent control reversal as Jenkins observed, but went on to verify that there were no control reversals, instead the “trim requirements of decreasing longitudinal cyclic with increasing collective pitch, more than offset the increase in thrust with collective at high advance ratio” . This report also highlights the presence of rotor control cross coupling at high advance ratio. Pitching and rolling moments were measured for longitudinal and lateral cyclic inputs. The results showed a substantial off-axis response, and that the effects were not orthogonal, indicating “that moment uncoupling cannot be achieved with a single phase angle choice” [11]. The RVR project was largely concerned with increasing rotor effective lift to drag instead of unloading the rotor however, and autorotation was not a major concern for the proposed powered rotor configuration.

Kuczynski and Sissingh [12] investigated hingeless rotor response characteristics at high advance ratio as part of a program with the United States Army Aeronautical Research Laboratory (USAARL). The tests, conducted at Ames Research Center and reported in 1971, investigated a rotor model that could be configured with a range of Lock numbers and non-dimensional flap frequencies. The Lock number was varied by the addition of tip weights, and the non-dimensional flap frequencies were adjusted by the addition of flexible flapping restraints and variation of rotor angular velocity [12]. The results include the rotor response derivatives with respect to control inputs as a function of advance ratio, and illustrate the rotor response coupling. The rotor steady state response derivatives were also compared to math model predictions. The math model considered centrally hinged rigid blades, and used the Lock number and non-dimensional flap frequency as the primary description of the blades [12]. The interesting result was the better correlation for the tests with the softer flapping restraint. The authors explain the differences by consideration of the mode shapes of the actual

blades. The math model provides a better description of the soft flexure, and they suggest an adequate math model may require a hinge offset parameter, or a first flap mode shape parameter [12]. The report concludes with a theoretical prediction of stability using Matrix Floquet Theory (MFT). The results predict a flapping instability for the configurations tested, but at advance ratios beyond the conditions tested. The highest advance ratio considered in this report was $\mu \sim 1.75$.

1.2.4 Analytical Investigations

Sissingh investigated the dynamics of rotors operating at high advance ratio [13] by solving the flapping equation through electronic analog simulation, and presented the results in 1967. Stability boundaries and response characteristics of "restrained and unrestrained blades at advance ratios from approximately 0.8 to 2.4" were reported. Reverse flow effects were included by portioning the rotor azimuth into regions for the calculation of the forcing terms. Bramwell et al. [14] used a similar approach to solve the flapping equation for articulated and teetering rotors with a range of spring and damper restraints. Flapping stability limit predictions were presented with the teetering rotor exhibiting stability up to at least $\mu \sim 5.0$. Perisho [15] analyzed the stability of one blade with torsional and bending degrees of freedom, and predicted the blade instability with a one-half per revolution motion as had been observed in model wind tunnel tests during the development of the McDonnell Aircraft XV-1 [15]. Peters and Hohensemser [16] investigated rotor stability for lifting rotors including cases with Delta-3 feedback and tilt-moment feedback using Floquet analysis. Stability boundaries are presented as functions of advance ratio and Lock number and results are compared to the results from Sissingh [13]. Features common to theses investigations are the study of essentially low frequency phenomena, which justifies the use of quasi-static airloads.

Floros and Johnson [17] [18] analytically investigated the flapping stability of a slowed-rotor compound helicopter. They used rigid flapping equations, based on Sissingh's equations, applied to a variety of hub types to assess the suitability for high advance ratio operation. The results include damping contours for a range of Lock numbers and advance ratios for the different hub types. Also presented were results for a rotor and wing model based on the CarterCopter Technology Demonstrator (CCTD). They modeled a teetering rotor with rigid and elastic blades in the comprehensive analysis code CAMRAD II, and investigated any differences that would be introduced by a more sophisticated representation of aerodynamics and blade motion. The results from the rigid flapping equations indicated that a teetering rotor was a good candidate for a high advance ratio rotor [17]. The CAMRAD II results showed that inclusion of the blade elasticity drastically reduced the flapping stability boundary compared to the rigid blade model. All stability predictions were made using Floquet theory, and only the damping of the least stable root was presented. The trim controls used were the tilt of the wing and rotor shaft, but no cyclic pitch was used, so the trim conditions are not representative of the full vehicle [17].

Berquist and Tanner [19] analyzed the effect of blade twist on a theoretical compound helicopter. Primary considerations were rotor performance and vibratory stress levels. Results suggest low rotor loading and low twist values produce the best performance and acceptable stress levels. However for the theoretical Sikorsky-type rotor to autorotate at the sea level conditions investigated, positive twist might be required [19], which represents a hover and low speed performance penalty.

Ashby et al. [20] further considered the reverse velocity rotor concept in response to NASA's interest in Runway Independent Aircraft (RIA) and the impact on the National Air Transportation System. Data from the Fairchild's wind-tunnel investigation were used as a validation of several of Sikorsky's proprietary codes. Sikorsky's concept

proposed a rotor slowed using a combination of a two-speed transmission and engine rpm control, utilizing thrust compounding, but not lift compounding, nor requiring the rotor to autorotate [20].

Shank [21] investigated constrained optimization of the aeroelastic trim process for high-speed compound rotorcraft with non-unique trim solutions. The rotor speed was incorporated directly into the vehicle trim algorithm, and an artificial neural network was used as a surrogate for blade stress and strain calculations, which served as the constraint on the trim process. Fixed rotor shaft and variable rotor shaft cases were considered, with the optimality objective being the total vehicle lift-to-drag. Results presented indicate the increase in lift-to-drag with the ability to tilt the rotor shaft, which effectively allows the rotor to operate a lower speed.

1.2.5 Autogyros

Numerous researchers, including Glauert [22], Lock [23], Bailey [24][25][26] Wheatley [27][28][29][30][31][32], Schrenk [33], and Hohenemser [34] contributed to the early literature on many aspects of rotating-wing systems, including performance predictions, and mathematical descriptions as functions of the design parameters. The intense interest in autogyros led to extensive wind-tunnel experiments, flight tests, and analytical analyses regarding nearly every aspect of autogyro operation in the 1930s. Authors such as Bennett [35] and Breguet [36] analyzed the high speed potential of autogyros and made comparisons with fixed wing vehicles to promote the concept.

More recently, flight dynamics of rotorcraft during autorotation has been investigated by Houston [37][38] using a generic simulation model that has been validated with flight test data. The coupling of the rotor speed degree of freedom with the phugoid mode was demonstrated, along with a discussion of several of the important

stability derivatives that affect the rotor speed mode and phugoid mode. Houston noted that out of the new stability derivatives added with the rotor speed degree of freedom, M_Ω , plays a key role especially for rotorcraft with large pitching moments due to collective, such as with rotors with a large flap hinge offset [39]. Houston used analytical expressions derived by applying the theory of weakly coupled systems in order to partition the longitudinal dynamics into two sets. The short period mode formed one set, with the phugoid and rotor speed forming the second. This partitioning allowed closed-form expressions to be developed to provide insight into the source of the placement of the longitudinal roots. Additional work by Houston [39][40] applied system identification techniques to identify the longitudinal and lateral dynamics of an autogyro from flight test data. The test article was a recreational-class vehicle with flight speeds below 100 mph, but still provides validated results for comparison regarding stability derivatives and root placement. Houston also emphasizes several issues that are relevant to all autogyros, namely the coupling of the rotor speed degree of freedom with the conventional rigid body degrees of freedom, and the importance of the vertical center of mass position with respect to the thrust line.

1.2.6 Compound Helicopters

Helicopters compounded with auxiliary lift and propulsive devices (compound helicopters) have been investigated as a means to increase the speed and maneuver capabilities of rotorcraft. Several compound helicopter research programs have provided insight into the issues associated with lift sharing in the concept vehicle, and to some extent autorotation in a compounded configuration.

Deal and Jenkins [41] [42] investigated a hingeless rotor compound helicopter to determine the speed stability, maneuver stability, and rotor-wing lift sharing in

maneuvering flight. The flight test revealed collective pitch settings for the maximum range of airspeeds the vehicle could be flown without adjusting the collective, and highlighted the relationship between collective pitch setting and aircraft attitude, especially at lower airspeeds [42]. Additionally, results were presented for rotor speed variation with load factor. These results are applicable to rotor over-speed considerations as well as rotor autorotation. The tests were conducted in a descending, banked turn at constant airspeed and jet thrust, with the rotor power at flight idle. The rotor RPM was allowed to decrease to 90 percent of design speed to establish the minimum load factor to prevent under-speed. The load factor was then increased until the rotor increased to 110 percent of design speed. This established a maximum load factor to prevent rotor over-speed. Tests were repeated at different collective pitch setting and wing spoiler settings. Increasing the collective pitch increased the maneuver over-speed boundary, while the spoilers could be used to decrease the autorotation under-speed boundary. The changes indicated that appropriate pilot action could be used to shift the boundaries, but would require the pilot to monitor the rotor speed [42], potentially adding complexity to the piloting strategy.

Van Wyckhouse reported on the flight tests of the Bell UH-1 compound helicopter maneuver flight test program in 1966 [43]. Wing and rotor lift contributions were reported in steady-level flight and during maneuvers. Example results indicated that the rotor, while carrying only about 30 percent of the lift in steady level flight, provided the majority of the load factor increment in maneuvers, with the wing contributing little to the load factor increment [43]. Based on rotor structural load and vibration limits, these results highlighted the need for more effective use of the airframe lifting surfaces, while restricting rotor loads during maneuvers [43]. Van Wyckhouse suggests in the conclusion that for “a compound helicopter using full airplane control, care must be taken to prevent inadvertently overloading the rotor during a maneuver”. Blackburn [44]

investigated load factor feedback to collective as a means to unload the rotor during accelerated flight, as demonstrated during tests of the Kaman UH-2 compound helicopter. Results indicated that the load factor feedback to collective was effective during symmetric pull-up maneuvers, and the test pilots reported and improvement in handling qualities [44], which was attributed to a reduced sensitivity of the longitudinal cyclic [44] below that previously exhibited in high speed flight without feedback. Orchard and Newman [45] suggest wing flaps as a means to increase wing loading during maneuvers, and indicate the potential benefits of flaps in hover for reducing download, and spoiling lift for autorotational landings [45] while recognizing that unconventional or more complex piloting strategies may result.

1.2.7 Additional Works

Several authors have contributed to the literature by providing summaries or historical perspectives. Leishman [46] provided an overview of the development of the autogyro, highlighting the technical challenges that were overcome, and a detailed description of the physical mechanism of autorotation. Hohenemser [47] described the flight dynamics of hingeless rotorcraft with numerous examples from existing vehicles, and highlights the potential for coupling between the rotor regressing flap mode and some body modes. The special problems associated with hingeless rotorcraft are summarized, as well as a discussion of the design parameters that effect flight dynamics.

1.3 Present Work

All the previous work cited in the literature review contributes to the basic knowledge that is relevant to the concept vehicle, however the inherently key aspects of the concept vehicle have mainly been considered as ancillary. These key aspects: reduced rotor

speed operation, reduced rotor thrust (unloading) and lift sharing, autorotation, and high advance ratio operation have appeared individually throughout the literature, but have not been studied collectively so as to thoroughly understand the combined characteristics unique to the concept vehicle. A notable except is the recent analytical work of Shank [21] concerning a similar high advance ratio compound autogyro configuration. The present work is intended to complement Shank's work in several ways. First, Shank determined "How to fly the vehicle" in terms of the optimized lift to drag ratio. In the actual flight vehicle other considerations may prevail that preclude operation at the optimum lift to drag ratio. For instance, modeling uncertainty or the inability of the pilot to monitor and adjust the operating conditions to achieve the optimum lift to drag ratio may result in operation in non-optimum conditions. Secondly, other factors could impose constraints that prevent operation at the optimum lift to drag ratio for flight safety reasons, such as vehicle stability considerations or the increased potential for hull strikes, etc. For these reasons it is desirable to identify stability and control trends over a wider range of operating conditions and to appreciate the sensitivities to the rotor parameters.

The objective of the present work is to consider the inherent features of the concept vehicle collectively, and identify stability and control characteristics relevant to the control system conceptual design and the impact of the rotor on the intrinsic flight dynamics characteristics of the concept vehicle. During the conceptual design phase, the primary vehicle and rotor parameters are constantly evolving as information is gained through multi-disciplinary analysis, testing, and the inevitable trade-offs are made to accomplish the top-level project goals. Therefore stability and control analysis on an ever-changing configuration can produce outdated or suspect results. Further, single-point or single-configuration analysis can produce results that are not easily understood without a means to connect them to more familiar results. Thus a primary task of this

dissertation was to perform a series of trim, stability, and control analyses for a baseline configuration over a wide range of operating conditions. Next trends associated with the rotor parameters were identified that clearly show the expected impact as design refinements are proposed and trade-offs considered.

Another equally important objective of this dissertation is to use the analysis results to develop insight into potential rotor control strategies for the concept vehicle. The primary rotor control function is the specification and regulation of the rotor speed. A secondary rotor control function is the management of cyclic flapping so as to avoid excessive structural loads and vibration. A number of rotor control strategies are possible. Of particular interest for the concept vehicle is the potential to use the swashplate controls and possibly tilting of the rotor shaft to accomplish rotor control. These analyses results provide insight into the effects of slowing the rotor, reverse flow, and changes to the rotor parameters, which must be understood before implementing any particular rotor control strategy.

Finally, an objective of the present work is also to assess the intrinsic vehicle flight dynamics characteristics due to the coupling of the rotor and airframe. Results of interest are the effect of the rotor on the presence of classical aircraft modes and the coupling of the rotor speed mode with vehicle motion.

In summary, an understanding of the stability and control characteristics when the key aspects of the concept vehicle are combined represents an open area of research. Research questions were formulated to guide the efforts in accordance with the stated objectives, and the research questions are summarized here under headings that reflect the major sections in the present work.

Rotor Trim and Performance – How to Unload the Rotor

1) *Under what conditions is autorotation possible?*
2) *How are the rotor speed, free stream velocity, rotor shaft incidence, and collective pitch related when the trim conditions of zero-torque, and zero average hub moments are imposed?*
3) *How can the rotor be unloaded, and what thrust results when the trim conditions are imposed?*
4) *What effect does the reverse flow have on the trim solution trends and the piloting or control strategy?*
5) *How is the rotor performance affected by imposing the hub moment trim constraints?*

Rotor Stability – What Effects Tend to Result in Reduced Rotor Stability

1) *How do the advance ratio, rotor speed, and the rotor parameters affect the rotor stability, and what effects tend to reduce stability?*
2) *How does the rotor speed degree of freedom affect the rotor stability?*
3) *How does the lead-lag blade motion affect the rotor stability?*

Rotor Pitch and Rolling Moment Sensitivities to Swashplate Control Inputs and Gusts

1) *How does the rotor speed degree of freedom affect the hub moment response to control inputs and/or disturbances?*
2) *What is the impact of slowed rotor operation at high advance ratio on the hub pitching and rolling moments produced by the swashplate controls?*
3) *How does the cross coupling depend on the rotor parameters and advance ratio?*

Slowed Rotor Dynamics

1) *What is the impact of operating at a reduced rotor speed on the rotor dynamics?*
2) *Is the quasi-steady rotor assumption valid, and what is the time scale of rotor transient hub moment response?*
3) *How does high advance ratio operation impact the rotor dynamics?*

Rotor Speed Response to Swashplate Controls

1) *Can the swashplate controls be used for rotor speed regulation and control?*
2) *Which control(s) are most effective for rotor speed control at high advance ratio?*
3) *How does the reverse flow alter the rotor speed control strategy?*
4) *Does the rotor speed control strategy vary with the rotor parameters?*
5) *How quickly does the rotor speed change when the rotor is disturbed from trim?*

Coupled Rotor and Airframe Interaction and Rotor Control

1) *What impact do the slowed rotor dynamics and the rotor speed degree of freedom have on the intrinsic flight dynamics characteristics of the concept vehicle?*
2) *How can the rotor speed be controlled, and what practical considerations impact the rotor control strategy?*

1.4 Organization of Dissertation

Chapter 1 provides in introduction to the concept of a slowed-rotor, high advance ratio compound autogyro, as well as the background literature review related to the concept.

The motivation for the current research is also described, and the particular issues of interest are identified in terms of the research questions for which answers are sought.

In order to investigate the identified issues related to the concept, detailed rotor and airframe models are required that specifically account for the effect of reverse flow, complex rotor blade motion, the rotor speed degree of freedom, and provide a means to vary the operating conditions and rotor design variables parametrically. A description of the models used in the analysis along with the analysis methods employed for addressing the research questions is presented in Chapter 2.

Chapter 3 presents the results pertinent to the isolated rotor models. Rotor trim is defined, and the relationships between rotor angular velocity, autorotation, swashplate control positions, and flight speed for trimmed rotors are presented in section 3.1. At high advance ratio the aerodynamic loads are highly periodic, and rotor stability analysis results are presented in section 3.2. In sections 3.3 and 3.4, the questions related to the swashplate control moment sensitivities and gust sensitivities are addressed by presentation of the rotor steady-state hub pitching and rolling moments resulting from gusts and control step input disturbances. Section 3.5 addresses the questions related to the slowed-rotor dynamics. The hub moment response to rotor shaft incidence angle is used as a means to excite the rotor transient response. System identification methods are applied to predict the rotor frequency response to disturbances for identification of the dominant rotor frequencies and the effect of the rotor parameters and advance ratio. Section 3.6 discusses the rotor speed response to swashplate control inputs and the relation to strategies for rotor speed control. Section 3.7 discusses the existence of multiple trim solutions and the sensitivity to the initial trim condition of the rotor speed response to swashplate inputs. Section 3.8 addresses the source of the non-linear rotor speed behavior observed in sections 3.6 and 3.7, as well as provides a detailed analysis of the effects that contribute to the rotor torque balance. Section 3.9 addresses moment

trim at high advance ratio and the steady-state flapping behavior on the trim contour presented in section 3.7. Section 3.10 addresses the effect of blade twist on the autorotational trim contour compared to the untwisted blade model. In section 3.11 rotor performance results for out-of-trim operation are presented by imposing the autorotation condition, but leaving the cyclic controls centered.

Chapter 4 takes the isolated rotor models and couples them with an airframe model to address the research questions related to the interactions of the rotor and airframe and rotor control strategies. Full vehicle trim is accomplished using swashplate controls, conventional airframe controls, and rotor shaft incidence as trim variables. Methods of rotor speed regulation are discussed in terms of steady-level trim and two aircraft quasi-steady maneuvers: a rotor speed transition maneuver (commanded change in rotor speed) and a climb/descent maneuver at constant rotor speed. Quasi-steady control and attitude trajectories for the maneuvers are presented and the rotor control strategies are discussed in section 4.2 and section 4.3. Coupled rotor and airframe flight dynamics characteristics are discussed in section 4.5.

Chapter 5 summarizes the conclusions drawn from this study and presents recommendations for future work.

CHAPTER 2

MODELING AND SIMULATION ENVIRONMENT

This chapter provides a detailed description of the models used in the analysis. Of concern here are the rotor models for prediction of the impact of the primary rotor design parameters, modeling of the rotor speed degree of freedom, and the baseline airframe model with conventional control surfaces. The last section of this chapter presents an overview of the analyses that were selected to answer the research questions using: trim results, Floquet analysis, time integration of the non-linear simulation, and system identification methods.

2.1 Rotor Model Formulation

Accurate prediction of the rotor behavior is a fundamental challenge for analysis of the concept vehicle. The interactions of the aerodynamics and rotor structure are complex, and in order to accurately characterize the rotor over a range of conditions beyond the conceptual design phase, a substantial effort would be required involving comparisons between computationally intensive modeling results and experimental data, likely with numerous iterations to refine the models to correlate with the experimental data. In the present work the analysis is focused on two primary areas: the impact of the rotor as related to the vehicle flight dynamics, and the rotor behavior related to the conceptual design of the control system. The concept vehicle is expected to utilize a rotor with stiff in-plane and out-of-plane characteristics which will be capable of generating large moments even as the thrust loading is reduced. Coupling of these hub moments with the vehicle dynamics is of primary interest in the present work. The control system is expected to provide a means to specify and regulate the rotor speed to avoid resonance

conditions due to operating at frequencies that coincide with structural frequencies while maintaining the rotor rotation. For this purpose an understanding of the rotor behavior as a function of the rotor speed and flight speed are essential.

For typical flight dynamics simulation models, Tischler [49] reports the frequency range of interest as ~0.3 to 12 rad/s and emphasizes that models of the rotor dynamics must be accurate near the frequency of the regressing flap mode as well. Analytical solution for the rotor frequencies are presented by Johnson [50] and others for the hover case. For rotors with three of more blades, the transformation of the roots to the non-rotating frame leaves the real part of the roots unchanged, but shifts the frequency by $\pm\Omega$, forming the low frequency regressing mode and the high frequency advancing mode, with the coning mode unchanged. The real part of the root is given by $-\gamma\Omega/16$ and the frequencies are determined by the flapping stiffness. For the concept vehicle the combination of heavy blades and high altitude operation results in a low Lock number, $\gamma \sim 2$, and the reduced rotor speed draws the regressing flap mode frequency to the same order of magnitude as the high frequency body motion. Thus the effects of primary concern in the present work can be considered relatively low frequency, even when the rotor dynamics are included.

The complex aerodynamic environment of the rotor is exacerbated by the reverse flow region which dominates the retreating side of the rotor at high advance ratio. The wake of an autorotating rotor is however above the rotor and with the combination of the forward flight speed, reduced rotor speed, and reduced thrust-load the flow though the rotor is likely dominated by the inflow due to the flight speed, with the shed vortices quickly left behind in the far field. For the purposes of identifying trends associated with the rotor operating conditions and the rotor parameters an elaborate, computationally intensive rotor wake model was deemed unwarranted.

The choice of the type of hub and method of blade attachment is a design choice. The literature review revealed high advance ratio studies involving teetering, articulated and hingeless rotors. For the present work the number of blades, the rotor radius, and the blade chord are assumed to be fixed from mission analysis and sizing considerations. In this case a rotor model formulation is preferred that accommodates the parametric variation of the operating conditions and rotor parameters. The concept vehicle as described in the literature is expected to use a hingeless rotor. The hingeless rotor provides several advantages over an articulated rotor such as “mechanical simplicity with a low parts count and low aerodynamic drag” [51]. Modeling of a hingeless rotor requires detailed information about the structural properties of the blade which may not be known in the conceptual design phase. Introducing a level of detailed modeling consistent with a hingeless rotor with elastic blades may also introduce instabilities into the model related to phenomena not under consideration in the present work, flutter, etc. Padfield [52] provides a discussion of the *center-spring approximation* and the associated trade-offs in fidelity, consisting primarily of errors in the mode shapes of the actual elastic blades. Further, the fundamental difference in the blade root attachment boundary conditions between hingeless rotors and articulated rotors precludes exact equivalence of the two formulations. Figure 3 from reference [52] shows the center spring approximation compared to the elastic and hinge offset blade models. Padfield [52] also cites several examples from the literature related to high speed flight in which the higher bending modes are important for flight dynamics of helicopters. For helicopters in high speed flight though the rotor is heavily loaded producing sufficient thrust for forward propulsion and lift.

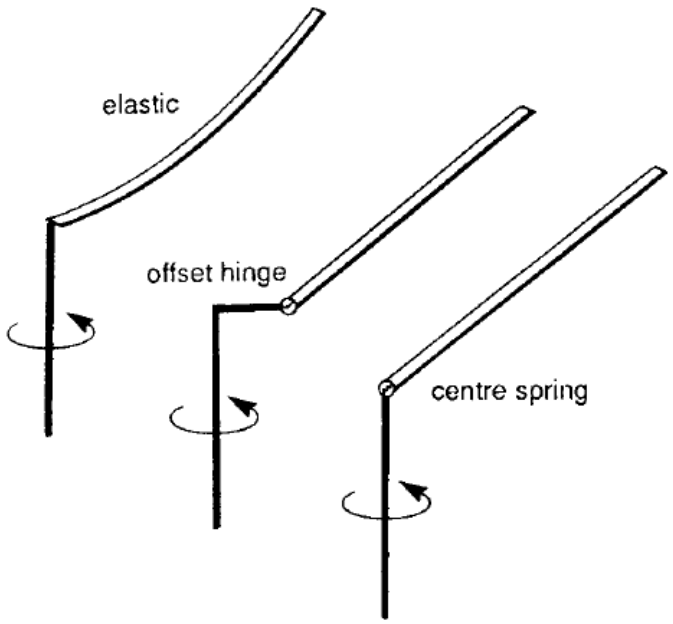

Figure 3: Center Spring Approximation Rotor Model from Ref. [52]

The inherent feature of unloading the rotor and the admissibility of an articulated rotor into the conceptual design justifies investigation using the center spring model for a parametric trends analysis of relatively low thrust and low frequency effects.

In addition to tailoring the model formulation to the specific problems to be addressed, the model fidelity in the various aspects should be balanced so as not to add unnecessary computational overhead or incorrectly imply a level of accuracy to the overall results. The model formulation selected for implementation in FLIGHTLAB™ [53] was the articulated rotor, blade-element model. Rigid blades were assumed and a dynamic inflow model was selected as the baseline configuration. The flapping frequency was determined by the addition of flapping hinge springs, and the models were created with zero hinge-offset so that the flapping spring stiffness completely determined the flapping frequency. When lead-lag motion was considered, the flap and lag hinges were coincident. The sequence of hinges in the FLIGHTLAB™ articulated

rotor model was: flap, pitch, lead-lag proceeding from the center of rotation toward the blade tip. Figure 4 shows a schematic from reference [54] of the physical implementation of the hinge sequence. Air loads were calculated in FLIGHTLAB™ using a table lookup quasi-steady model.

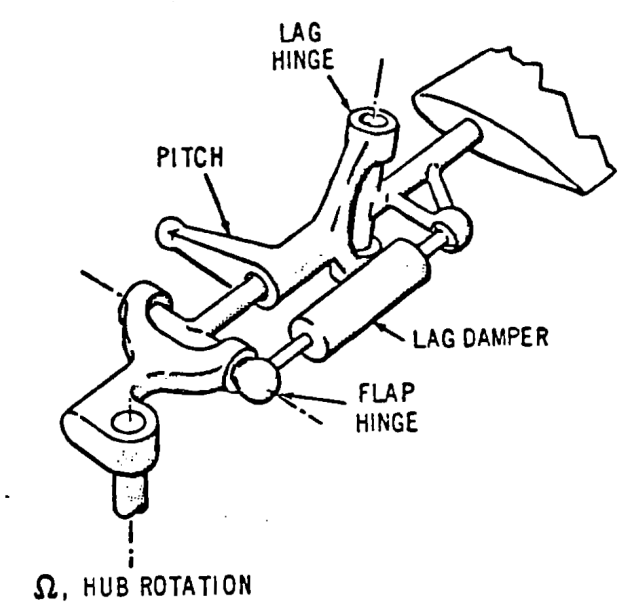

Figure 4: Articulated Rotor Model Hinge Sequence from Ref. [54]

The fixed baseline rotor parameters are shown in Table 1, and were common to all of the parametric models implemented in FLIGHTLAB™. The rotor blades were modeled as rigid bodies with constant mass properties, and the blade mass properties used for parametric analysis are shown in Table 2. These properties were chosen to be similar to values identified in the literature review for high advance ratio rotors, where heavy, stiff blades operating at low density implies low Lock numbers and high non-dimensional flapping frequencies.

Table 1: Fixed Baseline Rotor Parameters

Parameter	Value
Type of rotor	Articulated with Flap Springs
Number of blades	4
Nominal 40% Rotor Speed	12 rad/s
Rotor radius	21.5 feet
Blade chord	1.7 feet
Airfoil	NACA0012
Hinge offset	0
Blade Twist	0 deg.
Inflow model	Dynamic Inflow

Table 2: Rotor Mass Properties for Parametric Analysis

	Mass per unit length [sl /ft]	Weight per Blade [lbf]	Second Moment of Inertia with respect to the Flap Hinge [sl-ft^2]
Blade 1	0.1	69.2	331.3
Blade 2	0.2	138.5	662.6
Blade 3	0.3	207.7	993.8
Blade 4	0.4	276.9	1325.1

The FLIGHTLAB^{TM} input files require a description of the blade mass properties in terms of a table of radial station and mass-per-unit-length of the blade values. In this case, with constant mass properties, the second moment of inertia of the blade about the flap hinge was easily determined, and a straight-forward calculation of the Lock number was made. The Lock number itself is not a direct input to FLIGHTLAB^{TM}, but is a result of the mass properties input tables and the air density. The four blade-mass profiles were designated as blades one through four for ease of identification. The non-dimensional flap frequency, ν, was determined for each of the blade models as a function of the flapping hinge spring constant and the rotor speed. The 'Fan Plot' utility in

FLIGHTLAB™ was used to correlate the non-dimensional flapping frequency with the flapping hinge spring stiffness according to:

$$\nu = \sqrt{1 + \frac{K_\beta}{I\Omega^2}}$$

The calculations and the FLIGHTLAB™ results were consistent to within about 1%. The fan plot results are shown in Figure 5 for typical spring constant values. These four blade models formed the basis for the parametric analysis. Since a primary interest in the current work is the rotor behavior at a reduced rotor speed of 12 rad/s which corresponds to 40% percent of the nominal hover speed, the rotor properties also were summarized as in Figure 6, which shows the relationship between the different blades, the flap hinge spring constants, and the resulting non-dimensional flap frequency at the reduced rotor speed. Since the non-dimensional flap frequency depends on the ratio of the spring constant and the blade second moment of inertia, lighter blades require a smaller spring constant for a given non-dimensional flap frequency. The figure also demonstrates how the spring constants were varied between the blade models when analysis results at constant ν are presented.

In addition to the fixed baseline rotor parameters, a blade mass and spring stiffness combination was chosen as a parametric baseline to serve as a starting point for further analysis. The impact of the rotor parameters was then presented with respect to the baseline so that trends could be identified more readily. The parametric baseline stiffness and mass properties are shown in Table 3.

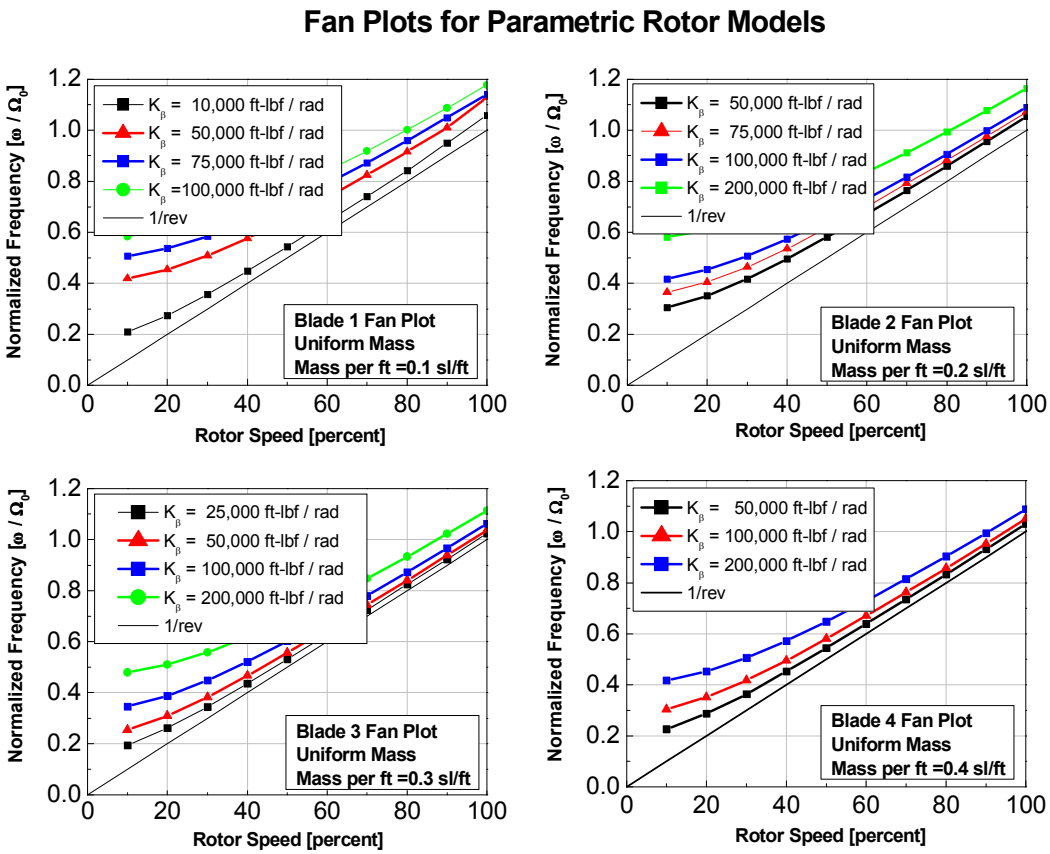

Figure 5: Fan Plots for Parametric Rotor Models

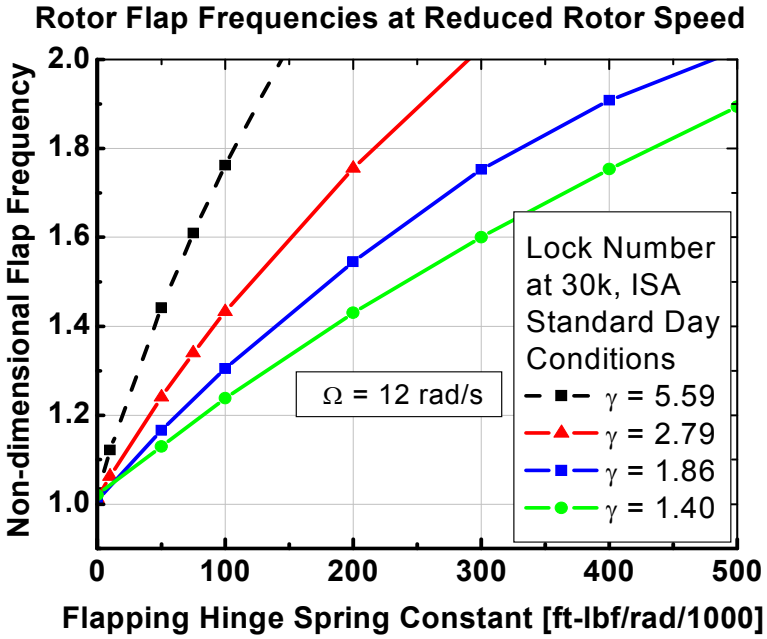

Figure 6: Flap Frequencies at Reduced Rotor Speed

Table 3: Parametric Baseline Rotor Properties

Analytical Quantity	FLIGHTLAB Input
Lock Number At 30k, ISA Standard day $\gamma = 1.4$	Mass per foot =0.4 slug/ft
Non-dimensional Flap frequency at 12 rad/s $\nu = 1.24$	K_β =100,000 ft-lbf/rad

2.2 Rotor Speed Degree of Freedom Model

The rotor speed degree of freedom is an inherent feature of autorotation, and its effects represent a significant portion of the knowledge gap associated with the concept vehicle. Therefore its inclusion was deemed a necessary feature and critical for the present work. The rotor speed degree-of-freedom was modeled using FLIGHTLAB™ library components including: drivetrain, shaft, gears, and a clutch component in conjunction with the constant-speed ideal engine. The clutch component allowed the rotor speed to remain constant during trimming routines, and provided a manual override to prevent any engine shaft torque from being applied to the rotor during the non-linear simulation of autorotation. The presence of an engine model is a feature of FLIGHTLAB™ for helicopter simulation, and is required in rotorcraft models. The ideal engine simply provides a constant rotor speed with no drive-train dynamics, and no torque limits. The shaft and clutch components allowed the rotor speed to vary under the influence of the aerodynamics, etc, with no effect from the constant speed shaft of the ideal engine. The clutch state was controlled through an on/off flag in the simulation.

Rotor speed behavior was investigated at hover conditions and in zero-density conditions to characterize the drive train model. Figure 7 shows the rotor thrust at hover versus the collective pitch setting for the parametric baseline model. A collective setting of nine degrees provided a thrust similar to the concept vehicle gross weight and was

used to demonstrate the rotor speed behavior with the clutch disengaged such that no input shaft torque was applied to the rotor. The right side of Figure 7 shows two test cases. In the first case the rotor speed decays in the presence of the atmosphere with the collective held constant, and the second case the rotor speed remains constant with the density flag set to the "off" position. The result was a rotor speed that varied depending on only the aerodynamics, with no losses in the drivetrain due to friction, etc. This feature augmented the modeling of steady state autorotation in trim with the capability to include the rotor speed degree of freedom in the non-linear simulation.

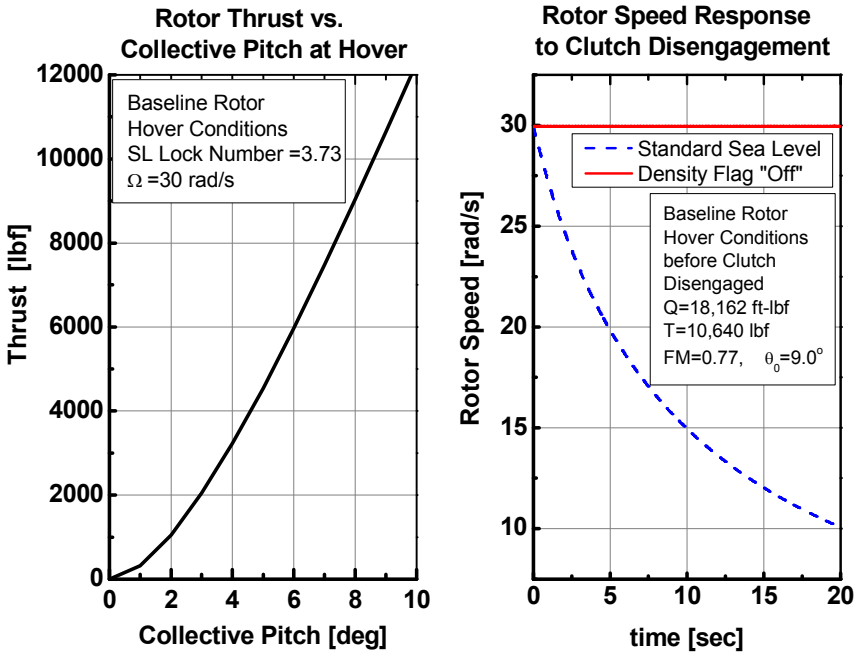

Figure 7: Rotor Drivetrain Response at Sea Level Hover

2.3 Airframe Model

The airframe configuration itself represents a design choice. A configuration was chosen as representative of the concept vehicle configuration from the publicly available information. The primary purpose of the airframe model was to investigate issues related to interaction of the rotor and airframe. Parametric analysis was restricted to the rotor parameters as the rotor represents the novel portion of the concept vehicle. The airframe model consisted of fuselage mass and inertia properties, and aerodynamic coefficient properties, along with horizontal and vertical stabilizers. The turbofan engines were modeled as point-forces with a fixed orientation in the body frame, but adjustable magnitudes for the trim process. Conventional fixed wing control surfaces were included for airframe control separate from the rotor controls. The airframe model properties are shown in Table 4.

Table 4: Airframe Model Properties

Airframe Model Parameters	
Gross Weight	10,000 lbs.
Fuselage Equivalent Drag Area	10 ft^2
Wing Span	30 ft
Airfoil	NACA 009 with Flap
Root chord	4.5 ft
Tip Chord	2.0 ft
Sweep Angle	5 degrees
Dihedral Angle	4 degrees
Horizontal Tail Planform Area	40 ft^2
Horizontal Tail Location	17 ft Behind Rotor Hub
Vertical Tail Planform Area	40 ft^2
Vertical Tail Location	17 ft Behind Rotor Hub
Auxiliary Propulsion System	Thrust force as required

2.4 Operational Envelope and Test Conditions

All analysis was conducted at test conditions of 30,000 ft altitude in the Standard Atmosphere. This condition was selected as representative of the concept vehicle cruise mission, where a substantial portion of the flight will be conducted. Achieving the maximum level flight cruise speed requires the rotor to be slowed to 40% of the nominal hover angular velocity with an advance ratio $\mu \sim 2.29$ to adhere to the advancing tip Mach number limit $M_{1,90} < \sim 0.85$. The relationship between the flight speed, rotor speed, advance ratio, and advancing tip Mach number is shown in Figure 8. The hatched region defines the envelope of test conditions considered for the present work.

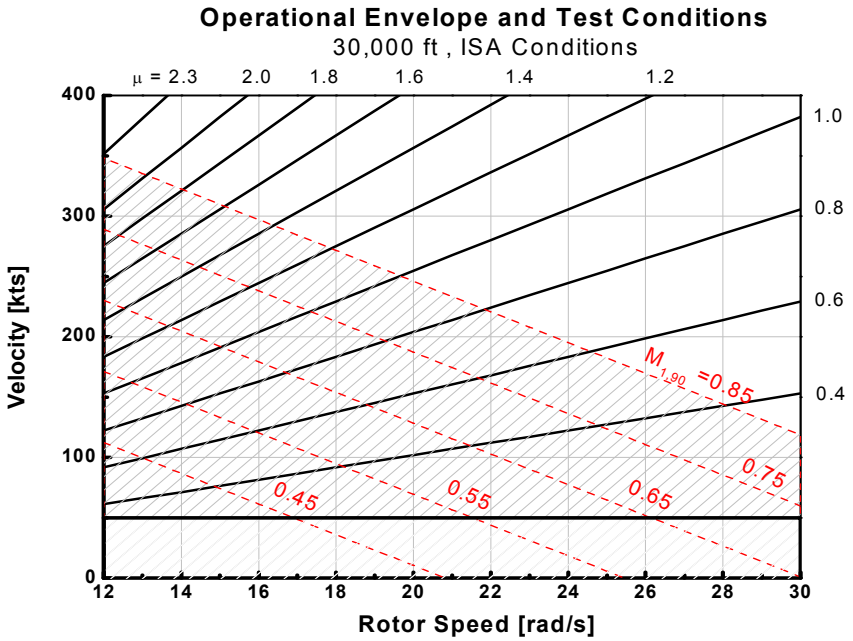

Figure 8: Test Conditions Envelope

2.5 Analysis Selection and Methodology Overview

This section describes the relationship between the inherent feature of the concept vehicle, the research questions, and analysis selected to answer the research questions. Most analyses began with trimming the model. This process of determining the control positions for a prescribed steady-state condition sets the model initial states for further analysis. Trim conditions imposed in the present work are defined in section 3.1.

Rotor stability was assessed by applying Floquet analysis, which is applicable to linear, periodic systems. A linear model with constant coefficients is a common approximation in helicopter theory. The effect of forward flight is to introduce periodic aerodynamic forcing on the blades, which results in periodic coefficients in the linear model. In many helicopter (relatively low advance ratio) applications, the periodic effect can be neglected. For the concept vehicle, high advance ratio operation implies the reverse flow covers essentially the entire retreating side of the rotor, such that on each rotor revolution, each blade experiences flow over the blade from leading edge to trailing edge on the advancing side, then from trailing edge to leading edge on the retreating side. The result is aerodynamic loads that strongly depend on the azimuth position (periodic variation with azimuth in steady state). These effects cannot necessarily be neglected in this application when considering the rotor stability trends. Built-in Floquet analysis routines in FLIGHTLAB^{TM} were used to produce the results, with scripting used to facilitate data collection and post-processing.

Rotor pitching and rolling moment sensitivities to swashplate control inputs were predicted using time-integration of the non-linear simulation. Step control inputs were applied, and the steady state hub moments were recorded after the rotor transient response decayed and the moments settled to a steady-state value. This analysis answers the research questions related to the effect of high flight speed on the

magnitude of the moments that can be generated per unit displacement of swashplate control. The cross coupling moments in terms of the phase angle response are also presented, which highlights the issues with changing cross coupling effects with flight condition. In helicopter applications it is often possible to choose a fixed geometry that connects the pilot controls to the swashplate actuators and serves as a compromise to provide acceptably low cross-coupling at most flight conditions. The concept vehicle is required to operate over wide ranges of rotor speeds and flight conditions, and the literature review indicated that longitudinal and lateral controls have differing phase responses at high advance ratio. Therefore the results in this section address the research questions related to control sensitivities, swashplate phase angle response and control cross-coupling.

In helicopter applications, the rotor transients generally occur on a much shorter time scale than the vehicle body motion, thus justifying the quasi-steady rotor assumption. For the concept vehicle, the rotor transients were expected to occur on a much longer time scale, the primary contributing factors being: high blade mass, low density at high altitude, reduced rotor speed, and potentially the effect of the reverse flow region. The slowed-rotor dynamics in this case are of a time scale that may couple with the body motion in a way that can make the piloting task more difficult, result in unacceptably large structural loads, or may lead to pilot-induced oscillations, increased pilot workload, etc. Transient rotor response may be seen whenever the rotor is disturbed by gusts, swashplate control inputs, or vehicle body motion. The magnitude and time scale of the moments generated by these disturbances may also lead to the need to suppress these moments through feedback control in the concept vehicle. The responses of interest are the hub moments in the non-rotating frame, which results from the combined effect of the blade flapping for all of the blades. Both time domain and frequency domain results are presented in the discussion of the slowed rotor dynamics.

The objective for the frequency domain analysis is to obtain low order transfer function models of rotor hub moment response to an input. In this dissertation the hub pitching moment response to changes in shaft incidence are used to answer the research questions related to the slowed-rotor dynamics. The transfer functions provide damping and frequency information about the rotor modes and the effect of the rotor parameters and advance ratio. Frequency domain data also provides information useful for the design of a hub moment suppression controller, when linear control theory would be a desirable starting point from a cost and complexity perspective. The time domain analysis consists of comparisons of the non-linear simulation and the low-order linear model response to step changes in shaft incidence. The analysis offers insight into the predictive capability of the linear models as compared to the non-linear simulation, the dominant frequencies present, and types of responses seen in the simulation that are not captured in the linear models.

Regulation and control of the rotor speed throughout the flight envelope was stated as a basis requirement of the control system inherent in the configuration. The effects of the swashplate controls on the rotor speed were investigated using the non-linear simulation. From trim, step control inputs were applied, and the model stepped forward in time to establish a rotor acceleration that was approximated using a two-point approximation. This analysis addresses the research questions related to rotor speed behavior and rotor speed control using swashplate inputs.

Coupling of the rotor and airframe was investigated using trim analysis, linearization of the non-linear models, system identification analysis, and time integration of the non-linear models. Rotor control strategies were further developed by considering two quasi-steady maneuvers using trim analysis for fixed rotor shaft, controllable rotor shaft, trimmed hub moment, and untrimmed hub moment cases. The intrinsic flight dynamics characteristics were investigated by comparing results predicted from

linearization of the non-linear models and system identification results based on surrogate flight test data from the non-linear simulation.

CHAPTER 3

ISOLATED ROTOR ANALYSIS

3.1 Autorotating Rotor Trim and Performance Trends

Basic trends for a trimmed rotor in autorotation were established using the parametric baseline isolated rotor model. The fundamental questions addressed in this section are related to the conditions under which autorotation is possible, what are the effects of advance ratio and the rotor parameters, and how the rotor load is reduced. The results presented were obtained using the 'trim' routine in FLIGHTLAB^{TM} where the steady-state trim condition for the rotor was defined in terms of the average rotor hub moments (pitch and roll) and the rotor torque being driven to zero. Trim was accomplished by adjusting the swashplate controls and the rotor shaft incidence to the freestream airflow for a specified rotor speed. The result was three quantities to drive to zero, with four quantities that can be adjusted, three swashplate controls: longitudinal cyclic, lateral cyclic, and collective pitch, and the shaft angle. As such, the collective was held fixed at zero degrees to establish the basic trends, and then adjusted to a new value on successive runs as a sensitivity parameter.

In order to present the rotor performance in a concise manner it was desired to establish if the relations between the rotor speed, freestream velocity, and rotor performance could be presented non-dimensionally. It was not assumed *a priori* that in the presence of reverse flow and complex blade motion the advance ratio was sufficient to describe the performance for all equivalent combinations of rotor speed and freestream velocity contained in the advance ratio. In order to address this question, the effect on rotor performance for different rotor speeds was investigated. This was accomplished by trimming the rotor over a range of freestream velocities up to the

advancing tip Mach number limit at different rotor speeds. The parametric baseline rotor thrust coefficient as a function of advance ratio is shown in Figure 9. The figure shows that in non-dimensional terms the curves all coincide except as the advancing tip Mach number approaches the imposed limit. The minimum advance ratio shown in the figure corresponds to a free stream velocity of 50 knots since some velocity is required to achieve autorotation. The thrust coefficient data also show that the effect of increasing advance ratio at a fixed rotor speed is to increase the rotor thrust. In dimensional terms, the unloading of the rotor (reduced thrust) comes about from allowing the rotor to operate at a lower rotor speed.

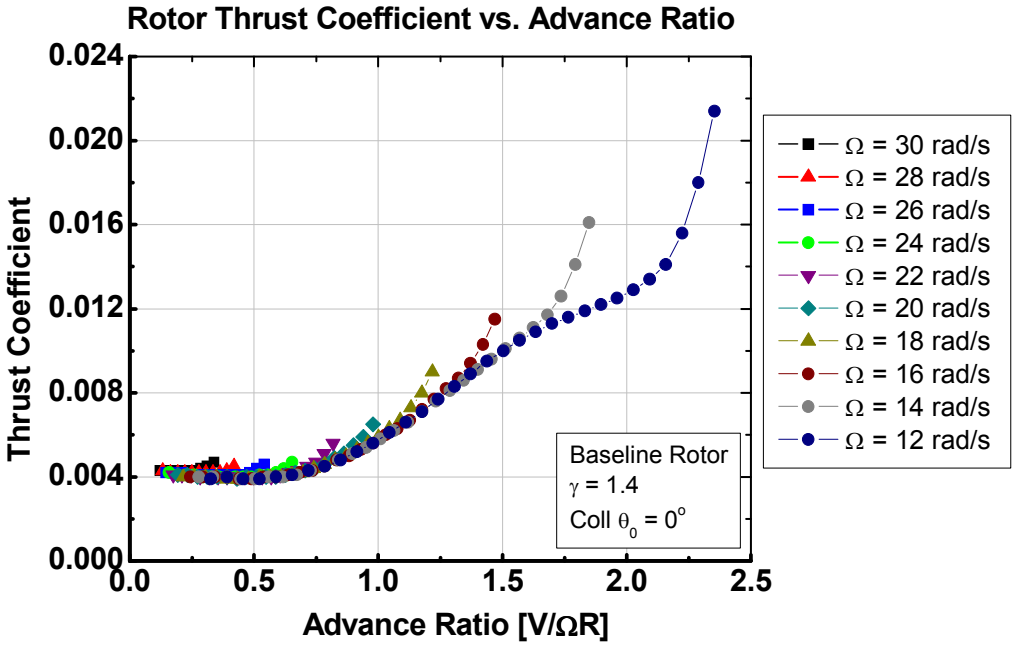

Figure 9: Baseline Rotor Thrust Coefficient vs. Advance Ratio

The rotor lift to drag ratio and the rotor shaft incidence to the freestream, shown in Figure 10 and Figure 11 respectively, also indicated consistent trends when presented

in terms of advance ratio. The rotor shaft incidence data, Figure 11, reveals that at low advance ratio a large shaft incidence is required such that sufficient air flow through the rotor is present to sustain autorotation. As advance ratio is increased however, lower shaft incidence is sufficient until at the highest advance ratio a slightly increased shaft incidence is again required likely due to the higher drag associated with the blade tip high Mach number condition. Similarly the thrust coefficient and rotor lift to drag ratio data show that at low advance ratio the rotor is essential producing little thrust and a large component is downstream (drag).

The cyclic control positions for these baseline trim cases are shown in Figure 12 and Figure 13. The control positions are generally within a narrow band of two degrees for the baseline rotor with the longitudinal cyclic passing through a maximum near an advance ratio of one, and the lateral cyclic remains relatively flat in the range beyond $\mu \sim 1.0$.

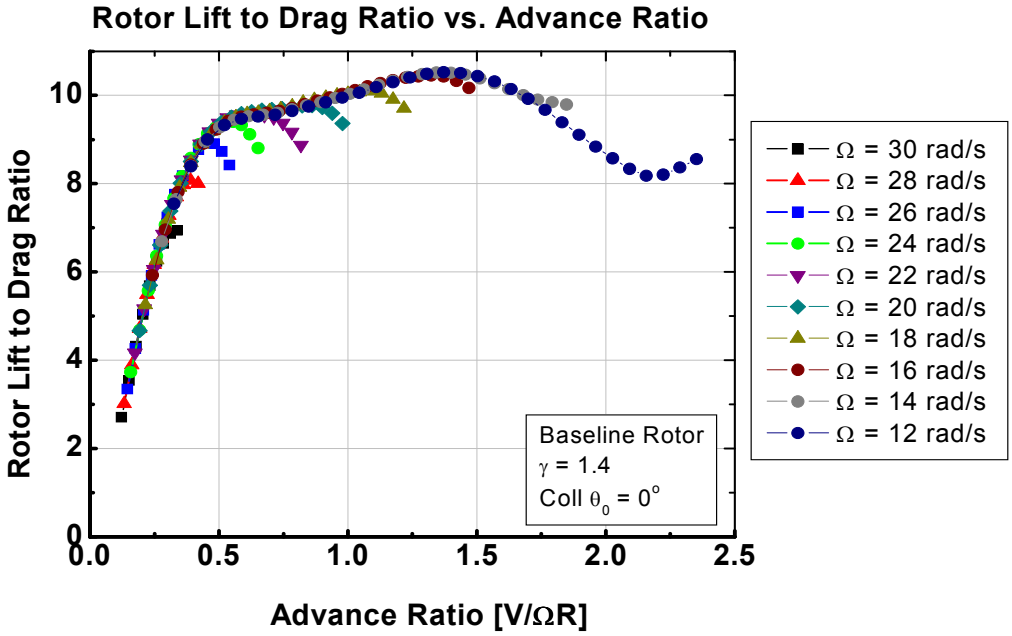

Figure 10: Baseline Rotor Lift to Drag Ratio vs. Advance Ratio

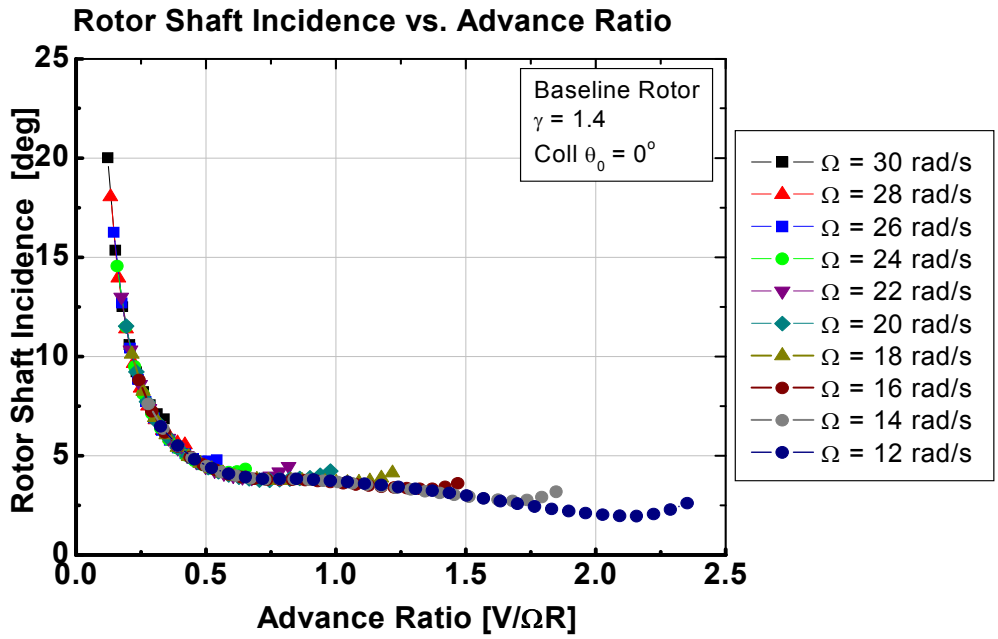

Figure 11: Baseline Rotor Shaft Incidence vs. Advance Ratio

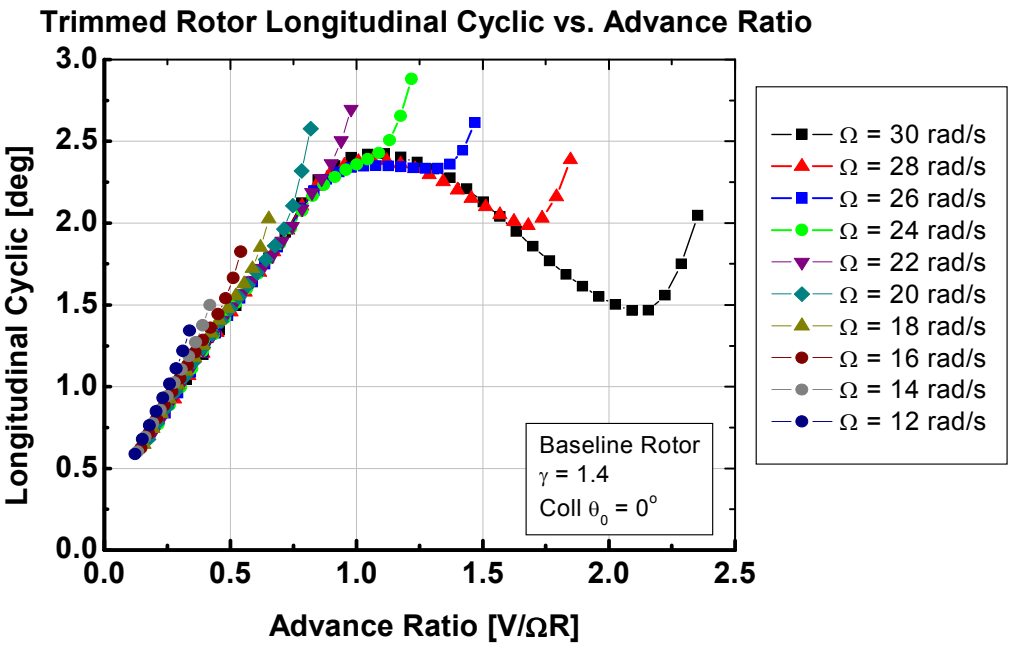

Figure 12: Baseline Rotor Longitudinal Cyclic vs. Advance Ratio

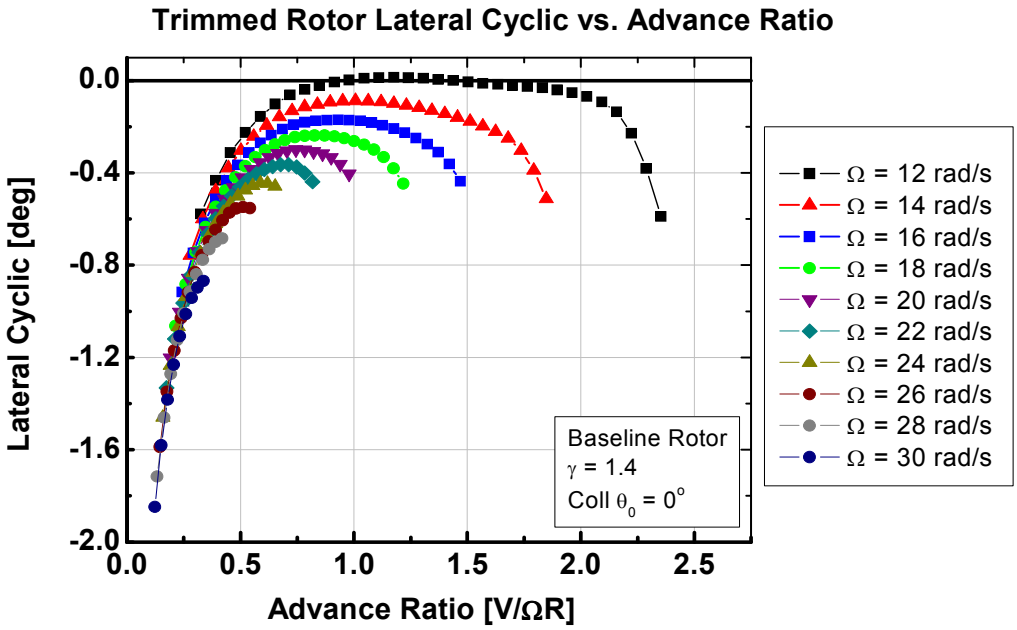

Figure 13: Baseline Rotor Lateral Cyclic vs. Advance Ratio

Based on the performance trends presented in terms of advance ratio, the trim and performance sensitivity analysis was conducted at the reduced rotor speed (12 rad/s) to simplify the presentation of the trends. Performance sensitivity to the Lock Number and the non-dimensional flapping frequency are shown in Figure 14 through Figure 16. The flap stiffness has minimal effect on the rotor performance in the ranges considered, and the Lock number shows only a weak effect with a slight decrease in thrust coefficient and lift to drag ratio with increasing Lock number. Cyclic control positions for trim, Figure 17 and Figure 18, show that the more lateral cyclic control input is required for higher Lock number (lighter) blades, suggesting the reverse flow forces the lighter blades to higher flapping, requiring more control input to trim the rotor. The cyclic control figures also show the magnitude of the inputs required for trim, which remain on the order of two degrees for the ranges of rotor parameters considered.

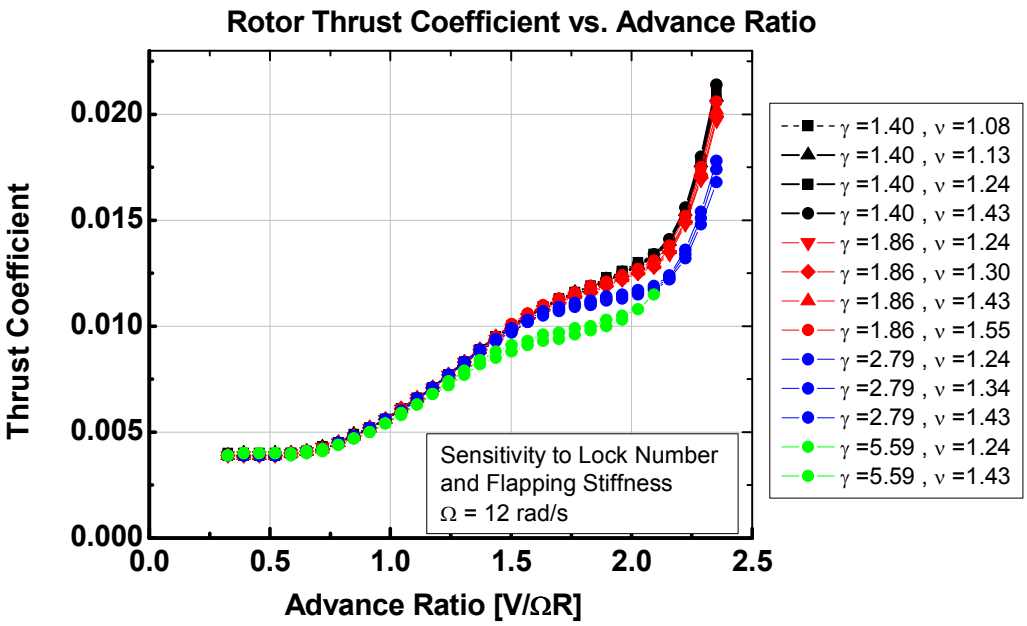

Figure 14: Thrust Coefficient Sensitivity to Rotor Parameters

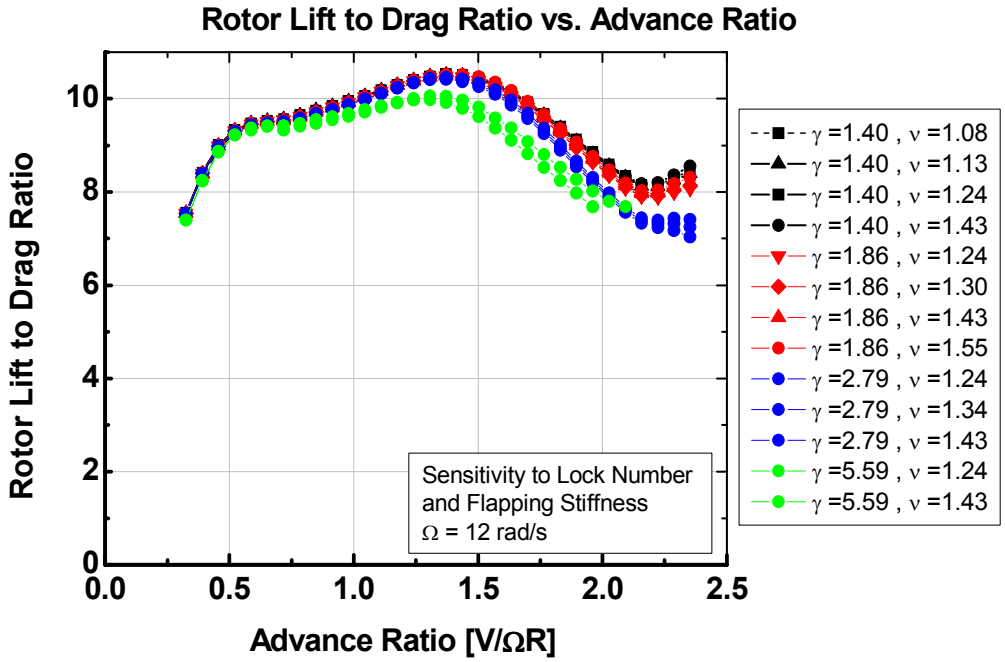

Figure 15: Lift to Drag Ratio Sensitivity to Rotor Parameters

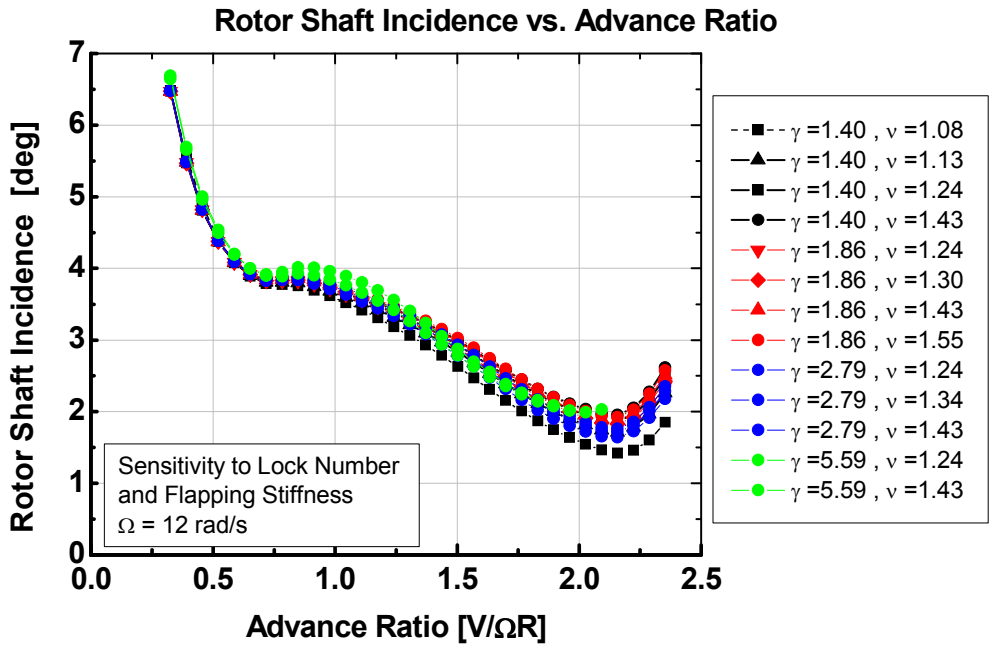

Figure 16: Shaft Incidence Sensitivity to Rotor Parameters

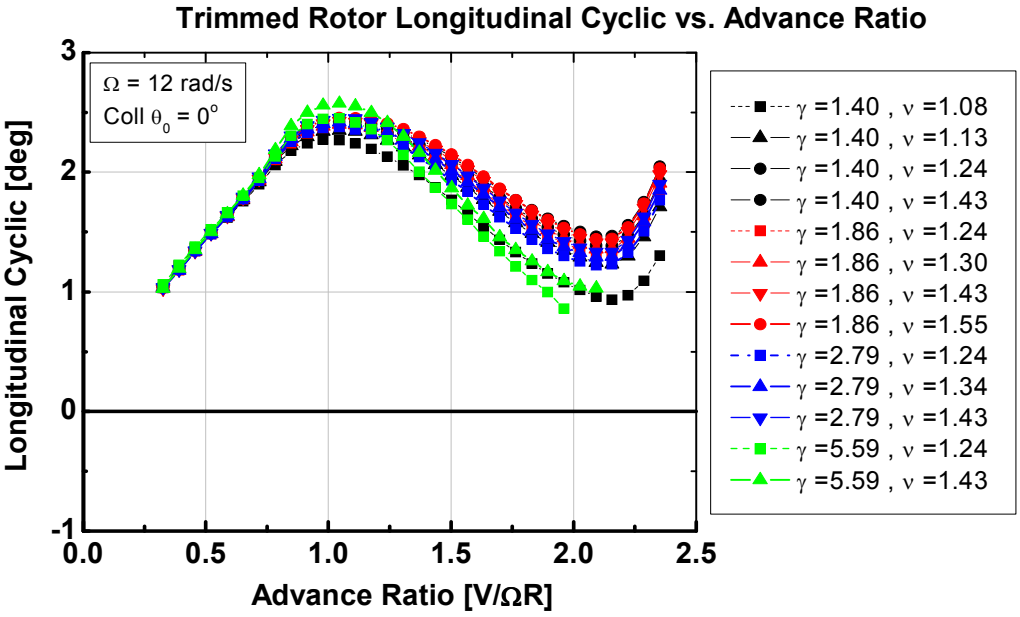

Figure 17: Longitudinal Cyclic Trim Sensitivity to Rotor Parameters

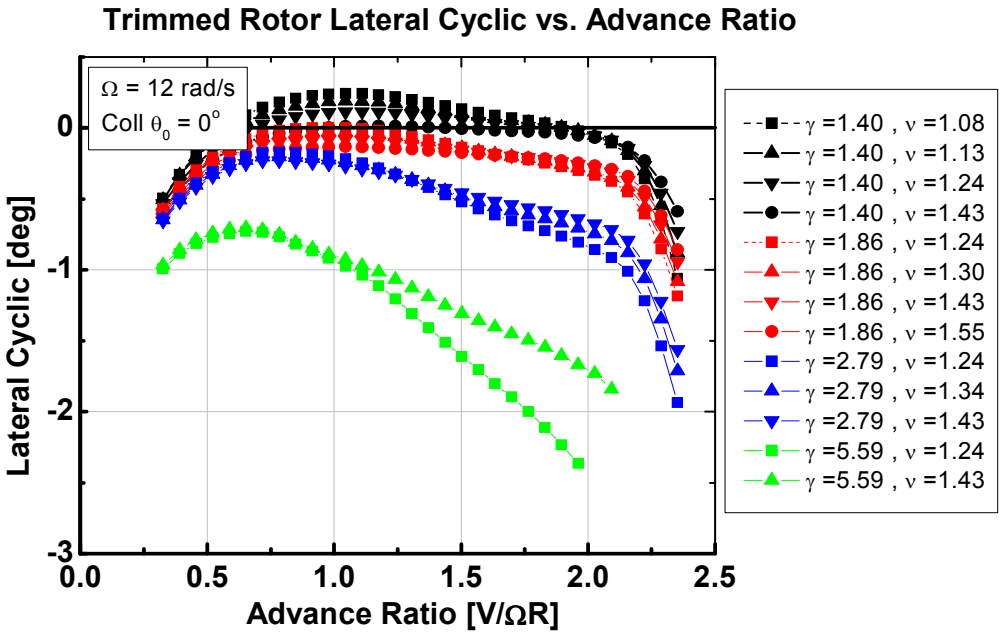

Figure 18: Lateral Cyclic Trim Sensitivity to Rotor Parameters

In the previous results, the performance trends were shown at a fixed collective pitch of zero degrees. The Lock number was also shown to provide a weak influence on performance. In order to determine the effect of the collective pitch setting, the analysis was repeated for collective pitch settings of +1 and -1 degrees for each of the blade models. The flap stiffness was held constant at $\nu = 1.24$ by adjust the flap hinge spring constant according to Figure 6. The thrust coefficient, lift to drag ratio, and shaft incidence trends with collective pitch and Lock number are shown in Figure 19, Figure 20, and Figure 21 respectively. The thrust coefficient data shows that thrust increment due to an increase in collective and re-trimming the rotor changes sign near an advance ratio of $\mu \sim 0.86$. This is the same trend observed by Jenkins [9] in a Langley Research Center wind tunnel investigation of a two-bladed teetering rotor, reported as occurring at $\mu \sim 1.0$, Ewans *et. al.* while investigating the RVR concept at Ames Research Center, with the reversal observed at $\mu \sim 0.9$, and Kuczynski and Sissingh [12] investigating

hingeless rotors, reported at $\mu \sim 0.79$. A physical explanation of the sign reversal is also given by Kuczynski and Sissingh [12] from the experimentally determined lift derivatives. The effect can be expressed:

$$\left.\frac{\partial(C_T/\sigma)}{\partial\theta_0}\right|_{trim} = \frac{\partial(C_T/\sigma)}{\partial\theta_0} + \frac{\partial\theta_s}{\partial\theta_0}\frac{\partial(C_T/\sigma)}{\partial\theta_s}$$

Beyond advance ratio $\mu \sim 0.79$, "the reduction in rotor lift due to the trim cyclic pitch is greater than that produced by the collective pitch", such that at high advance ratio the relative contribution of the two terms causes the sign change.

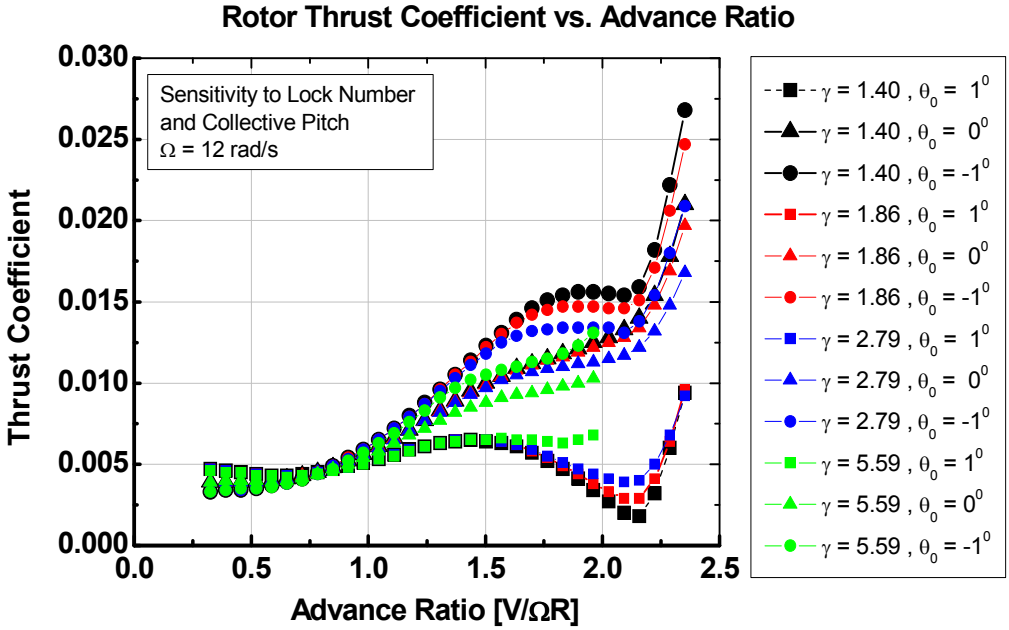

Figure 19: Thrust Coefficient Sensitivity to Collective Pitch

The lift to drag ratio and shaft incidence data show that at high advance ratio, higher collective pitch reduces the lift to drag ratio and requires a higher shaft incidence to maintain autorotation. The Lock number trends show that the thrust coefficient and lift to drag ratio tend to vary in a narrower range with increasing Lock number but the shaft incidence range increases with increasing Lock number.

The cyclic control positions are shown in Figure 22 and Figure 23. The longitudinal cyclic data shows little variation with Lock number, but the collective pitch effect is to shift the curves so that a reduction in collective requires a reduction in longitudinal cyclic. The lateral cyclic trim data show that the collective has very little effect on the lateral cyclic control position with the range of travel still generally within two degrees.

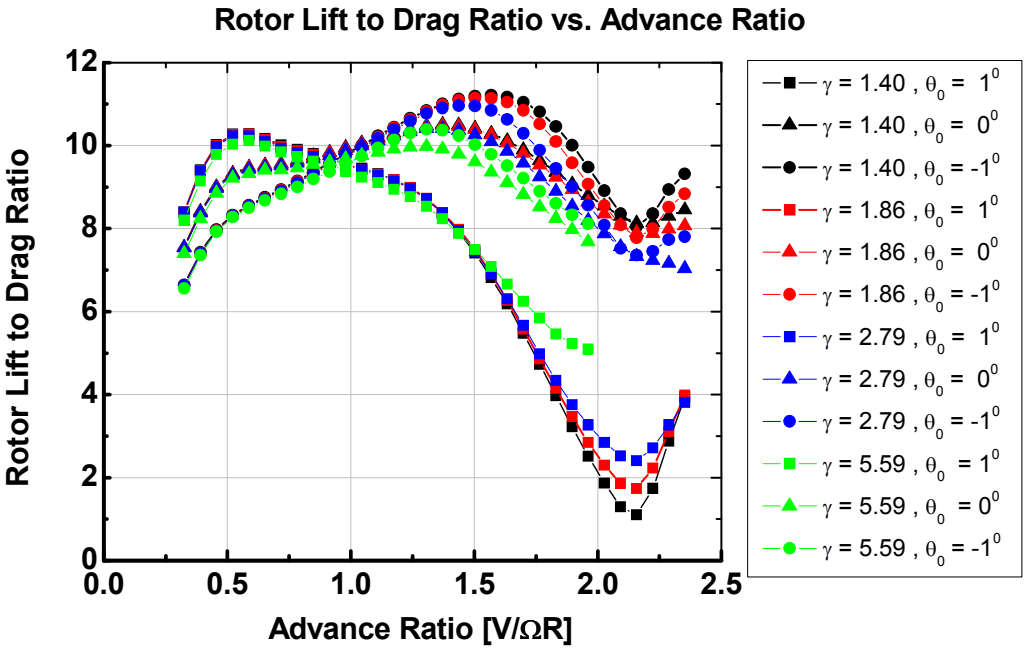

Figure 20: Lift to Drag Sensitivity to Collective Pitch

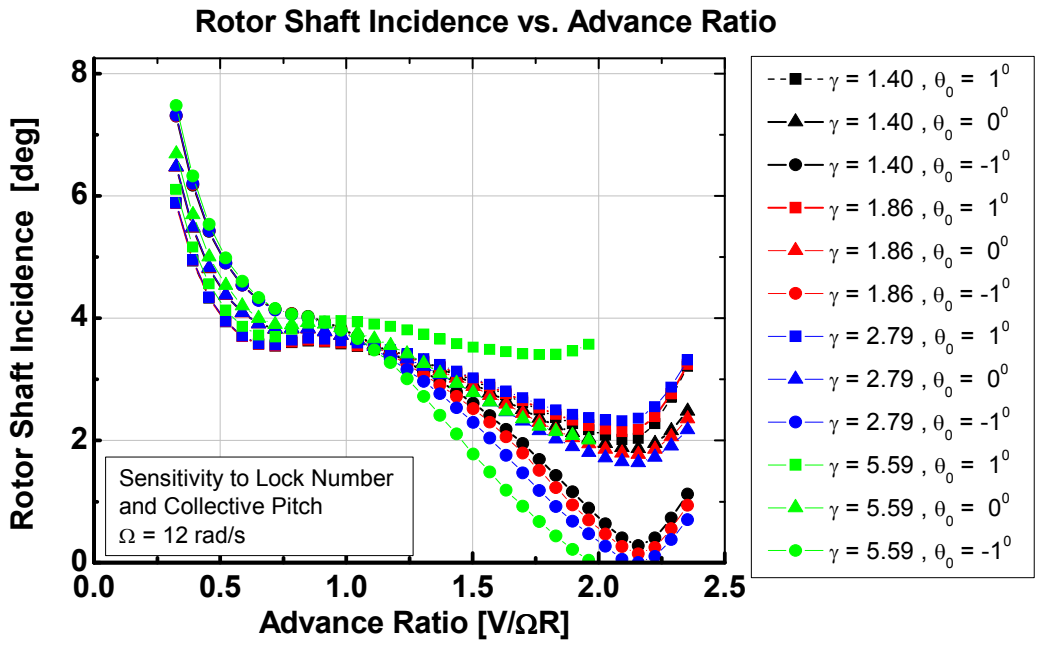

Figure 21: Shaft Incidence Sensitivity to Collective Pitch

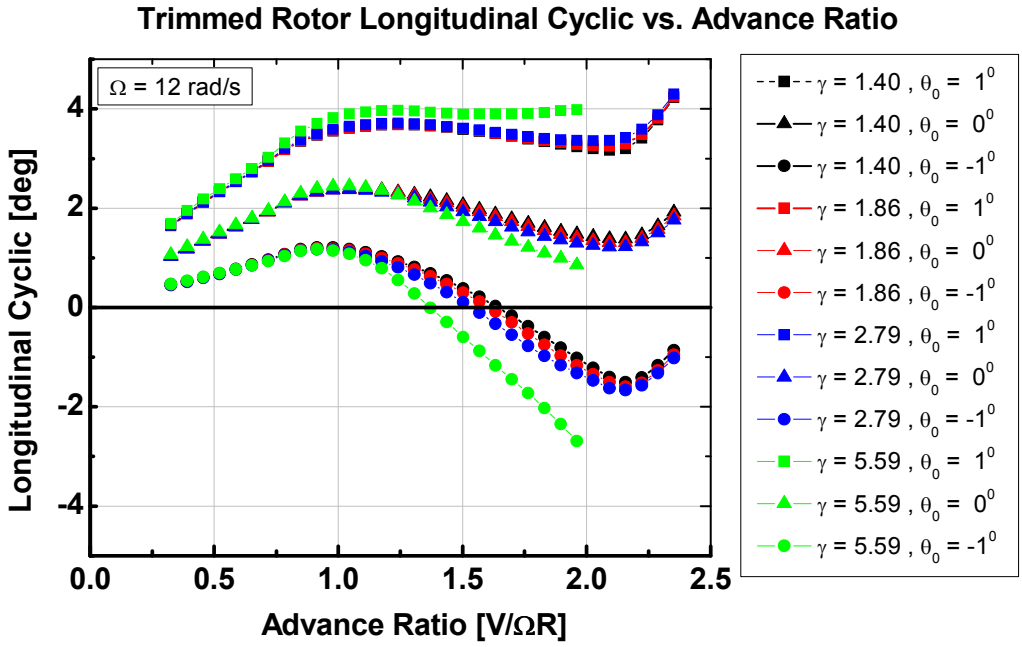

Figure 22: Longitudinal Cyclic Trim Sensitivity to Collective Pitch

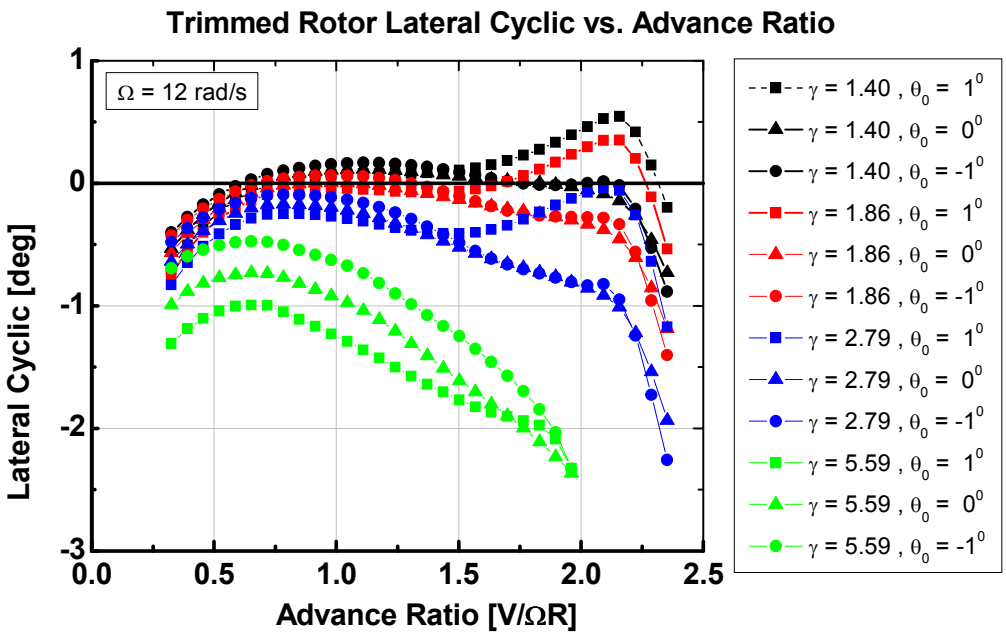

Figure 23: Lateral Cyclic Trim Sensitivity to Collective Pitch

The trimmed, autorotating rotor performance analysis predicts some of the conditions under which autorotation is possible as well as the performance trends in terms of rotor parameters. The collective pitch sensitivity data shows that multiple trim solutions are possible at a particular flight condition with varying performance. Additionally, The highest Lock number blade (blade 1, $\gamma = 5.59$) results were only presented up to an advance ratio of $\mu \sim 1.9$. At higher advance ratios the trim process tended to failed for this model indicating the combinations of cyclic controls for zero hub moments did not allow for a zero-torque solution. This was evidenced in the trim process as the solution converging, but not within the numerical tolerance of 10 ft-lbs used in this study.

Autorotation of the rotor is a fundamental characteristic of the concept vehicle. Autorotation is achieved when “the inflow angle is such that there is no net in-plane force on the blades, therefore no contribution to rotor torque” [50]. The components of the rotor aerodynamic forces in the rotor shaft plane were extracted from the blade element

model in FLIGHTLAB™ to establish the portions of the rotor azimuth that serve to absorb power from the relative air flow (driving region) and the regions that consume power (driven region). FLIGHTLAB™ calculates the aerodynamic forces in the local wind frame at each aerodynamic computation point (ACP). These forces were transformed to the rotating hub frame so that the component contributing to the torque was determined for each azimuth position. Script files written in SCOPE facilitated the data processing. Figure 24 shows the rotor in-plane forces and the angle of attack contours at $\mu = 0.33$. The angle of attack contour shows a small reverse flow region at this low advance ratio covering roughly one third of the blade radius as would be predicted from analytical considerations. The in-plane force contour shows values below zero covering the advancing side of the rotor, which opposes the rotation, whereas the retreating side of the rotor provides positive in-plane forces which drive the rotor.

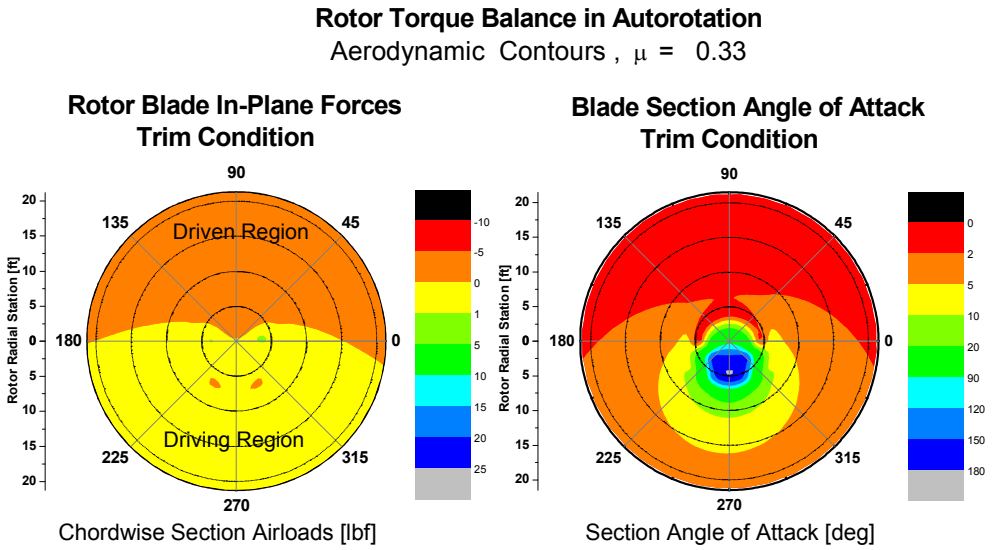

Baseline Rotor, Ω = 12 rad/s, γ = 1.40, μ = 0.33

Figure 24: Baseline Rotor Aerodynamic Contours at μ=0.33

Figure 25 shows the aerodynamic contour at the cruise condition, $\mu \sim 2.29$ where the retreating side of the rotor is dominated by the reverse flow region. The in-plane force contour shows that the driving and driven azimuth regions remain similar to the low advance ratio case, but with larger magnitude forces and a reduction in the driving region azimuth range.

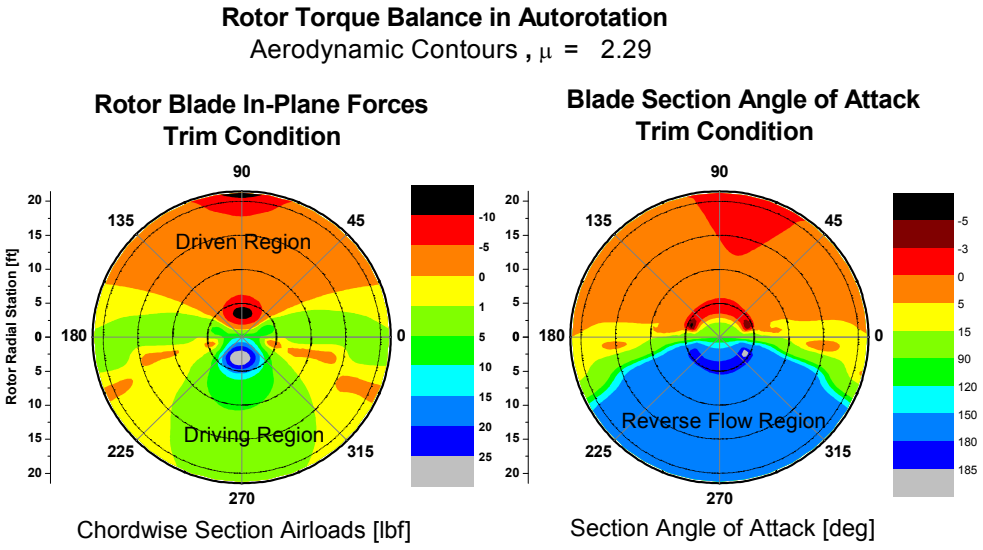

Figure 25: Baseline Rotor Aerodynamic Contours, μ=2.29

3.2 Rotor Stability

The rotor degrees of freedom in the rotating frame are the flapping of the individual blades and the rotor speed. At high advance ratio the aerodynamic forcing of the rotor is highly periodic due to the extreme differences in the flow that the rotor experiences between the advancing and retreating sides. In order to assess the rotor flapping

stability and identify conditions of reduced stability, Floquet analysis was applied through a built-in routine in FLIGHTLAB™. Johnson [50] describes the analysis of linear periodic systems by determining the state transition matrix, φ, over one period of the system. The eigenvalues, θ_i, of φ then determine the stability of the system, with the stability boundary $|\theta_i| < 1$. The roots in the θ plane are related to the λ plane by:

$$\lambda = \frac{1}{T}(\ln|\theta| + i\angle\theta) + n\frac{2\pi}{T}i$$

Such that a "multiple of the fundamental frequency may be added, depending on the branch of the logarithm that the root is on" [50]. Roots of the state transition matrix may be real numbers or complex conjugates. When the θ roots are complex, the λ roots will be complex conjugates as well. A positive, real θ root will transform to a single λ root with a frequency that is a multiple of the fundamental frequency of the system. A negative, real θ root will transform to a single λ root with a frequency that is one-half the fundamental frequency plus a multiple of the fundamental frequency [50]. Movement of the θ roots on the real axis will then correspond to movement of the real parts of the λ roots *locked* to a multiple of the fundamental frequency of the system.

For a lightly-loaded rotor, autorotating at high advance ratio the fundamental frequency (rotor speed) will be considerably decreased with increasing flight speed (slowed to avoid violation of the advancing tip Mach number constraint). Reduction of the rotor speed shifts the fundamental frequency of the rotor, and the frequencies to which the Floquet roots may become locked. It is therefore, of primary interest to investigate the stability in terms of the rotor speed and advance ratio. The baseline isolated rotor model was used to establish these trends by trimming the rotor (hub moments and torque) for a specified rotor speed and wind tunnel free stream velocity, and executing the Floquet analysis routine. Scripts written in the native FLIGHTLAB™ programming language, SCOPE, were used to facilitate the loops associated with

increasing the wind tunnel speed, re-trimming the rotor, and repeating the Floquet analysis. The eigenvalues of the FTM (Floquet Transition Matrix) were transformed to the λ plane, and the mode with the smallest magnitude real-part was retained. The rotor modes are in the non-rotating system (multi-blade coordinates) as described in the literature by Johnson [50], Padfield [52], and others. Typical results obtained in this analysis are shown in the root locus plots of Figure 26. When the roots remain complex conjugates, the transformed roots simply shift in the complex plane with changes in advance ratio (one oscillatory pair is shown on the left side of Figure 26).

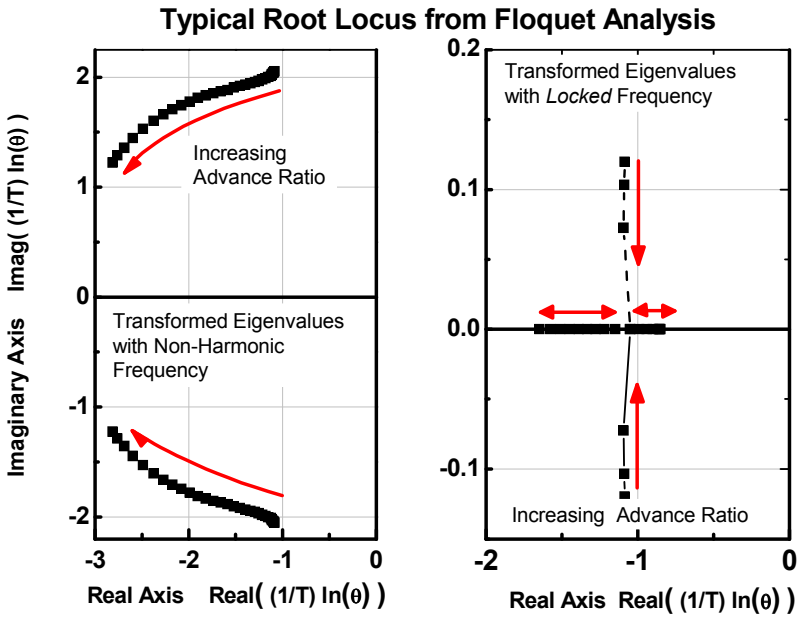

Figure 26: Typical Root Locus from Floquet Analysis

When the frequency of the oscillatory pair becomes locked to a particular frequency, the roots move in opposite directions with one root moving closer to the

stability boundary and the other moving away from the stability boundary as shown on the right side of Figure 26. Stability from the Floquet analysis is presented here in terms of the root with the smallest real part, which represents the mode with the least damping. Since a multiple of the fundamental frequency, or half the fundamental frequency, may be added, the damping ratio is not automatically known. The frequencies can be determined from physical insight into system if necessary. In helicopter applications for example, the absence of periodicity at the hover solution provides a convenient point from which to obtain the frequencies of the rotor modes. Then the introduction of periodic effects with forward flight can be assumed to occur as a continuous function. In the present work, the damping of the least stable root is presented without determining the actual frequencies of the modes as a means to identify trends of increasing or decreasing relative stability.

Figure 27 shows the effects of slowing the rotor and increasing the advance ratio for the baseline rotor. For a particular rotor speed, the effect of increasing advance ratio is to increase the damping within the advance ratio range considered. The baseline rotor illustrates the case where the roots remain as oscillatory pairs, never becoming locked to a particular frequency. The advancing tip Mach number limit for each rotor speed is also shown in Figure 27. This limit line passes through a minimum damping value near an advance ratio $\mu \sim 1.0$, which could represent a critical case when flexible blades with additional degrees of freedom are considered.

Since the reduced rotor speed operation represented the lowest damping cases, this rotor speed was retained for the sensitivity analysis with respect to rotor flapping stiffness and Lock number. Figure 28 shows the effect of varying the flapping stiffness of the baseline rotor.

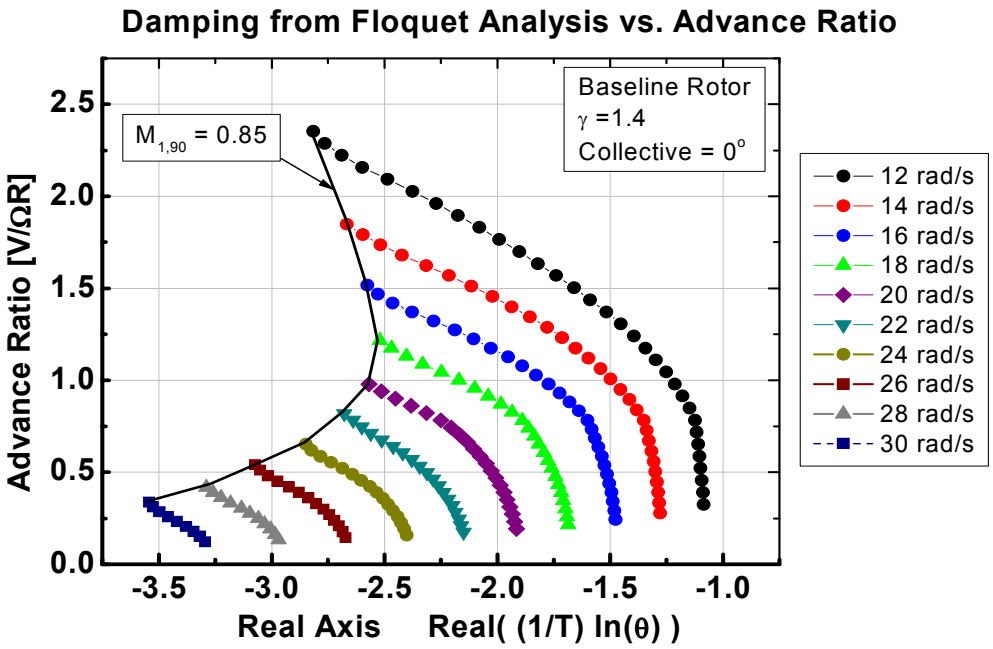

Figure 27: Baseline Rotor Stability from Floquet Analysis

The damping curves only differ when the frequency becomes locked. The frequency of the roots for the low stiffness rotors start out closer to a fundamental frequency, and become locked at a lower advance ratio than the higher stiffness cases which remain non-harmonic in the ranges presented here. The Lock number sensitivity, Figure 29, shows that higher lock number rotors have higher damping at low advance ratio which is expected since the damping in hover is given analytically as $\gamma\Omega/16$, but tend to become locked at a much lower advance ratio and tend toward the unstable region with advance ratio.

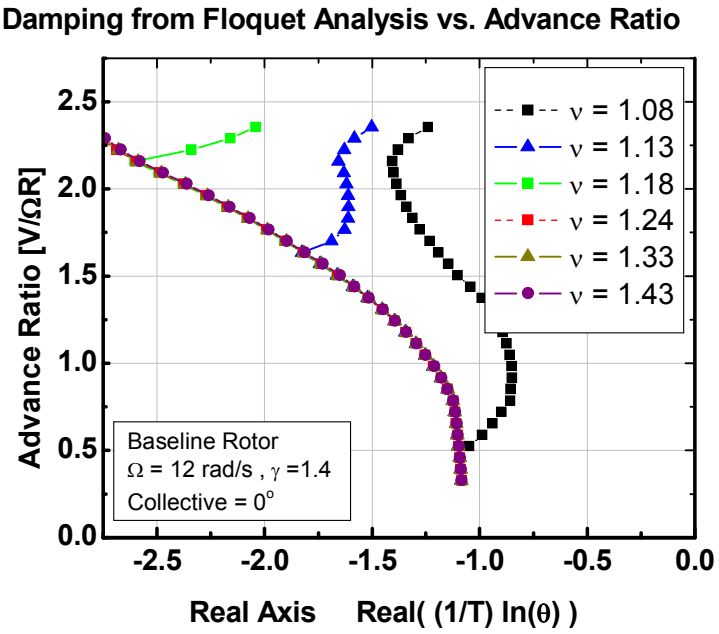

Figure 28: Rotor Stability Sensitivity to Flapping Stiffness

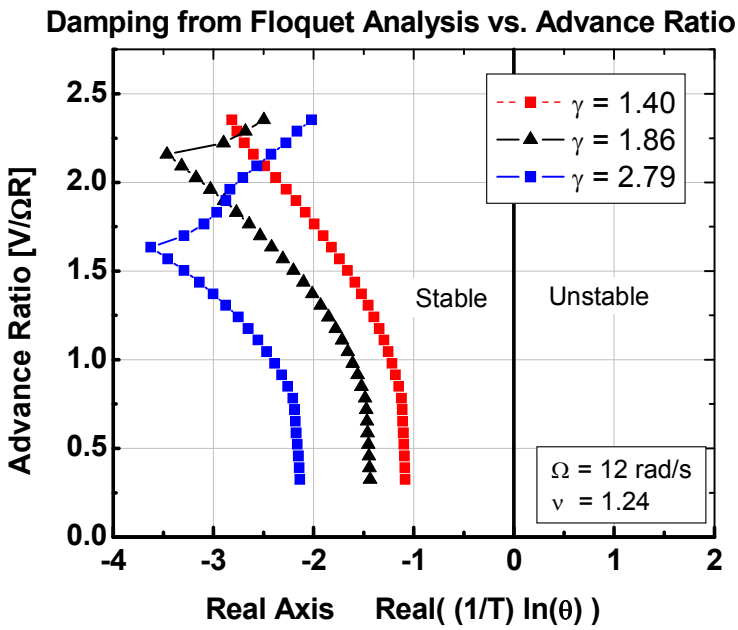

Figure 29: Rotor Stability Sensitivity to Lock Number

Inclusion of the rotor speed degree of freedom adds a first order mode to the rotor. With the clutch disengaged, the rotor speed responds to changes in the torque balance similarly to the hover case shown in Figure 6. The primary factors affecting the location of the rotor speed eigenvalue are the advance ratio and the Lock number as shown in Figure 30, with the rotor stiffness (not shown) providing a negligible effect. The largest increase in damping occurs at any rotor speed when the advancing tip Mach number approaches the limit, suggesting the effect of the increase in drag with Mach number. The eigenvalue is also seen to reach a minimum near $\mu \sim 0.78$. In all cases for the baseline rotor, the magnitude of the eigenvalue is very small, indicating low damping and a long time constant for rotor speed changes.

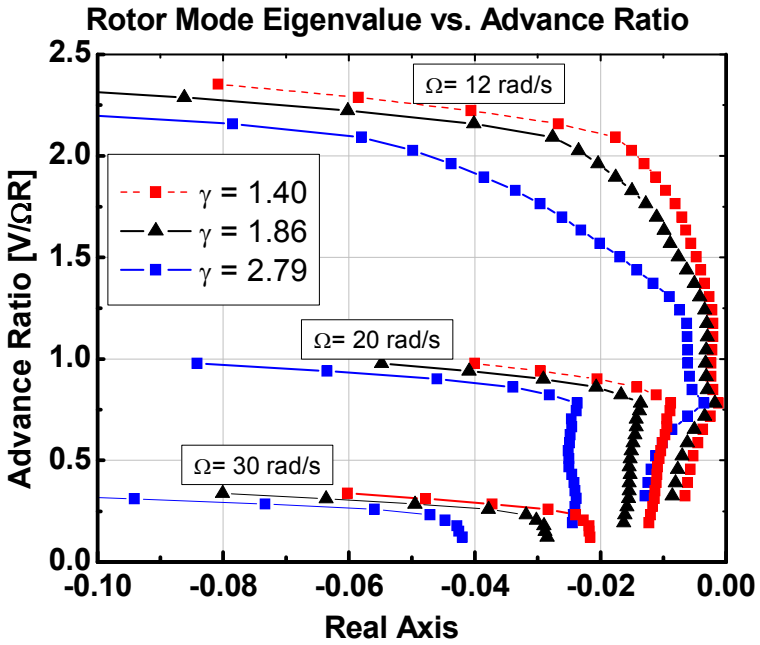

Figure 30: Rotor Speed Mode Eigenvalue Sensitivity

The inclusion of the lead-lag motion adds additional degrees of freedom to the rotor. The damping of the lead-lag motion is related to the drag of the airfoil, which by design is lower than the lift. Since the rotor model utilizes the articulated formulation, damping can be added to the lead-lag motion by including a mechanical damper component on each blade. The real parts of the eigenvalues including the lead-lag motion are shown in Figure 31. The results are presented in terms of the non-dimensional parameter:

$$C_\varsigma^* = \frac{C_\varsigma}{I_b \Omega}$$

where C_ς is the dimensional damper constant which is a FLIGHTLAB™ input. The damping shows very little sensitivity to advance ratio and non-dimensional lead-lag stiffness. The primary factors that affect the damping are the Lock number and the added mechanical damper.

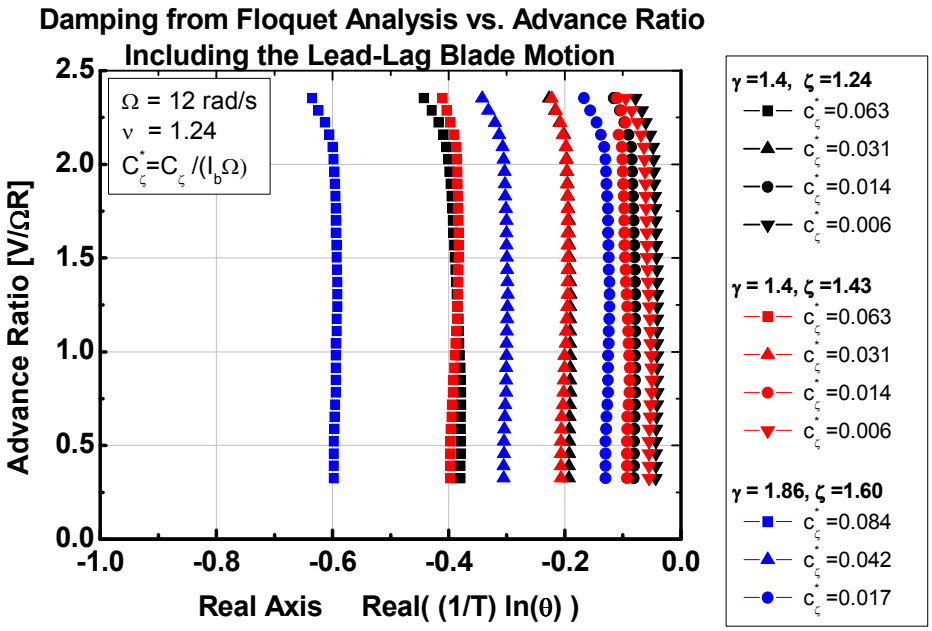

Figure 31: Eigenvalue Damping vs. Advance Ratio Including Lead-Lag Motion

Johnson [50] reports typical values for hingeless rotor structural damping coefficients in the range 0.01 to 0.03. Values associated with elastomeric dampers on the Bell 412 Advanced System Research Aircraft are reported as 0.075 per damper with two dampers per blade [55]. These reported values relate to helicopter applications.

The predicted damping of the lead-lag motion and the rotor speed mode are both low and have the potential to interact since the in-plane motion of the blades affects the torque balance on the rotor. The results presented in Figure 31 did not include the rotor speed degree of freedom because this interaction tended to produce somewhat erratic numerical results making the identification of trends difficult. The non-linear simulation however provides additional insight into the coupling. Figure 32 shows the non-linear simulation time history for the rotor with no control inputs, but with the rotor speed and lead-lag degrees of freedom active. The rotor torque and hub moments were trimmed prior to these runs to a tolerance of 1 ft-lbf to minimize the trim tolerance residual effect. The left side of Figure 32 shows the low advance ratio case. Low values of the damping parameter results in the growth of an unstable oscillation in the rotor speed behavior. The right side of Figure 32 shows the high advance ratio case, where the increase in dynamic pressure and the variation of the aerodynamic loads around the azimuth results in increased oscillations even for the stable values of the damping parameter. Figure 33 summarizes the cases shown in Figure 31 in terms of the damping and the value of the damping parameter, and shows the real part of the root tends to vary linearly with the damping parameter. Also shown is the stability boundary as ascertained from the non-linear simulation data, with increasing advance ratio requiring an increase in the damping parameter for rotor speed stability. These results suggest a minimum value of the damping parameter for the baseline rotor of $C_{\varsigma}^{*} = 0.094$ when the lead-lag and the rotor speed degrees of freedom are included in the analysis.

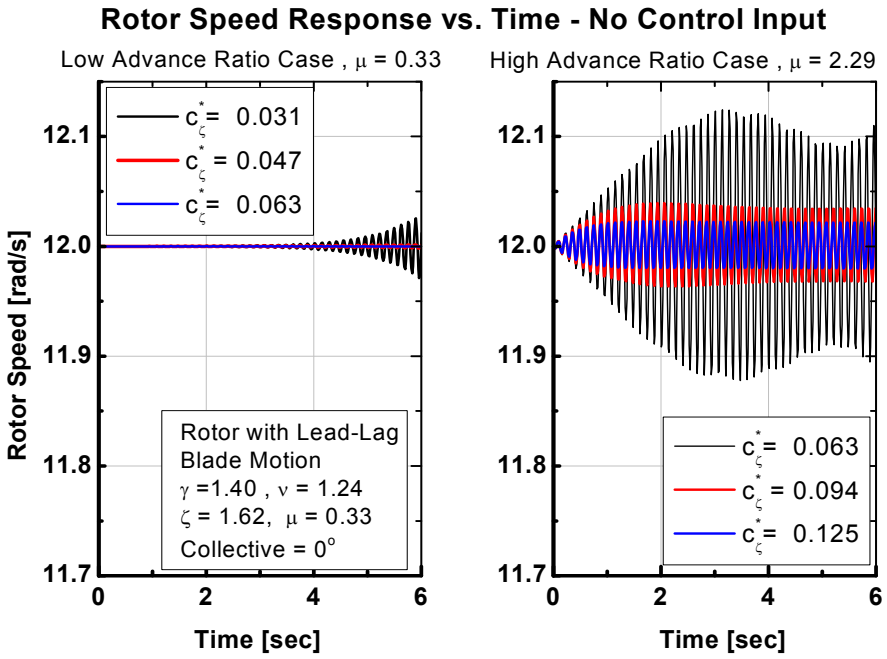

Figure 32: Non-linear Rotor Speed Response with Lead-lag Motion

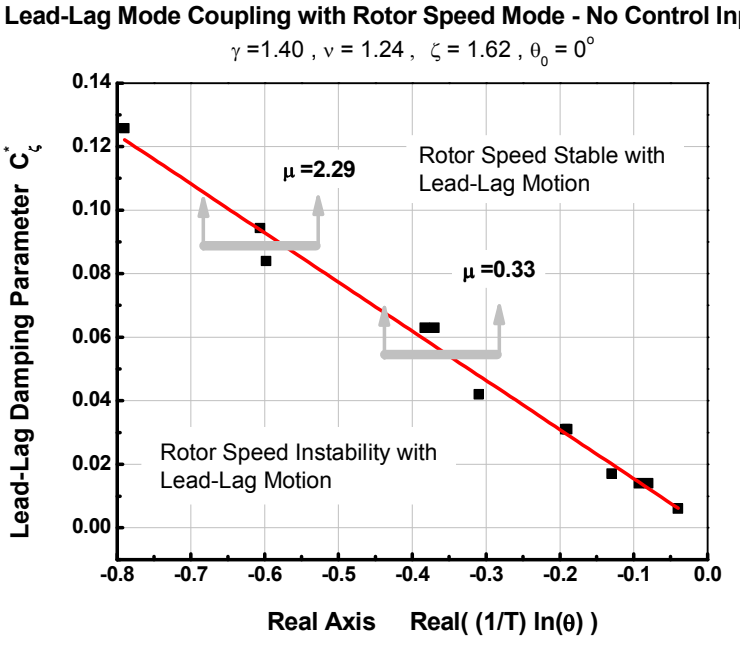

Figure 33: Lead-Lag Mode Sensitivity to Damping Parameter

3.3 Steady-State Control Hub Moments and Cross-Coupling

The moments generated by swashplate control inputs were investigated by perturbing the individual swashplate controls and running the isolated rotor non-linear simulation forward in time. The objective was to assess the magnitude of the moments generated as a function of the advance ratio, and to access the time scale of the rotor transient response for hub moments and rotor speed changes. The time history of the rotor pitching moment transient response to a longitudinal cyclic step is shown in a short time scale (6 seconds) in Figure 34 with the clutch in the "off" position, meaning the rotor speed was allowed to varying under the effects of the aerodynamic forces on the blades. The time scale for the rotor moment transient response can be seen as on the order of two seconds. At the same time the rotor speed is changing, and the time history in this short time scale is shown in Figure 35. In this short time scale the rotor moments reach an essentially constant steady-state value even as the rotor speed changes, and the rotor speed is seen to change relatively slowly. When the same response is considered over a much longer time scale (100 seconds), the rotor moments are seen to change only as the rotor speed changes significantly and approaches the new steady-state rotor speed corresponding to the torque balance at the new cyclic control position. Figure 36 shows the pitch and roll moments at two different advance ratios in the long time scale, and Figure 37 shows the rotor speed response in the long time scale. The rotor speed is seen to change in the order of the long time scale (~100 seconds) while the hub moment transient response is on the order of the short time scale (~2-3 seconds). This difference in time scales admits an approximation to the steady-state control moment sensitivity as being essentially at constant rotor speed. On the basis of the assumption of constant rotor speed in the short time scale, rotor hub moments due to swashplate control inputs are presented with constant rotor speed in non-linear simulation.

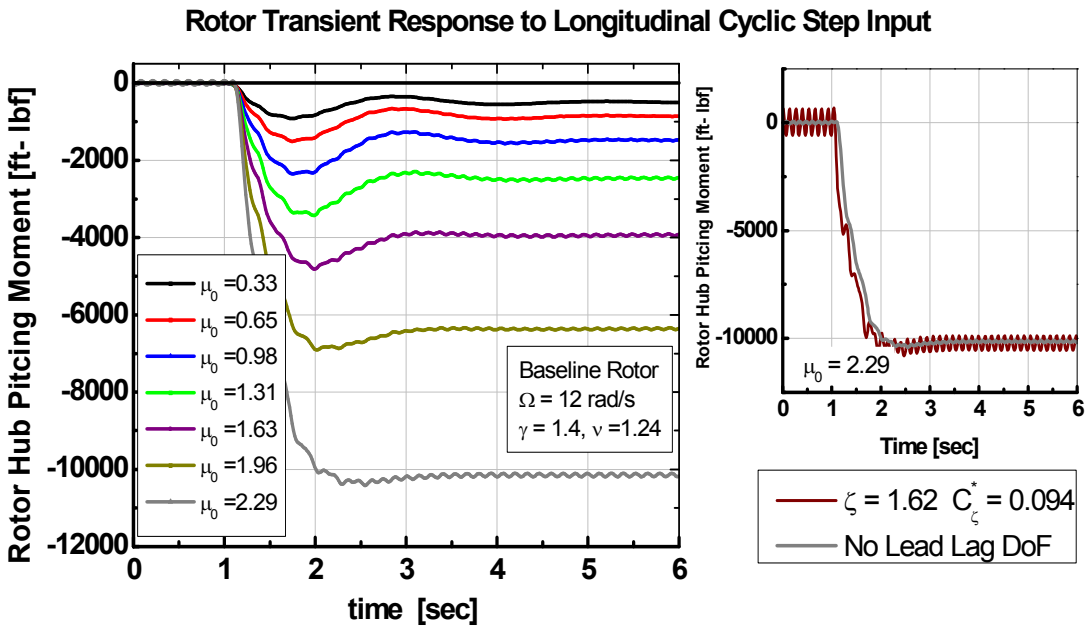

Figure 34: Rotor Pitch Moment Transient Response to Longitudinal Cyclic Step

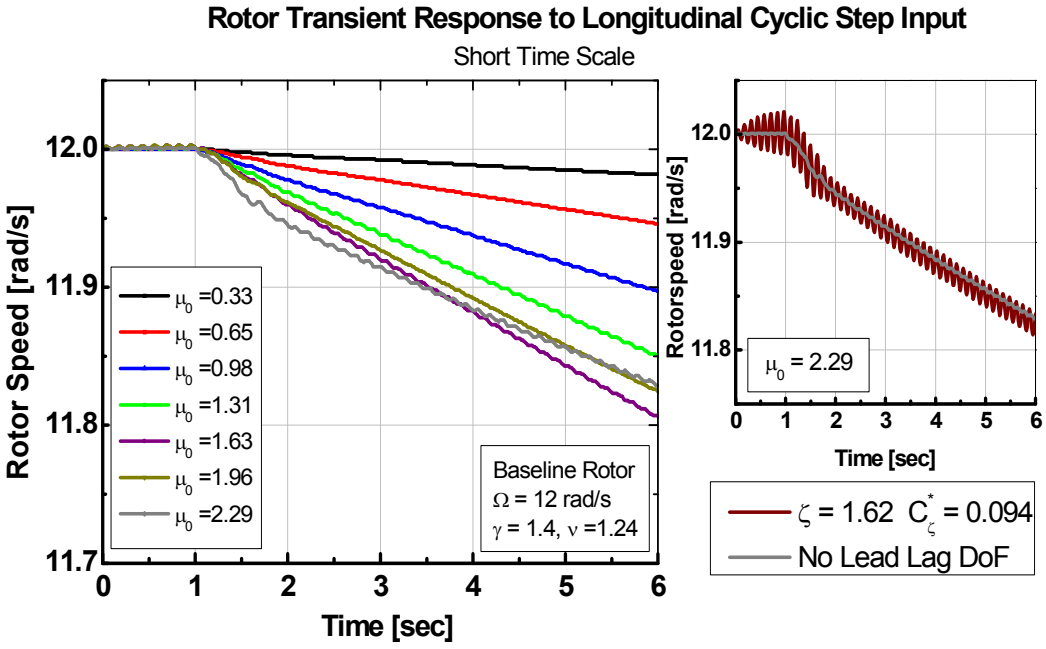

Figure 35: Rotor Speed Response to Longitudinal Cyclic Step – Short Time Scale

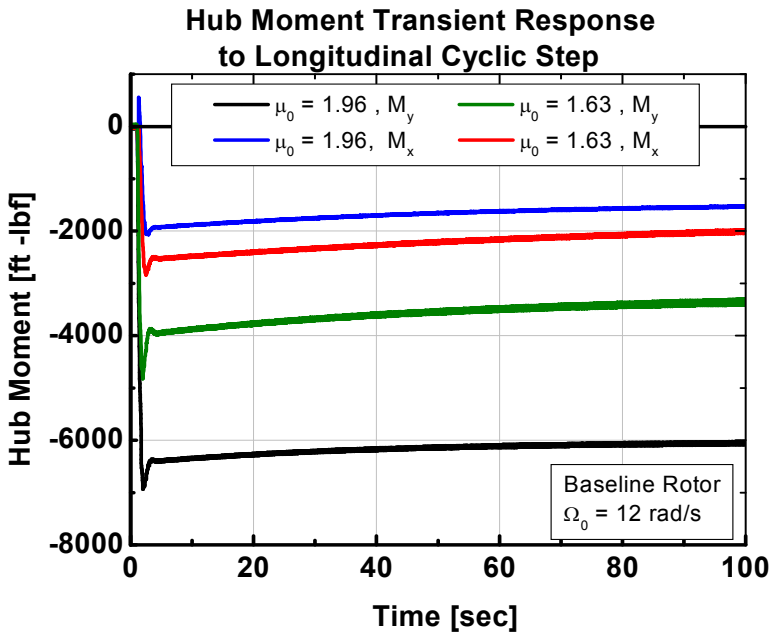

Figure 36: Long Time-Scale Hub Moment Response to Cyclic Step

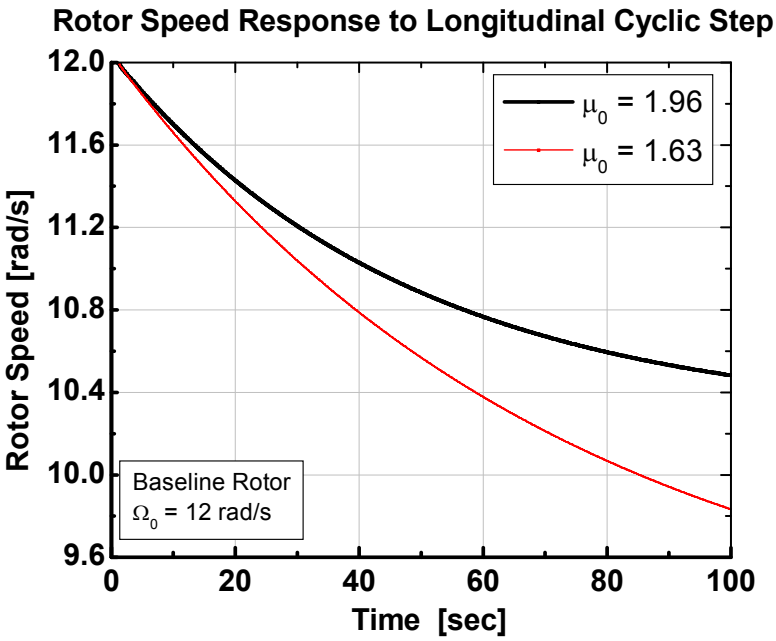

Figure 37: Long Time-Scale Rotor Speed Response to Cyclic Step

The insets to Figure 34 and Figure 35 also show a comparison of the response with and without the lead-lag degree of freedom when the damping parameter is selected based on the minimum value identified in section 3.2, $C_{\zeta}^{*} = 0.094$. The magnitude and low frequency response is essentially identical indicating that with sufficient damping to ensure rotor speed stability, the effect of lead-lag motion is negligible for the presentation of the steady-state moment sensitivity. Hub moments generated by longitudinal, lateral, and collective pitch inputs were thus determined at constant rotor speed and without the lead-lag degrees of freedom. Steady-state pitching moment values for one degree of longitudinal cyclic input are shown for the parametric baseline rotor as a function of advance ratio in Figure 38. The effect of operating at higher rotor speed is an increase in the magnitude of the moments generated. The advance ratio also increases the sensitivity to very large values at high advance ratio indicating the rotor will be very sensitive and capable of producing large moments with small inputs. In addition to the pitch moment from the longitudinal cyclic, a roll moment is also produced. This control coupling exists due to the flapping stiffness of the rotor, and also varies with the advance ratio. The roll moment response is shown in Figure 39. The combined effect of the pitching and rolling moment can be seen by calculating the rotor moment phase response as in Figure 40. A phase response of ninety degree would indicate no cross-coupling (only on-axis response). The small phase angle at low advance and low rotor speed indicates the primary effect of longitudinal cyclic would be off-axis because of the associated increase in non-dimensional flap frequency.

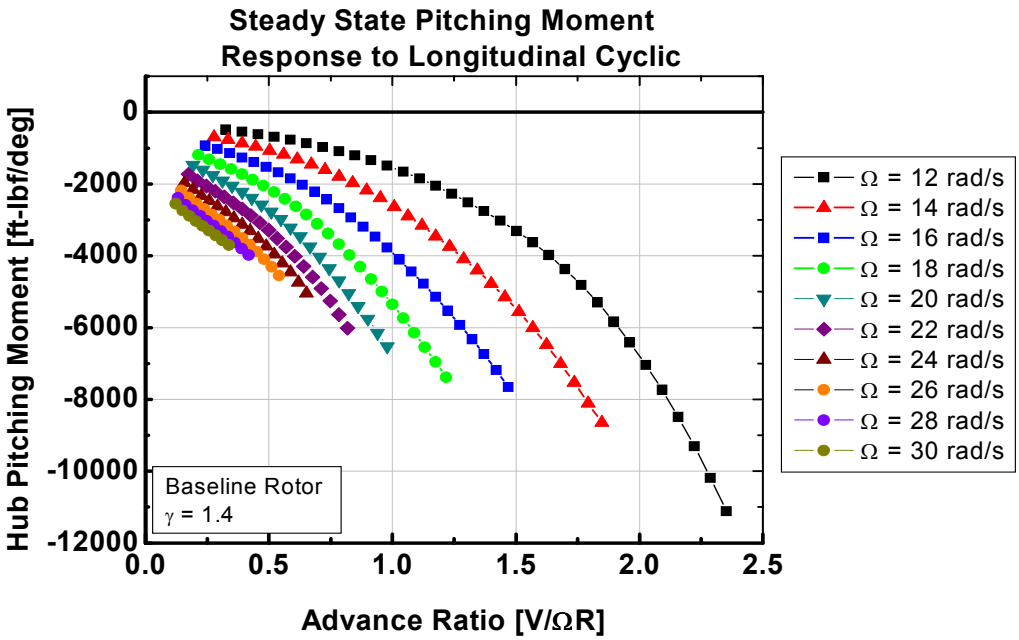

Figure 38: Steady State Pitch Moment Response to Longitudinal Cyclic Step

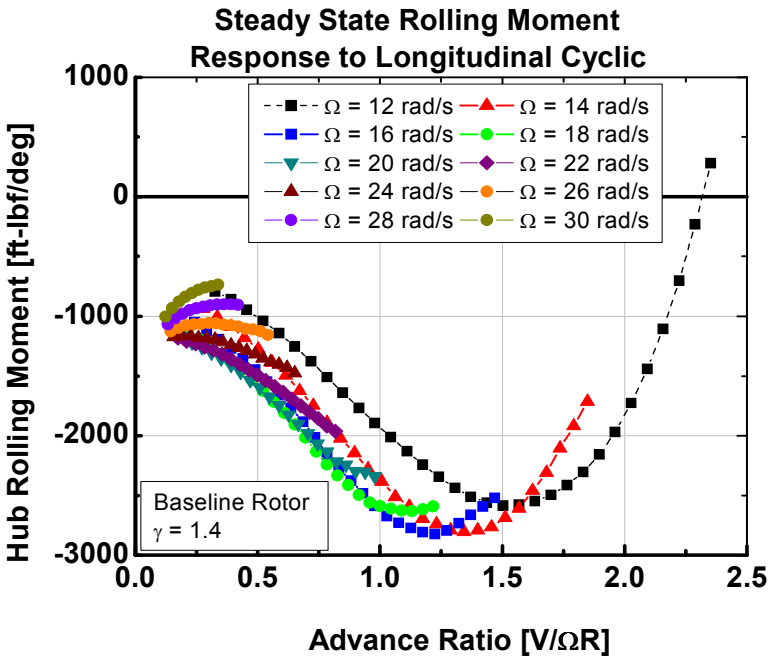

Figure 39: Steady State Roll Moment from Longitudinal Cyclic

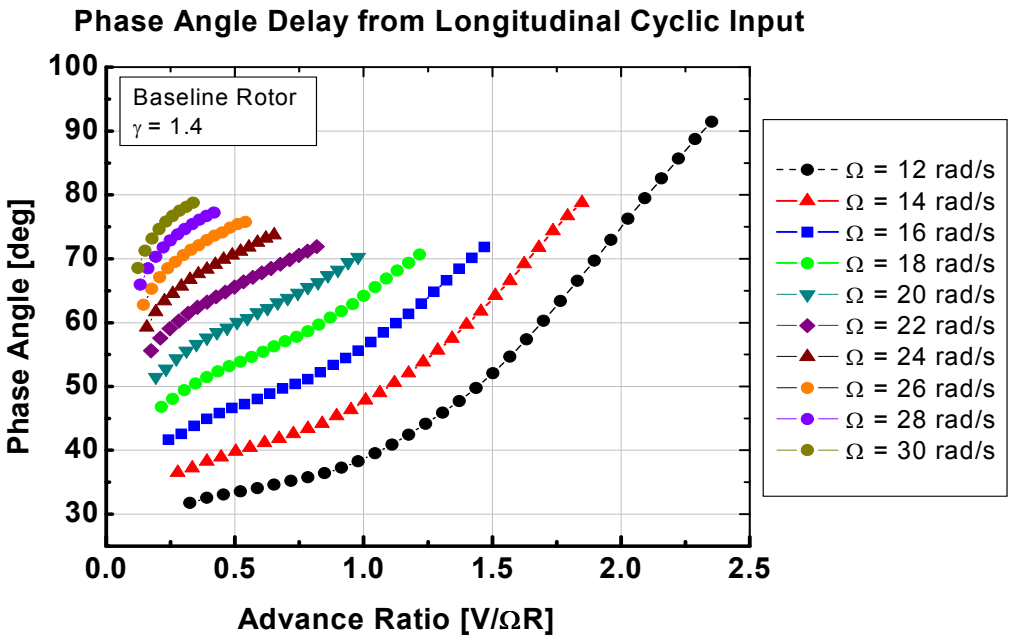

Figure 40: Steady State Hub Moment Phase Response to Longitudinal Cyclic

The effect of increasing advance ratio is to shift the phase back toward an on-axis response. This behavior would be a consideration in adopting a flight profile for rotor speed, altitude, and flight speed since this effect would also result in a complex control or piloting strategy. Figure 41 shows the steady state rolling moment from lateral cyclic steps for the baseline rotor. The same trend of increasing magnitude with advance ratio is present; however the high advance ratio magnitude is much lower than the longitudinal cyclic case. The phase angle response exhibits a smaller sensitivity to advance ratio, but with different phase angles between longitudinal and lateral cyclic responses, as well as the sensitivity to rotor speed and advance ratio, choosing a fixed mechanical swashplate phasing to eliminate the cross-coupling would difficult.

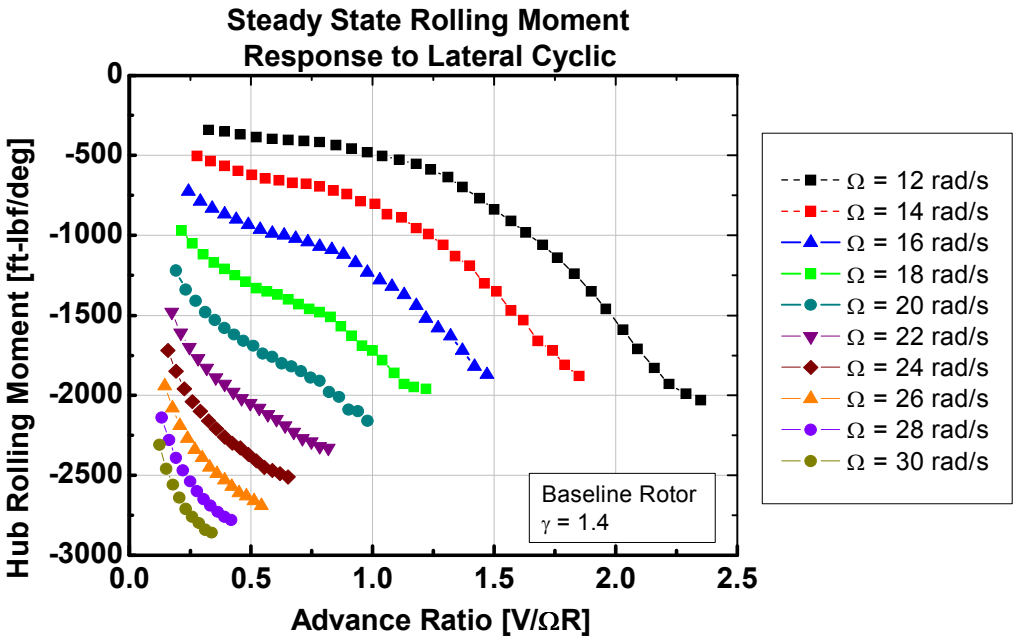

Figure 41: Steady State Roll Moment Response to Lateral Cyclic Step

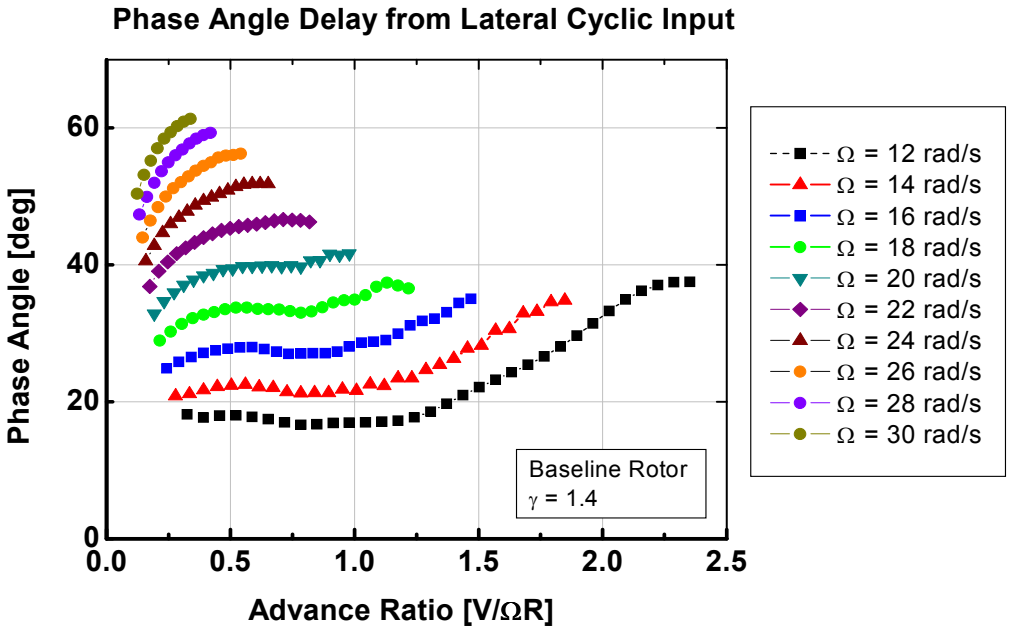

Figure 42: Steady State Hub Moment Phase Response to Lateral Cyclic

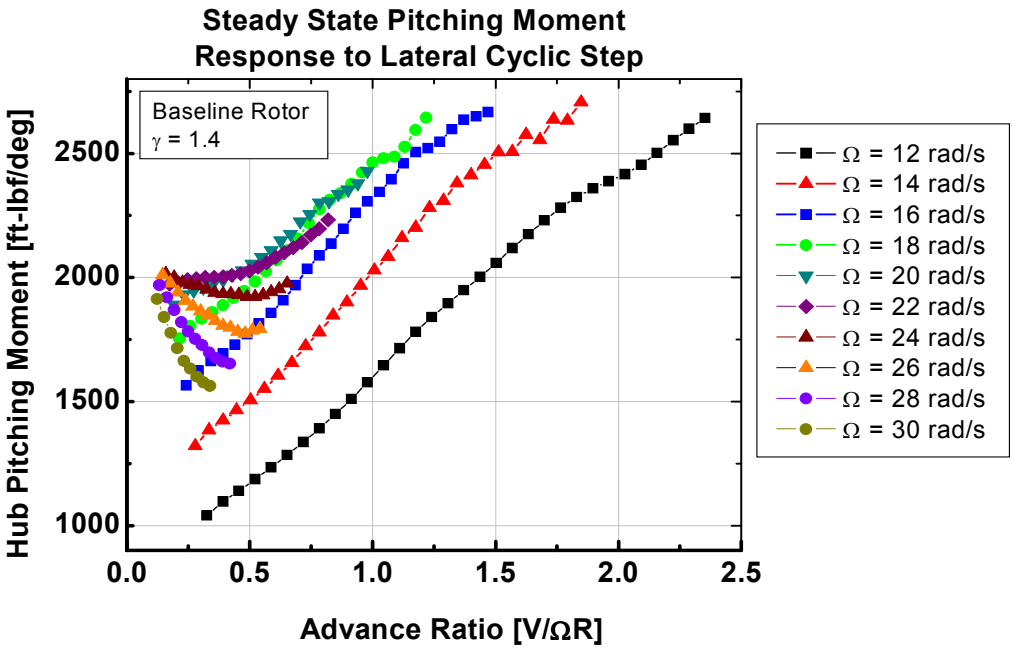

Figure 43: Steady State Pitch Moment from Lateral Cyclic

Collective control inputs also result in both pitching and rolling hub moments. The steady state pitching moments as a function of rotor speed and advance ratio are shown in Figure 44. The trends are similar to the effect of the longitudinal cyclic control with large magnitude at high advance ratio. Figure 45 shows the steady state rolling moment response to collective. At low advance ratio the effect of the positive collective step is to produce a steady state negative (right) rolling moment, with and increasingly positive (left) rolling moment with higher advance ratio.

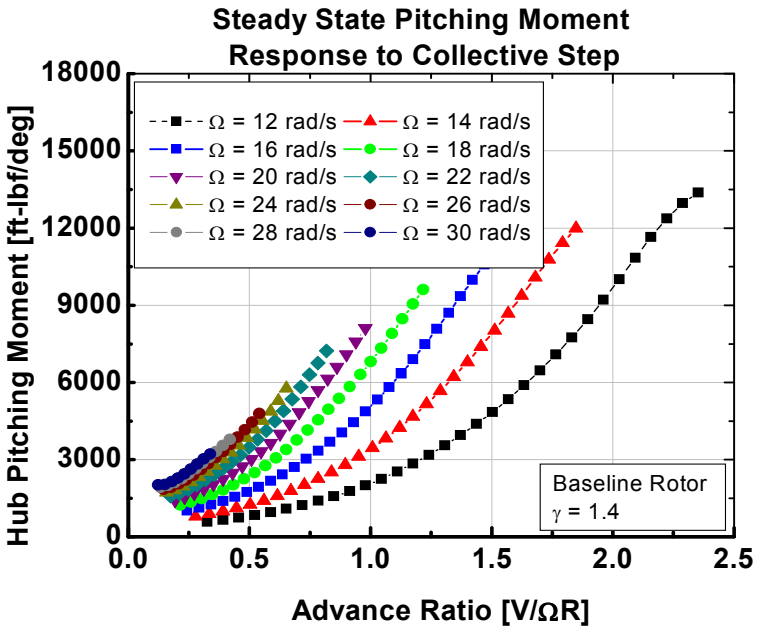

Figure 44: Steady State Pitching Moment Response to Collective Step

The steady state moment sensitivities to rotor non-dimensional flapping frequency are shown in terms of the on-axis response and the phase angle delay response for both longitudinal and lateral cyclic inputs. Figure 46 shows the pitching moment response for varying flapping stiffness. At low advance ratio the sensitivity is low and the curves essentially coincide, but at high advance ratio the reverse flow effect changes the flapping behavior. The inset of Figure 46 shows the steady state moments at $\mu = 2.29$ versus the flapping frequency. A maximum occurs near $\nu \sim 1.2$ with even higher stiffness values producing smaller moments suggesting the stiffer blades result in lower flap angles and lower restoring moments from the hinge springs, where as the low stiffness values may admit higher flap angles, but with lower spring constants, lower restoring moments result. The phase angle response is shown in Figure 47. Lower stiffness values increase the phase angle response closer to the familiar ninety degrees,

and the effect of advance ratio increases the phase angle still further until at high advance ratio the rolling moment reverses sign as can also be seen in Figure 39.

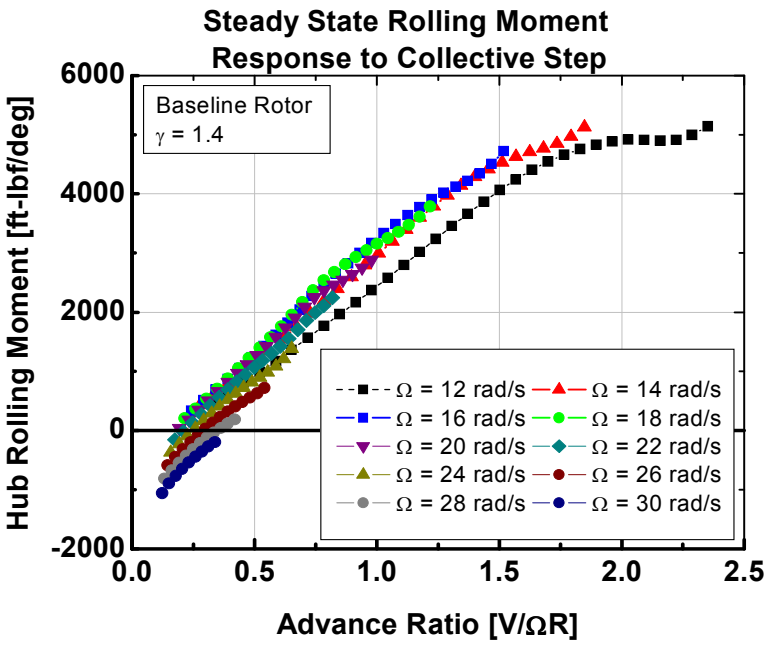

Figure 45: Steady State Rolling Moment Response to Collective Step

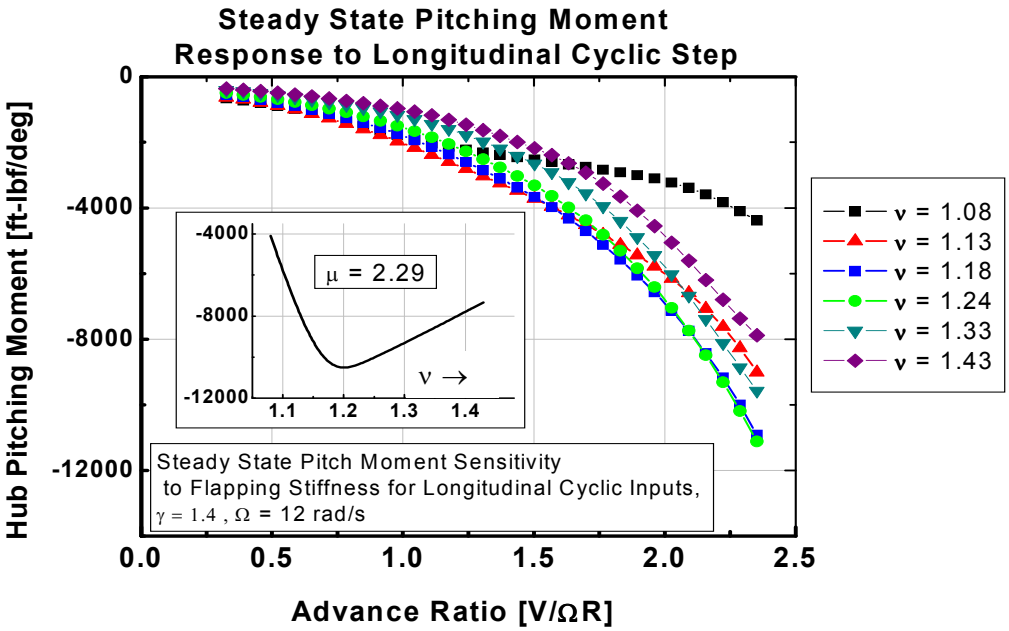

Figure 46: Steady State Pitching Moment Response Sensitivity to Flap Frequency

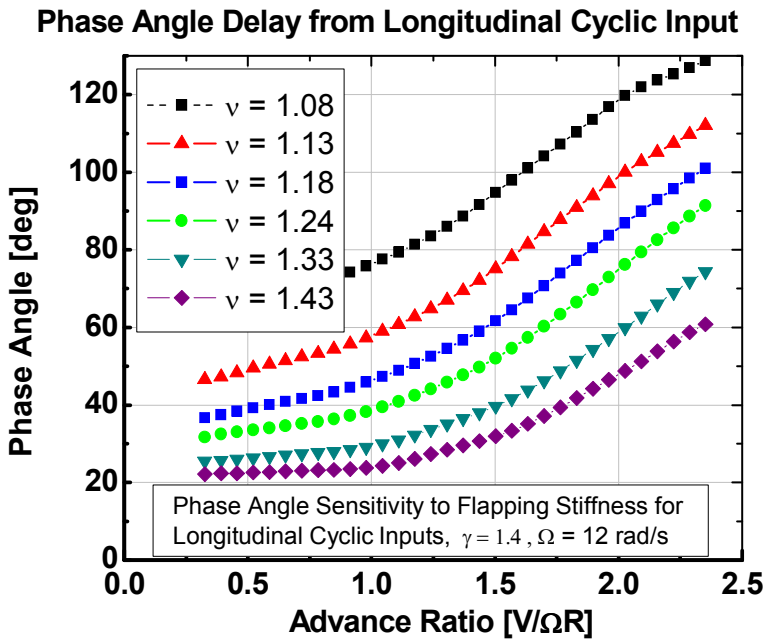

Figure 47: Longitudinal Phase Angle Sensitivity to Rotor Flap Frequency

Roll moment steady-state response to lateral cyclic for varying rotor stiffness is shown in Figure 48. The inset again shows a maximum magnitude response near $\nu \sim 1.2$, but with a smaller variation in magnitude with flapping stiffness. Phase angle sensitivity to flapping stiffness for lateral cyclic inputs is shown in Figure 49. Similarly to Figure 42, the effect of increasing advance ratio is smaller than the longitudinal response, and higher flapping stiffness values reduce the phase angle indicating significant off-axis response.

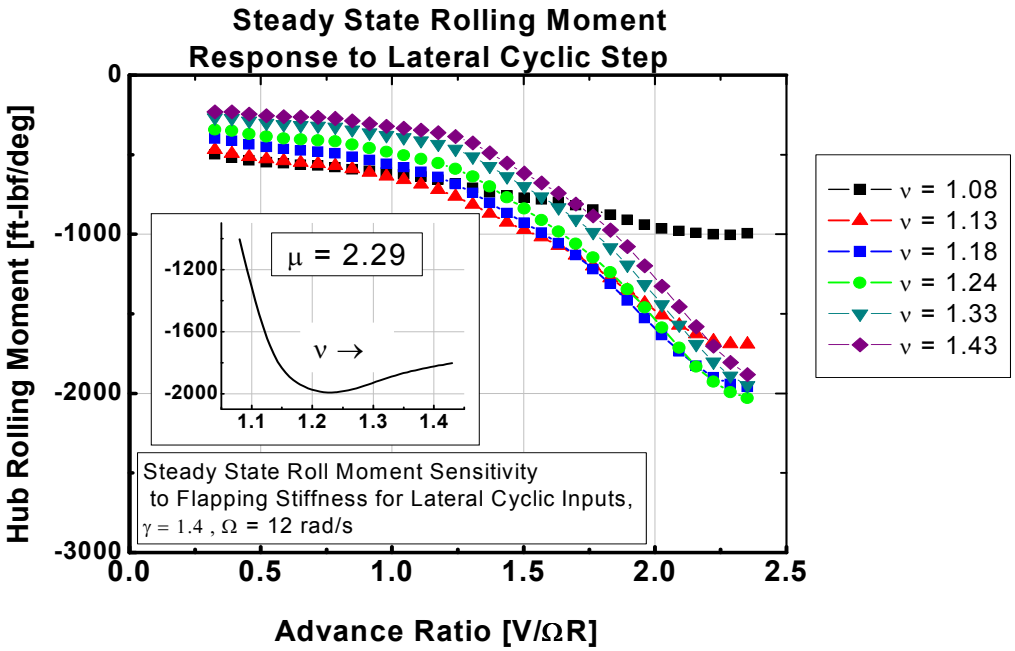

Figure 48: Steady State Rolling Moment Sensitivity to Flapping Frequency

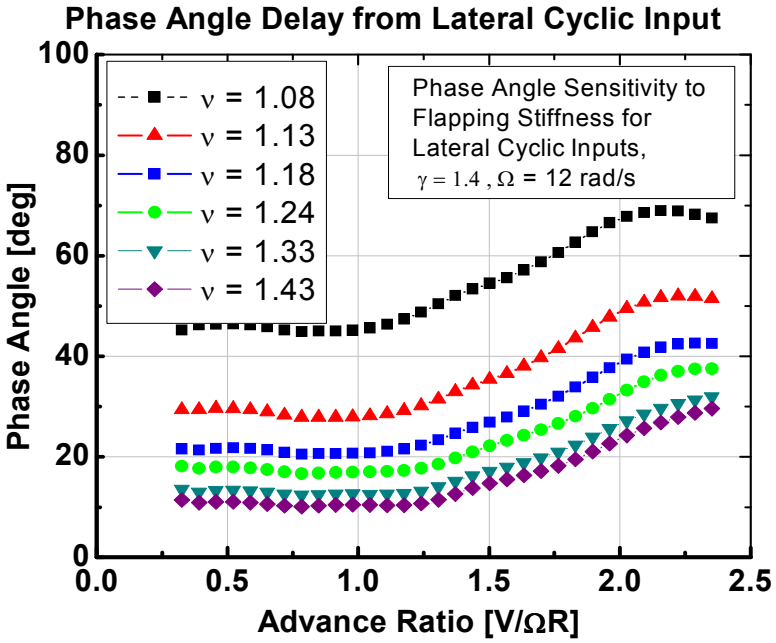

Figure 49: Lateral Phase Angle Sensitivity to Rotor Flap Frequency

The steady-state moment sensitivity to Lock number is shown for longitudinal cyclic in Figure 50. For the ranges of Lock number consider, the effect is small except for the highest Lock number blade (blade 1), which tends to diverge from the basic trend near an advance ratio of $\mu \sim 1.0$. The phase angle sensitivity to Lock number, Figure 51, shows the increase in phase angle with advance ratio and Lock number. The blade 1 response follows the trends of the other blades more closely because of the generally smaller magnitude of both the on-axis and off-axis responses. Phase angles higher than 90 degrees occur at lower advance ratios for increasing Lock number and indicate a sign reversal for the off-axis moments generated. Steady-state rolling moment sensitivity to Lock number is shown in Figure 52, with the phase angle response shown in Figure 53.

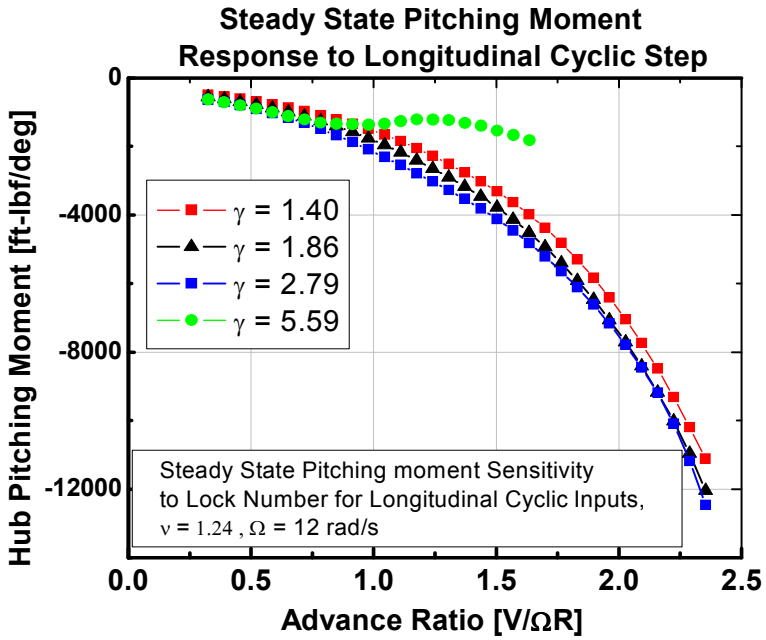

Figure 50: Steady State Pitching Moment Sensitivity to Lock Number

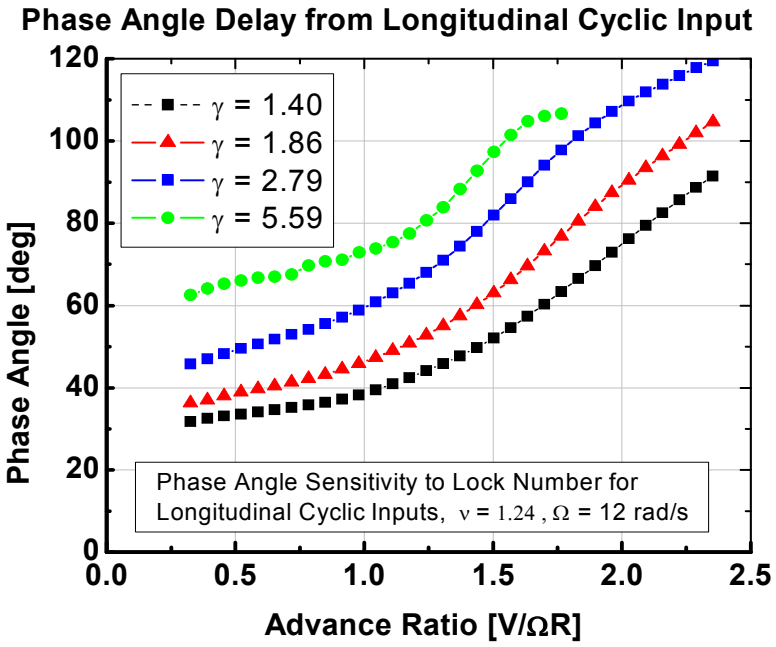

Figure 51: Longitudinal Phase Angle Sensitivity to Lock Number

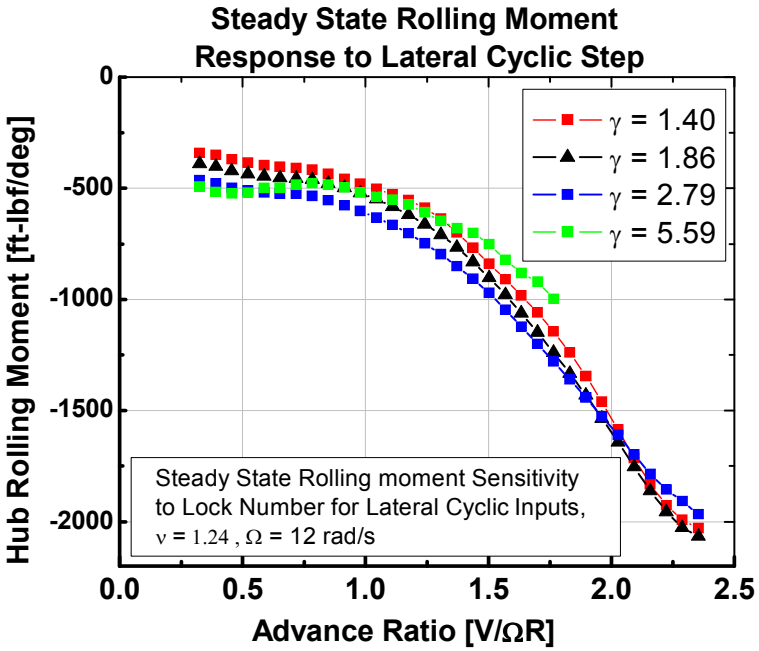

Figure 52: Steady State Rolling Moment from Lateral Cyclic

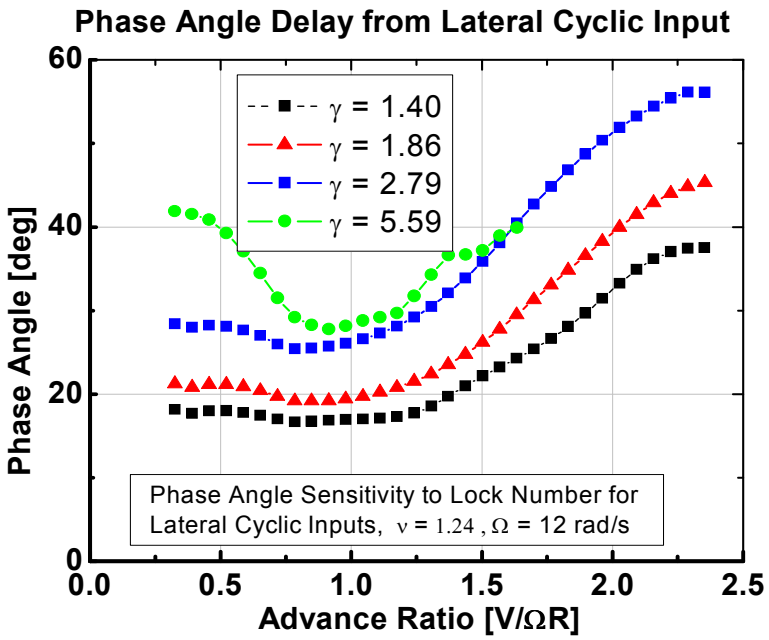

Figure 53: Lateral Phase Angle Sensitivity to Lock Number

The primary conclusions from the steady-state hub moment sensitivity study are related to the increased sensitivity with advance ratio, the strong cross coupling effects, and the non-linear effects at high advance ratio with varying flapping hinge spring stiffness. Also shown was the sign reversal in the off-axis moment response at high advance ratio, which occurred at a lower advance ratio for lighter blades. The phase angle results were presented to highlight the cross-coupling in the context of swashplate with a fixed mechanical phasing to emphasize the difficulty with choosing a single phase angle that would provide primarily on-axis response at all flight conditions. This effect would make it difficult for a human operator to control the swashplate inputs since the magnitude and signs change with flight condition, and an automatic controller design would need to account for this effect as well.

3.4 Rotor Steady-State Gust Sensitivity

Rotor steady-state moment responses to atmospheric gusts were investigated using step wind magnitude inputs with the isolated rotor models. The responses investigated were selected as being related to familiar static stability derivatives: angle of attack static stability (M_w), speed static stability (M_u), and dihedral effect (L_v), although they represent steady-state values and cannot be considered instantaneous values as in the quasi-steady rotor assumption. The gust responses do however provide valuable insight into the rotor behavior as far as its tendency to provide stabilizing and destabilizing effects (moments). Vertical gusts represent an angle of attack change on the rotor. The rotor contribution to angle of attack stability in helicopter theory is destabilizing since an increase in angle of attack leads to a positive (nose-up) pitch moment, leading to a further increase in angle of attack. In the simulated wind tunnel experiment the same phenomenon was observed. Figure 54 shows the steady state pitch moment per increment in vertical gust velocity, dimensionally as ft-lbs of moment per ft/s of gust velocity.

Speed static stability in helicopter theory implies a nose-up pitching moment with increases in speed relative to the freestream velocity as providing a stabilizing moment which tends to return the speed to the undisturbed value. Steady state pitching moment response to horizontal gusts were investigated as a predictor for the rotor behavior using step increments in the free stream wind tunnel velocity, and the results for the baseline rotor are shown in Figure 55. Higher magnitude response in seen at higher rotor speed, when shaft incidence is high, while advance ratio sensitivity is low except as the advancing tip Mach number limit is approached.

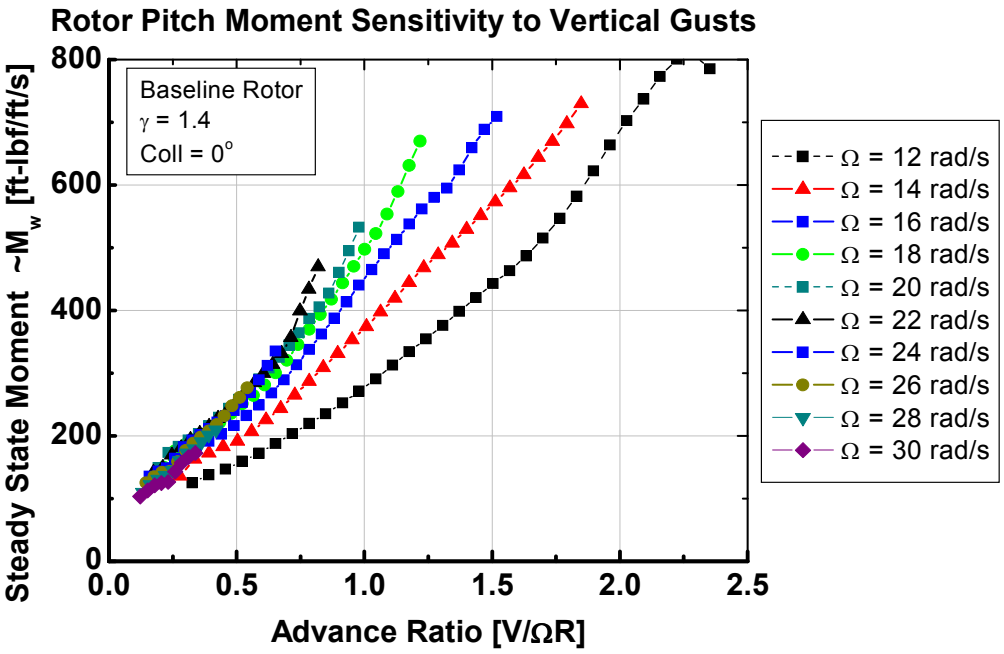

Figure 54: Baseline Rotor Pitch Moment Sensitivity to Vertical Gusts

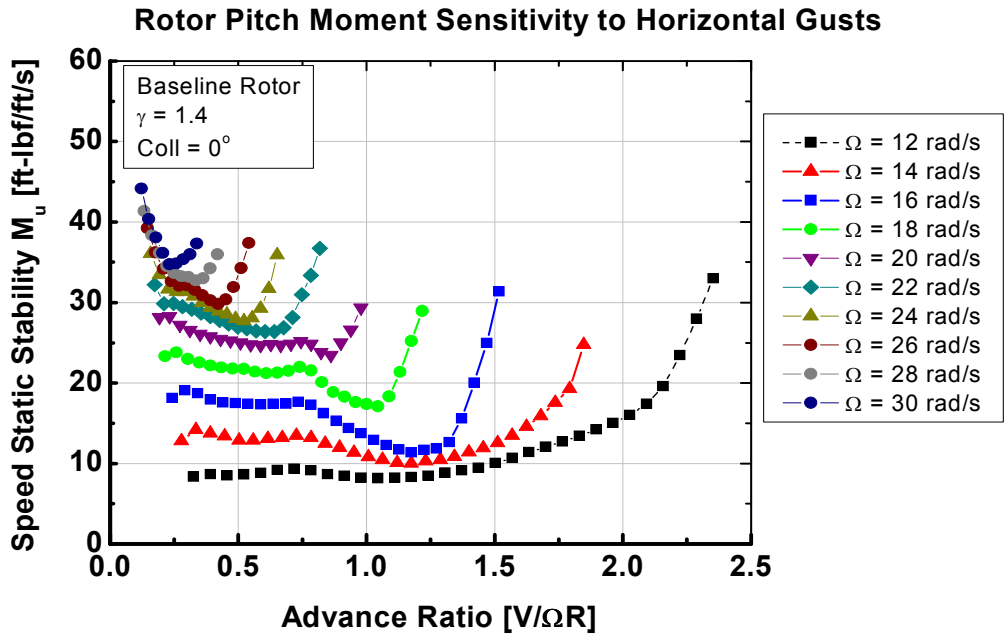

Figure 55: Baseline Rotor Pitch Moment Sensitivity to Horizontal Gusts

The dihedral effect in helicopter theory provides a stabilizing rolling moment in response to side gusts that tend to roll the helicopter so as to eliminate the sideslip. The steady state response of the baseline rotor to side gusts shows that at high rotor speed the response provides a stabilizing effect where the moments are shown as the negative of the values in the hub frame so as to be consistent with the common interpretation of the dihedral effect where negative values are stabilizing. With reduced rotor speed however the response to side gusts produces moments which tend to increase the sideslip (destabilizing) with little sensitivity to advance ratio. In the case of the baseline rotor, the explanation of this destabilizing effect can be attributed to the blade flapping behavior. At low advance ratio and low rotor speed, the heavy blades are producing little thrust. The result is a negative coning angle such the blades are drooped slightly. At high advance ratio, the thrust has increased such that the coning angle is positive.

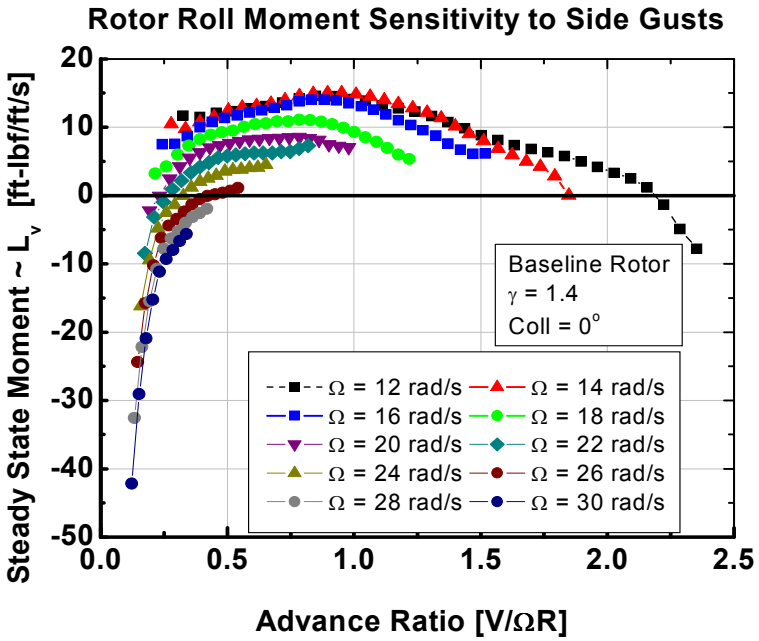

Figure 56: Baseline Rotor Sensitivity to Side Gusts

3.5 Rotor Transient Response and Slowed-Rotor Dynamics

Rotor transient hub moment response was shown to occur on a much faster time scale than the rotor speed changes, thereby justifying the presentation of the steady state hub moment results. However the slowed-rotor dynamics themselves are such that the assumption that the rotor responses instantaneously ("quasi-steady assumption") is not correct. Consideration of the time history of the non-linear simulation hub moment response to cyclic step inputs, Figure 34, indicates that the transient rotor responses require on the order of one to three seconds to reach a steady-state value. It can also be seen that the response is generally dominated by the low-frequency content. In analytical helicopter work the regressing flap mode is typically the dominant mode, with the damping given by the quantity $\gamma\Omega/16$ for the hover case. Heffley *et. al.* [56] summarized the Lock number-rotor speed product for existing helicopters, and note that the quantity $\gamma\Omega/16$ is in the neighborhood of 12 to 15 s^{-1}. The concept configuration parameters place the quantity $\gamma\Omega/16$ below this range due to three main factors: reduced rotor speed, heavy blades, and high altitude (low density). For the parametric baseline rotor at the reduced rotor speed, the quantity $\gamma\Omega/16$=1.05 s^{-1}. This low value means the time scale of rotor transient response to disturbances or inputs may be on the same order of magnitude as the vehicle motion. In the present work experimental transfer functions are determined from application of system identification methods. These transfer functions are linear describing functions for the input-output relationships for rotor control inputs or disturbances to hub moments in the non-rotating frame. Rotor transient dynamics can be excited by any swashplate control input, gust, or rotor orientation disturbance from the trim condition. In this dissertation, the hub pitching moment frequency response to changes in shaft incidence angle are studied. This hub moment response results when the airframe undergoes a change in pitch attitude due to

gusts or airframe pitch control input. In the case of an automatic feedback controller designed to suppress the hub moments, determination of frequency response models would be a logical first step. Kuczynski and Sissingh [57] determined experimental transfer functions for a 45-inch radius hingeless rotor and compared results from theoretical predictions. Advance ratios up to $\mu \sim 1.44$ were considered, and a first-order lag feedback control system, "described most accurately as a steady-state gust alleviation device" [57], was evaluated. In the present work, the frequency response is used to investigate the effect of advance ratio and the rotor parameters at the reduced rotor speed. Comparison of step response for the low-order identified model and the non-linear simulation is used to highlight the effect of advance ratio and the sensitivity to rotor parameters in the time domain, as well as discuss the response components not captured in the low-order model. The comparison provides relevant background information that would influence the architecture of the feedback control system. For instance, a linear feedback controller versus a controller designed for a non-linear or periodic system represent different architecture choices with varying cost and complexity.

The experimental transfer functions were obtained according the methods described by Tischler and Remple [49]. The system identification process involves collecting time history data of system inputs and outputs as the system is excited by a variable frequency input sweep. The time history data is then transformed into the frequency domain. The software program CIFER® [58] was used to accomplish the transformation and facilitate data post-processing. CIFER®, developed by the U.S. Army Aeroflightdynamics Directorate at Ames Research Center, has been used extensively for rotorcraft and aircraft dynamics model identification from flight test data. In the present work, time history data from the FLIGHTLAB™ non-linear simulation was used as

surrogate flight test data. The input frequency sweeps were conducted over a frequency range of 0.001 to 5.0 Hz with a total time history for each record of two hundred seconds. Figure 57 shows the experimental frequency response for the hub pitching moments resulting from shaft incidence perturbations. The coherence function "can be interpreted physically as the fraction of the output spectrum that is linearly attributable to the input spectrum" at a particular frequency [49]. Coherence values will be between 0 and 1 with higher values providing more confidence in the model.

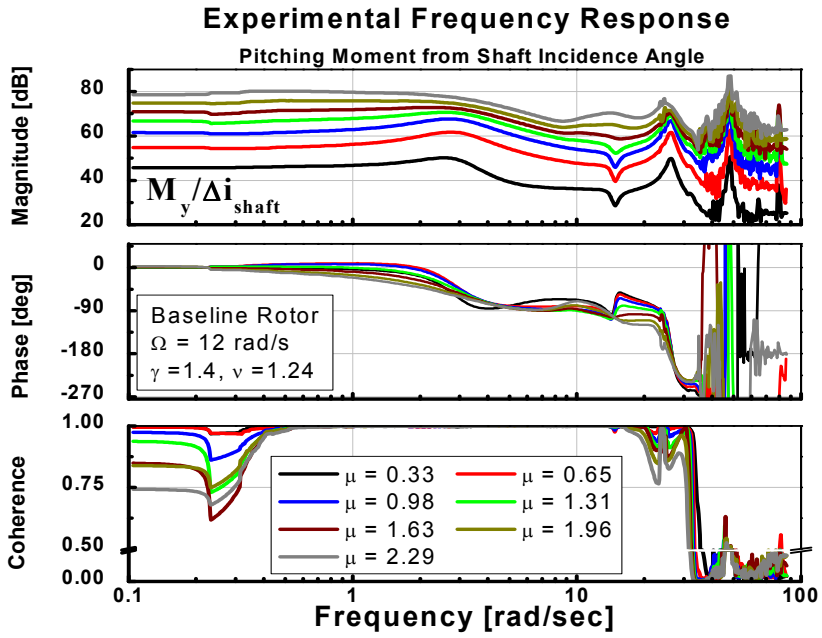

Figure 57: Experimental Frequency Response – Advance Ratio Sensitivity

Transfer function models were identified using the NAVFIT component of CIFER®. NAVFIT identifies the coefficients for a particular transfer function form using an optimization process to curve fit the frequency response of the identified transfer function to the experimental data. Low frequency effects were of primary interest so that the range of the curve fitting process was restricted to $0.1 \le \omega_n \le 10$ rad/s, which

includes the regressing flap mode for the baseline rotor, but neglects the coning and advancing flap modes. A proper fourth order transfer function form was found to accurately fit the data in this range, as reflected by low cost functions, ranging from $J = 0.6$ for the $\mu = 0.33$, up to $J = 11.1$ for the $\mu = 2.29$ case. Figure 58 shows the frequency response of the low-order identified models of pitching moment response to shaft incidence angle changes.

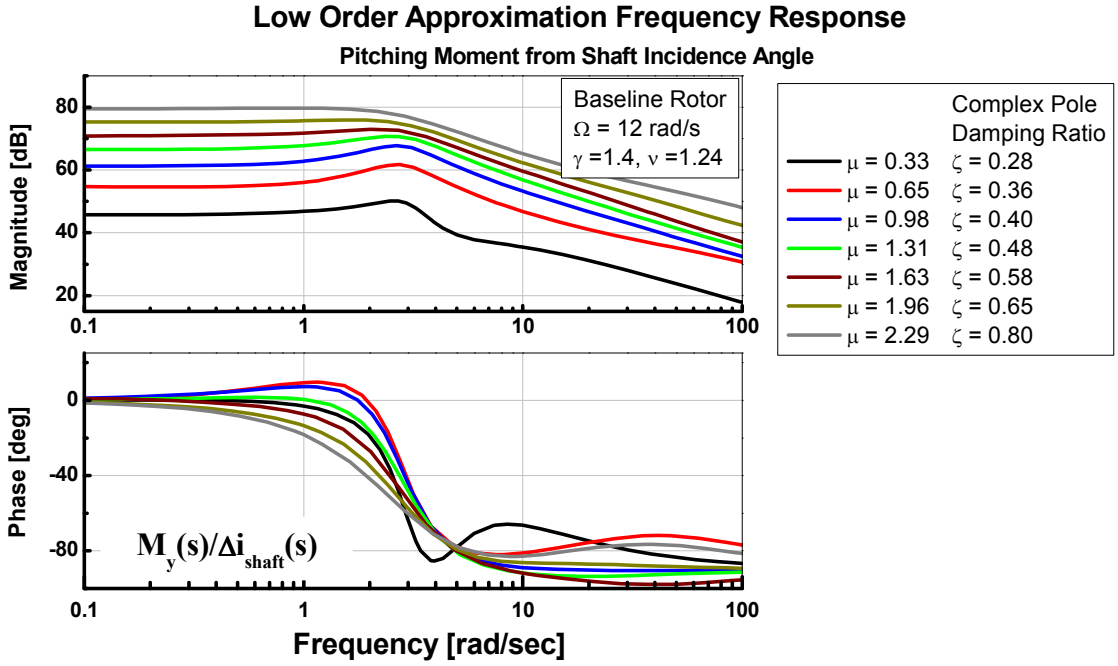

Figure 58: Hub Pitching Moment Frequency Response to Shaft Incidence Angle

The magnitude plot shows the increase in steady-state value with increased advance ratio as was seen in the steady-state analysis. Also show is the amplitude peak value which is indicative of the damping, where an increase in the peak amplitude implies a decrease in damping. The identified models contain a complex pole-pair with a damping

ratio that increases with advance ratio at an essentially constant natural frequency, $\omega_n \approx 2.8$ rad/s.

Rotor hub pitching moment response to shaft incidence step inputs was used to compare the non-linear simulation and the low order models from system identification. Beyond just the frequency response plot, the time history provides several important conclusions regarding the use of low-order linear models to predict the rotor behavior. Figure 59 show the effect of advance ratio on the rotor response. From an initial trim condition, the steady-state magnitude increases in the same manner as the steady-state control input data presented earlier. At still higher advance ratios the effect is a reduction in overshoot and a reduced response settling time. Also visible in Figure 59 is a high frequency oscillations. This high frequency response peak-to-peak magnitude increases with advance ratio as the effect of increased sensitivity and will be seen in the fixed system as an increase in 4/rev vibration.

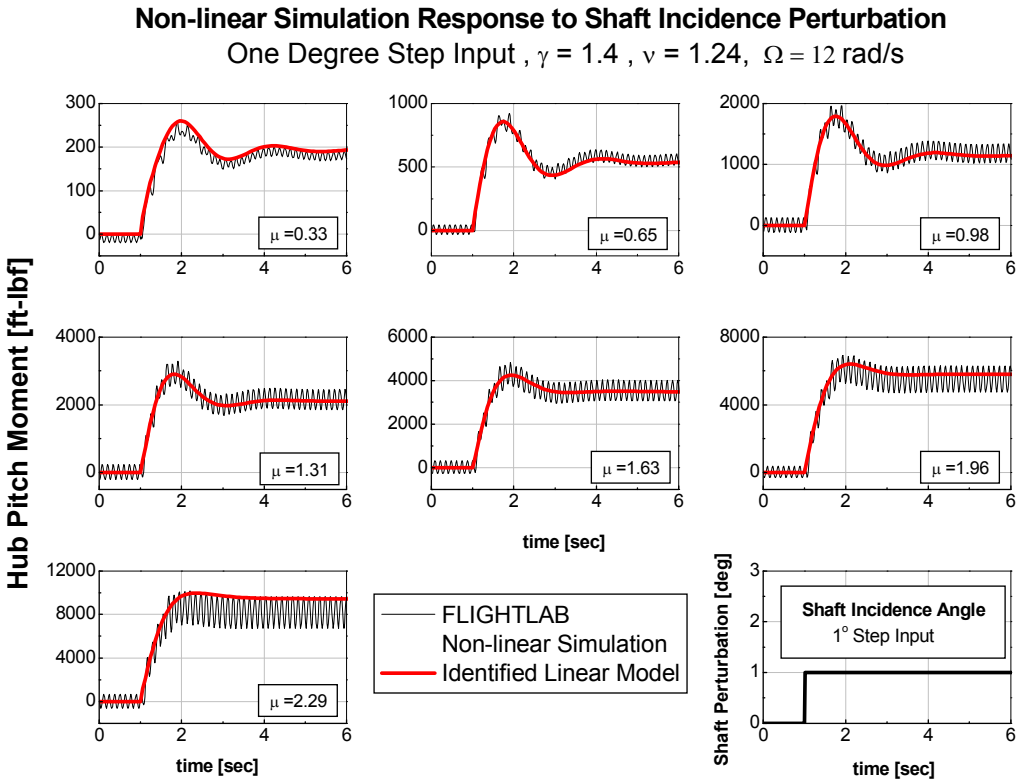

Figure 59: Advance Ratio Effect on Slowed-Rotor Transient Response

Figure 60 shows the experimental frequency response sensitivity to non-dimensional flapping frequency at the cruise condition. The frequency response for the higher flap stiffness shows a higher amplitude peak at a higher frequency, indicating a reduction in damping ratio. For the low stiffness values the low frequency rotor response appears as real roots, not an oscillatory pair, and the frequencies near the rotor speed appear more prominently. Figure 61 shows the identified model based on the dominant low frequency modes, with the effect of the frequencies near the rotor speed retained.

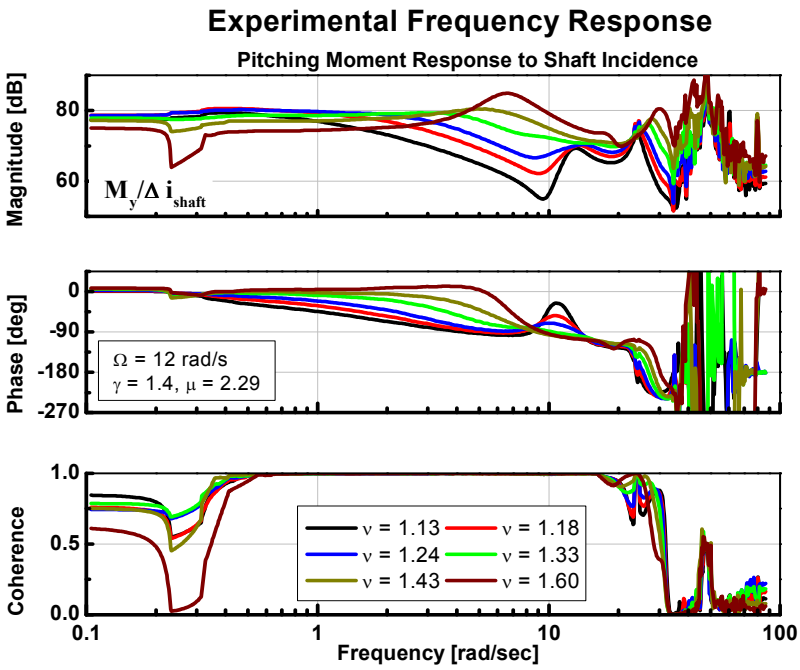

Figure 60: Experimental Frequency Response – Flap Stiffness Sensitivity

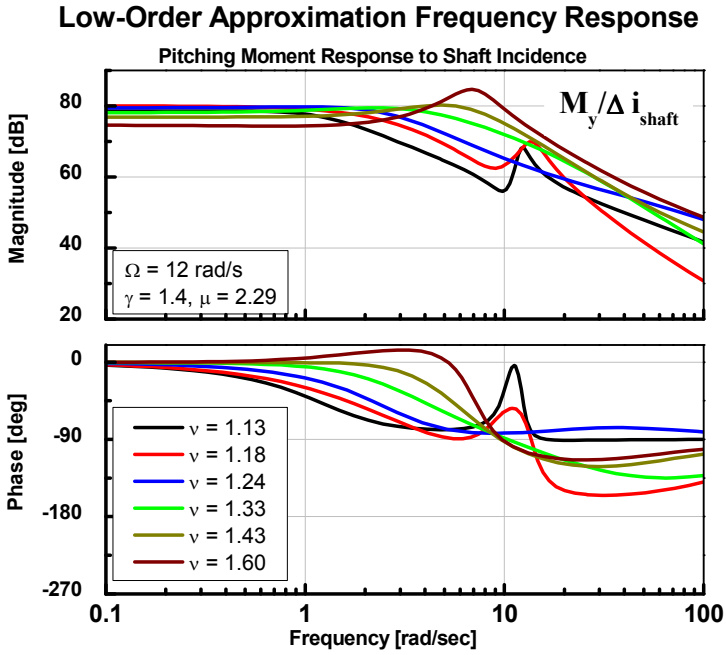

Figure 61: Frequency Response Sensitivity to Flapping Stiffness

Figure 62 shows the step response at the cruise condition for the sensitivity to flapping stiffness. The lowest flapping stiffness response shows an overdamped behavior, with the effect of increasing flapping stiffness being an increase in overshoot and oscillatory behavior indicative of an underdamped response.

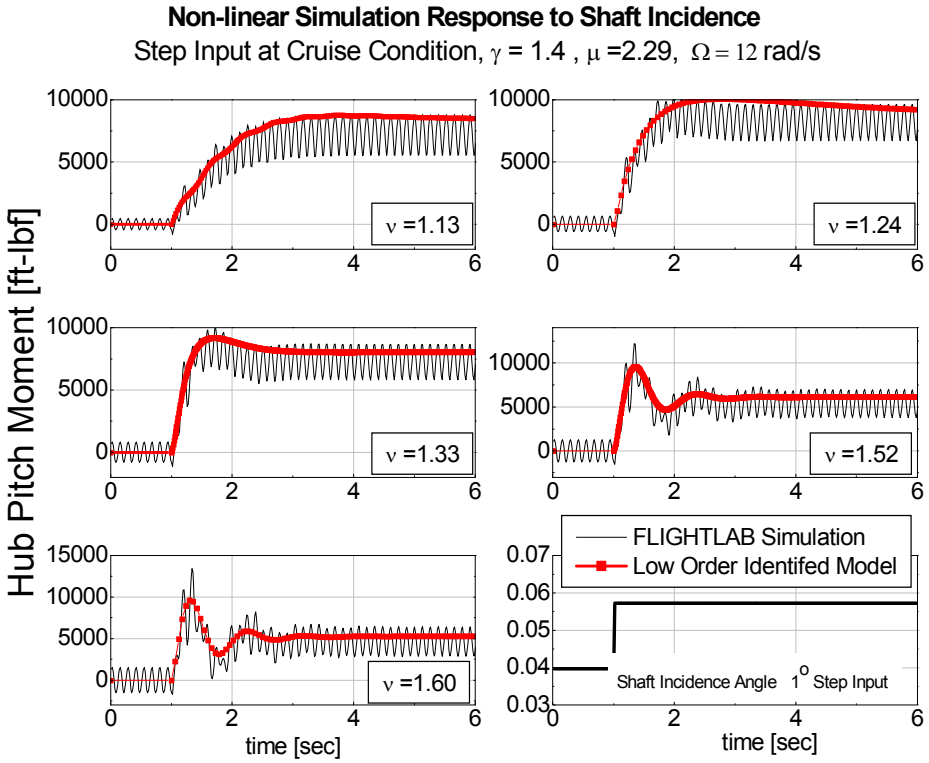

Figure 62: Rotor Flapping Stiffness Effect on Slowed-Rotor Transient Response

Experimental transfer function sensitivity to Lock number is shown in Figure 64. A small steady state magnitude increase with Lock number can be seen in the magnitude plot. The step response comparison is shown in Figure 65. At constant flapping frequency, the increase in Lock number results in an overdamped response. In the non-linear simulation, the primary trend with increasing Lock number is an increase in the 4/rev

vibration content, indicating that the lighter blades are experiencing higher cyclic flapping when disturbed from trim.

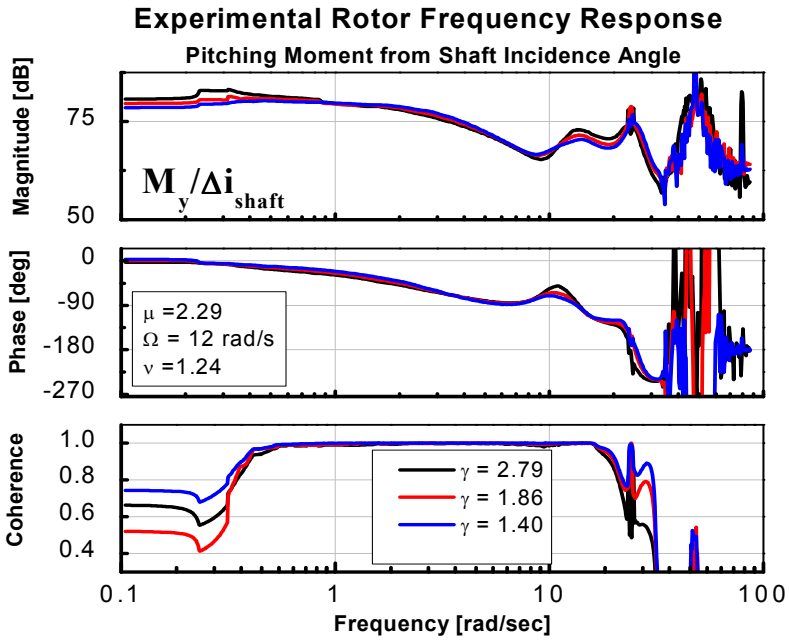

Figure 63: Experimental Frequency Response – Lock Number Sensitivity

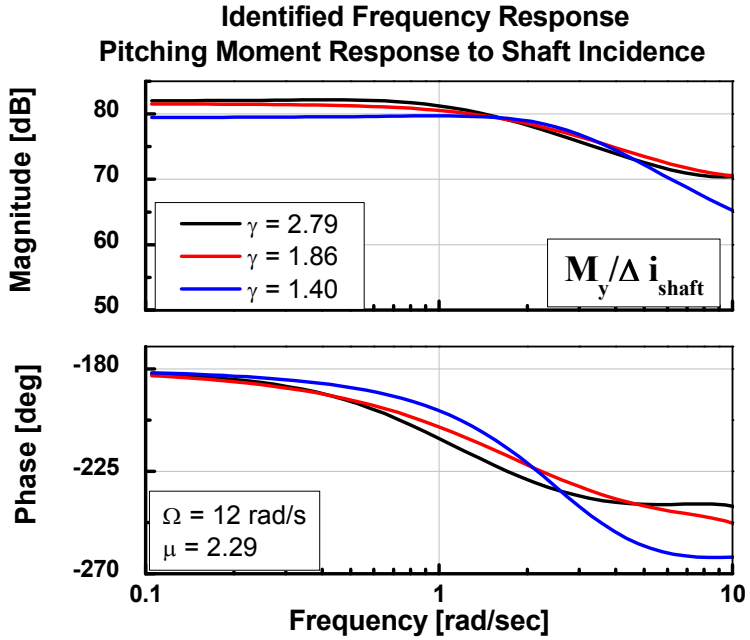

Figure 64: Identified Hub Pitching Moment Frequency Response to Shaft Incidence

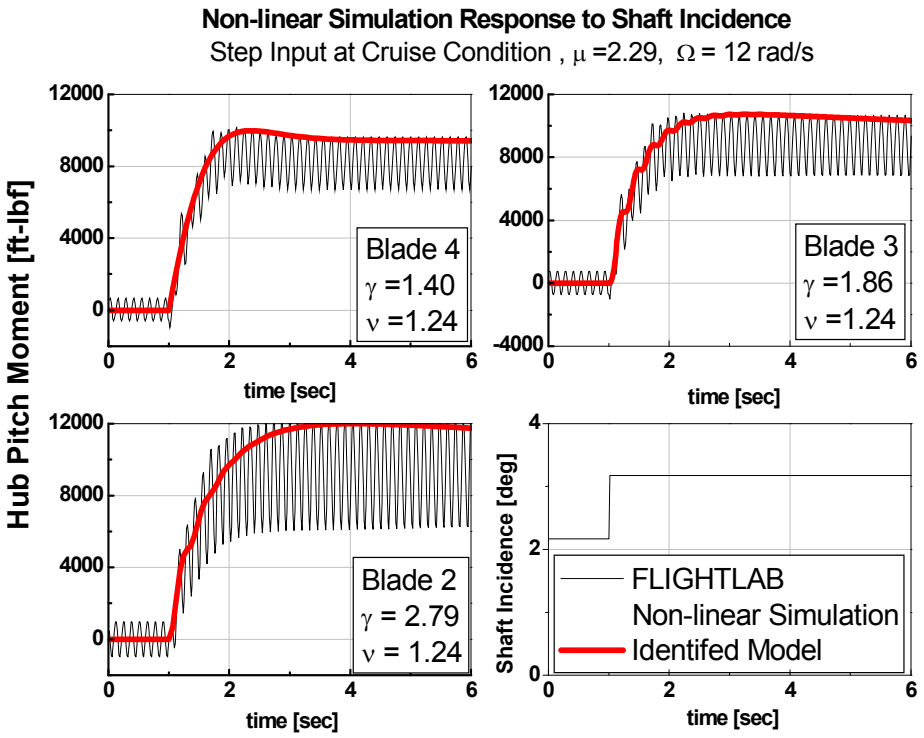

Figure 65: Lock Number Effect on Slowed-Rotor Transient Response

3.6 Rotor Speed Response to Swashplate Controls

Some means of rotor speed regulation has been discussed as an inherent feature of the concept vehicle. Earlier the hub pitching and rolling moment response to swashplate control inputs was presented in terms of the steady state response to a one degree step input at constant rotor speed. Rotor control using only swashplate controls represents a possible strategy, and in this section the rotor speed response to swashplate control inputs is presented. The rotor speed response is a result of the torque balance on the rotor, and the response was shown to occur on a much longer time scale than the rotor hub moments, justifying the constant rotor speed approximation in section 3.3. The changes in rotor speed due to swashplate inputs cannot however be presented in

exactly the same manner as the hub moment data because of the observance of a non-linear behavior in the simulation. The non-linear behavior is apparent because the sign of the output depends on the magnitude of the input. Figure 66 illustrates the non-linear behavior through the rotor speed time history to a slow, ramp longitudinal cyclic perturbation from trim. In this example, the small magnitude step results in a decrease in rotor speed, while the large step initially results in a reduced rotor speed, but when a certain magnitude input is reached the rotor speed begins to increase. For this reason the rotor speed response to swashplate control inputs is shown in terms of the magnitude of the input. The source of this non-linear behavior is investigated in section 3.8.

The nonlinear simulation time response of the isolated rotor model to swashplate inputs showed that the rotor acceleration could be estimated using a two point approximation of change in rotor speed over simulation time, $\Delta\Omega/\Delta t$, where swashplate control step inputs were applied as in Figure 66. This procedure was repeated for positive and negative step inputs for each of the swashplate controls. Figure 67 shows the rotor acceleration due to longitudinal cyclic inputs as a function of advance ratio. At low advance ratio the behavior is nearly linear with only a small magnitude, but with increasing advance ratio the magnitude increases and the non-linear behavior appears for positive inputs. Figure 68 shows the rotor acceleration for lateral cyclic inputs. The magnitude for lateral inputs is an order of magnitude smaller than the longitudinal cyclic results, and does not display the same non-linear response. Collective pitch results are shown in Figure 69. The non-linear response is again present at high advance ratio, for negative collective pitch inputs, but the magnitude is smaller than the longitudinal results.

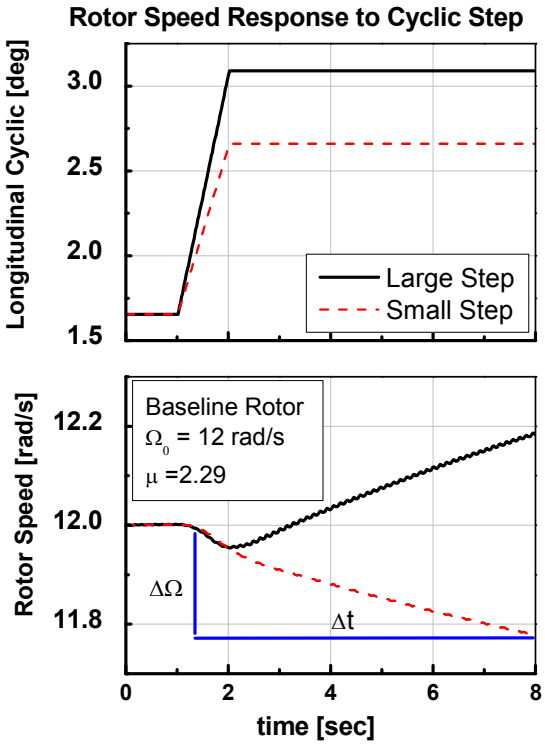

Figure 66: Rotor Speed Response to Small and Large Longitudinal Cyclic Steps

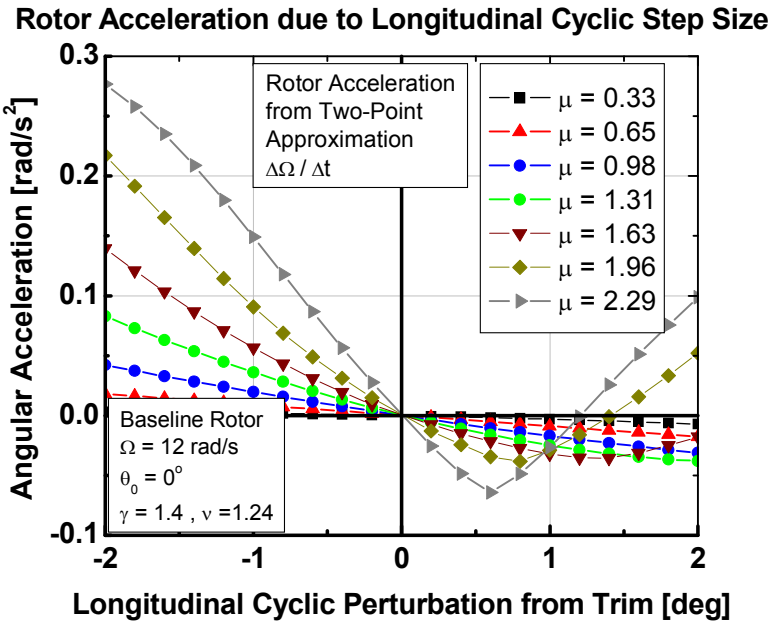

Figure 67: Advance Ratio Effect on Rotor Speed Response to Longitudinal Cyclic

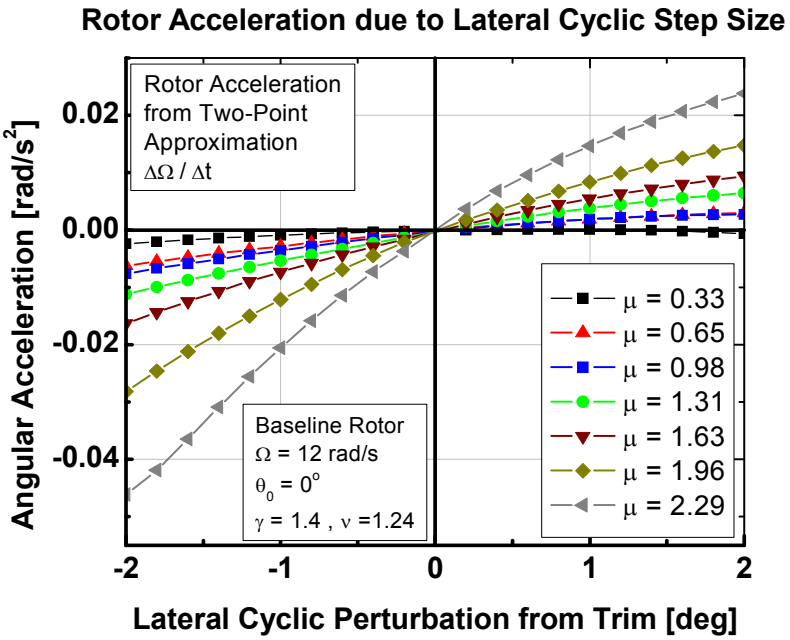

Figure 68: Advance Ratio Effect on Rotor Speed Response to Lateral Cyclic

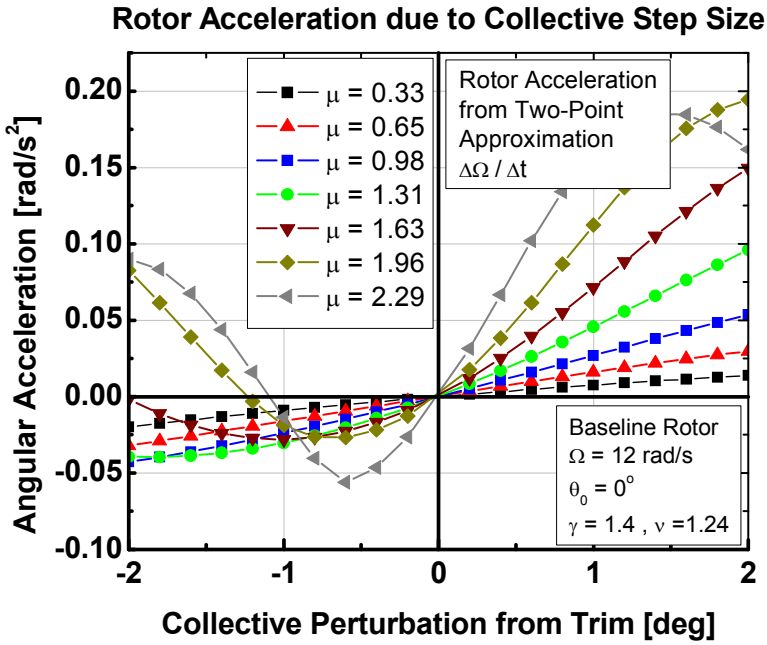

Figure 69: Advance Ratio Effect on Rotor Speed Response to Collective

The rotor acceleration data were presented for the baseline rotor at zero degrees of collective pitch. The sensitivity to the collective pitch setting is addressed in Subsection 3.7 where sensitivities to trim condition and the existence of multiple trim solutions are presented. Sensitivity to rotor parameters is addressed in Subsection 3.8 in the investigation of the source of the non-linear behavior.

3.7 Cruise Condition Rotor Performance and Multiple Trim Solutions

A more detailed investigation of the cruise condition was made with the isolated rotor model since a considerable portion of the concept vehicle mission would be flown in this condition. The wind tunnel conditions were set to the cruise condition, and a series of sweeps were made using the collective control and the rotor shaft incidence to the tunnel velocity as parameters. At a fixed collective, the shaft incidence was swept from -3 degree to plus 3 degrees and the rotor rolling and pitching moments were trimmed at each point. Figure 70 illustrates the rotor torque vs. the rotor shaft incidence to the tunnel free stream velocity at the cruise condition.

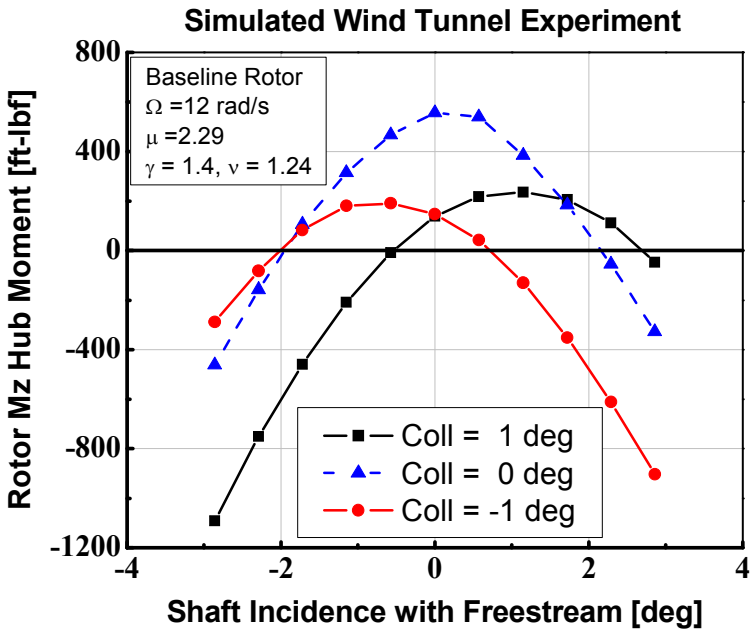

Figure 70: Trimmed-Rotor Torque Curves – Cruise Condition

The collection of points at the zero-torque crossing was retained as possible autorotational trim operating points. The result was a contour of combinations of rotor shaft incidence and collective control. The left side of Figure 71 shows the contour in terms of the collective pitch settings and the right side of the figure shows the contour in terms of the lift produced by the rotor. The points designated as “Trim Point 2” and Trim Point 6” are points that provide nearly equivalent rotor lift (~1,500 lbs.), but differ in that Trim Point 2 has an aft shaft orientation with respect to the freestream flow, and Trim Point 6 has a small forward tilt into the freestream flow. These two trim points are identically the conditions discussed by Rigsby and Prasad [59] when considering the application of system identification methods to identify models for the prediction of rotor speed behavior. In both cases the point represents a trimmed, zero-torque condition. Points one through six are used to investigate the differences between the multiple trim

conditions for the baseline rotor configuration at the cruise condition in terms of the rotor speed response to control disturbance from trim.

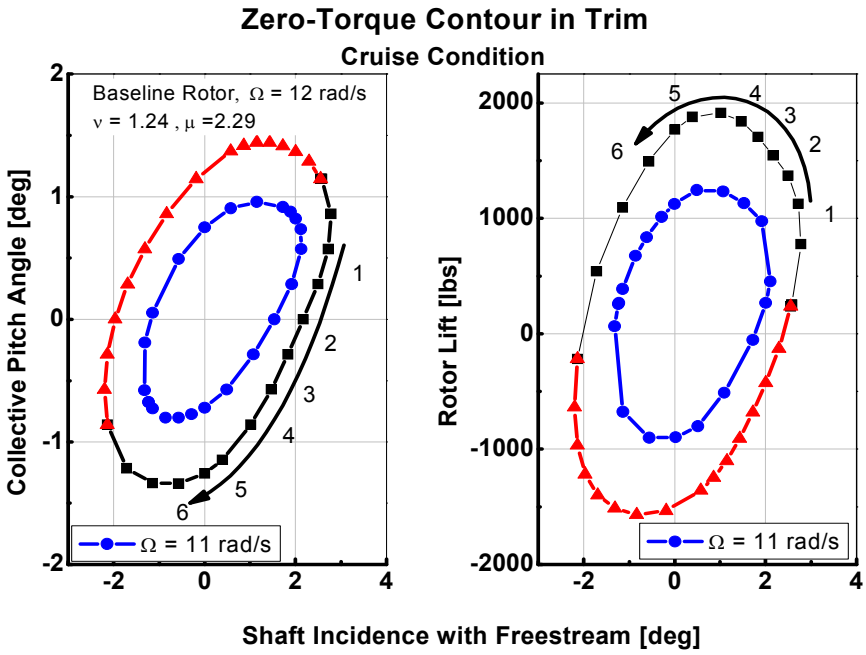

Figure 71: Rotor Trim Contours - Cruise Condition

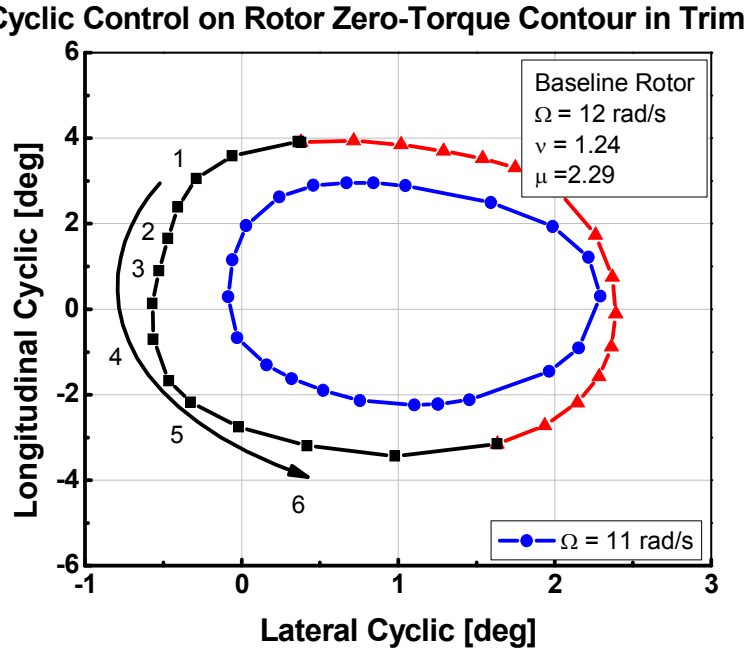

Figure 72: Cyclic Control Positions on Trim Contour – Cruise Condition

The orientation of the rotor shaft to the free stream represents a design decision that may or may not be adjustable in flight. The decision to tilt the shaft adds complexity and cost to the design, but allows for greater flexibility in choosing the rotor operating point. In addition to the differences in performance for the trim points, the rotor speed response to swashplate inputs also depends on the choice of trim point. Figure 73 shows the rotor acceleration due to longitudinal cyclic step versus the magnitude of the step. Trim point 2 exhibits the behavior that negative steps tend to speed up the rotor while positive steps tend to slow down the rotor for steps of at least as large as one degree of cyclic even though the positive steps show nonlinear behavior starting near ½ degree. Trim point 6 exhibits a similar trend for negative steps but the positive direction shows a small negative effect until about ½ a degree then a sign reversal for larger inputs. Figure 74 shows the effect of the lateral cyclic on rotor acceleration and similarly Figure 75 shows the effect of the collective. The behavior highlights the nonlinear effects. A fundamental principle in the concept of a vehicle utilizing a lightly loaded rotor autorotating at high advance ratio is the need to tightly control the rotor speed either with pilot inputs or automatic feedback control. The nonlinearities and sign reversals indicate that complex piloting strategies would be required or a feedback control system that can accommodate changing sensitivities and partial derivative signs would be required in order to utilize swashplate inputs for rotor speed control when this behavior is present. The origin of the non-linear behavior is discussed in Section 3.8.

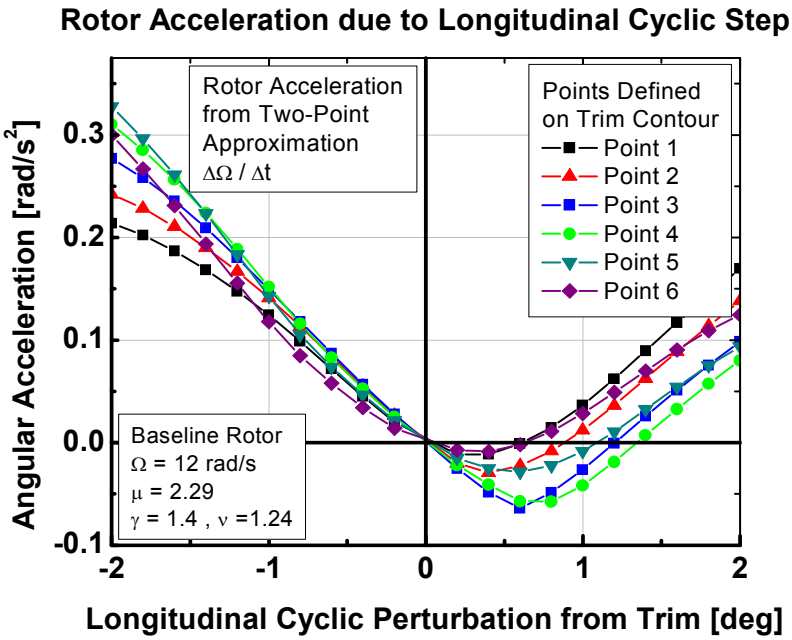

Figure 73: Rotor Acceleration Sensitivity to Longitudinal Cyclic Step Magnitude

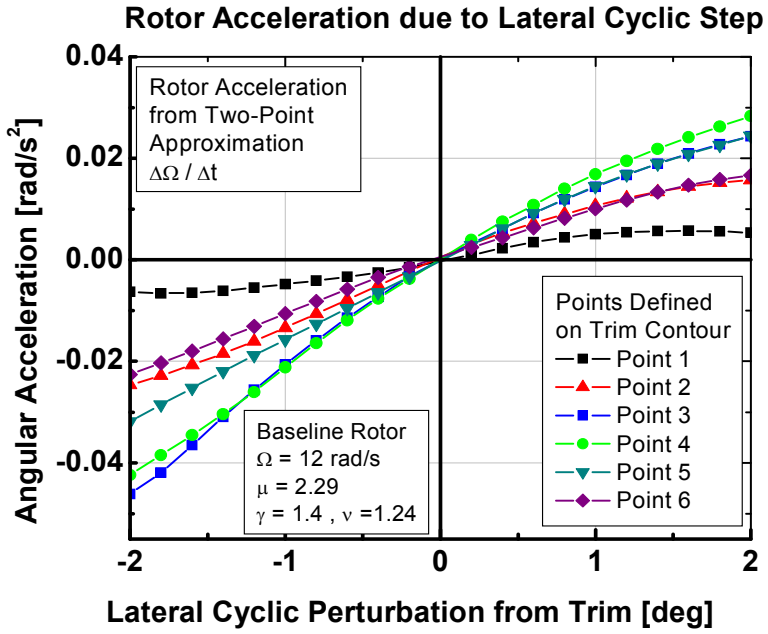

Figure 74: Rotor Acceleration Sensitivity to Lateral Cyclic Step Magnitude

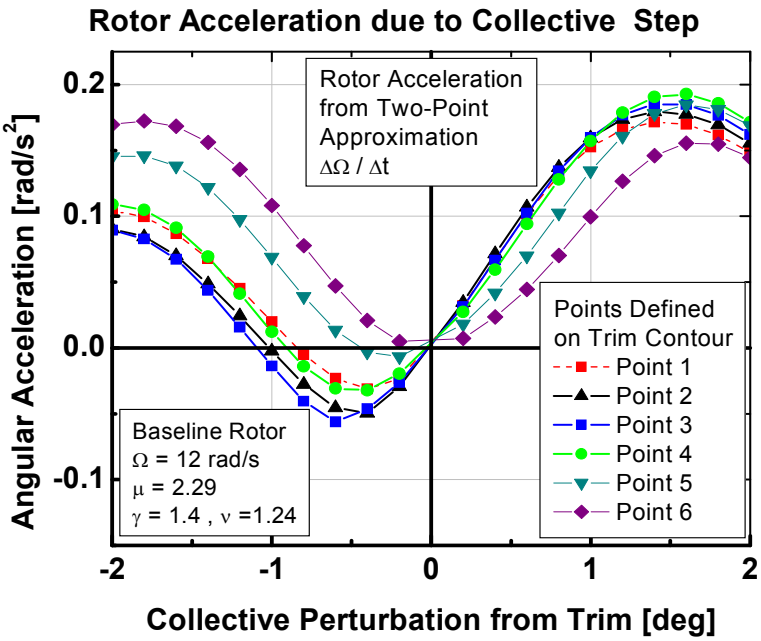

Figure 75: Rotor Acceleration Sensitivity to Collective Step Magnitude

3.8 Source of Rotor Speed Non-linear Response to Control Inputs

Non-linear rotor speed response to swashplate control inputs was presented in subsection 3.6. A study was performed to identify more specifically the source of this non-linear behavior. Initially, factors considered as potentially contributing to the behavior were the inflow model, flapping stiffness, and the Lock number. These factors were investigated parametrically and compared to the baseline rotor. Subsequently, a detailed accounting of the contributions to the torque of a single rotor blade was made to provide additional insight into the origin of the non-linear behavior.

To assess the impact of the inflow model on the non-linear rotor speed behavior, the longitudinal cyclic perturbation analysis was repeated using two other inflow models: Glauert uniform inflow, and a finite state inflow model. The finite-state inflow model used a fourth order polynomial for the span-wise variation. The rotor inflow model results are shown in Figure 76. The results indicate very little impact on the rotor speed behavior

likely due to the reduced thrust loading on the rotor in the cruise condition. The literature review revealed no clear findings on the applicability of dynamic inflow to the lightly-loaded rotor autorotating at high advance ratio, nor suggested the superiority of inflow models such as the prescribed or free wake models. For work beyond the conceptual design phase, higher fidelity wake models would however be appropriate when higher fidelity blade structural models are available. Next, the sensitivity to the rotor flapping stiffness was investigated by adjustment of the flapping hinge spring constant. Figure 77 shows the sensitivity to changes in the flap hinge spring, which alters the flapping frequency. Lower stiffness values results in a smaller range where negative rotor acceleration is possible, while larger stiffness values tend to straighten and flatten the curve resulting in a lower sensitivity to the inputs. Figure 78 shows the sensitivity to blade mass changes (Lock Number effect) with the hinge spring adjusted to maintain the non-dimensional flapping frequency at the baseline value of v~1.24.

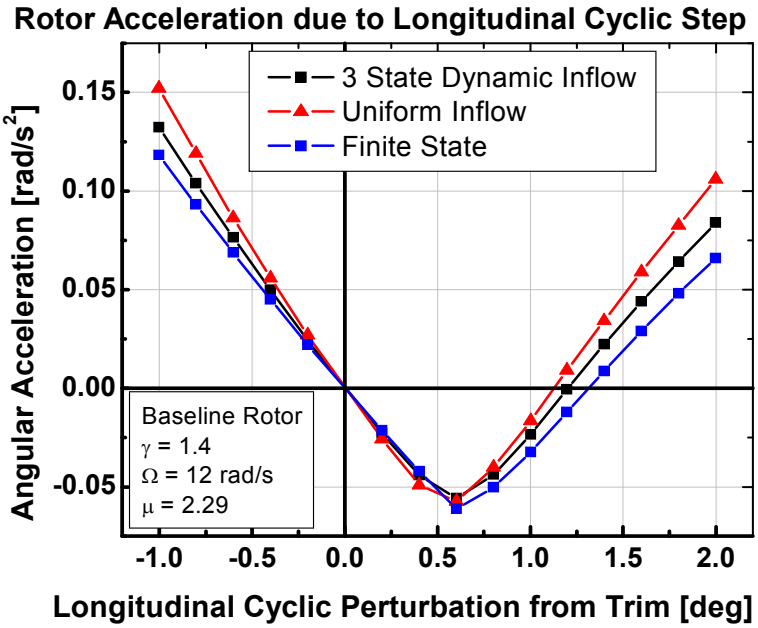

Figure 76: Sensitivity to Rotor Inflow Model - Baseline Rotor

The results show that reducing the blade mass (increased Lock number) produces a similar effect as a reduction in stiffness, namely a steeper slope and a reduction in the range for negative rotor acceleration, and a more parabolic curve shape. Figure 77 also shows the limiting case of an infinitely stiff rotor which has no flapping degrees of freedom. In this case the longitudinal cyclic effect on the torque is essentially linear, indicating the non-linear effects are associated with the blade flapping. Considering the sensitivity to flapping stiffness and Lock number, the non-linearities appear more severe in cases where the blade flapping response to the cyclic input results in larger magnitude flapping angles. In other words the lighter blades with lower stiffness tend to result in more severe non-linearities as also confirmed with the infinitely stiff rotor case.

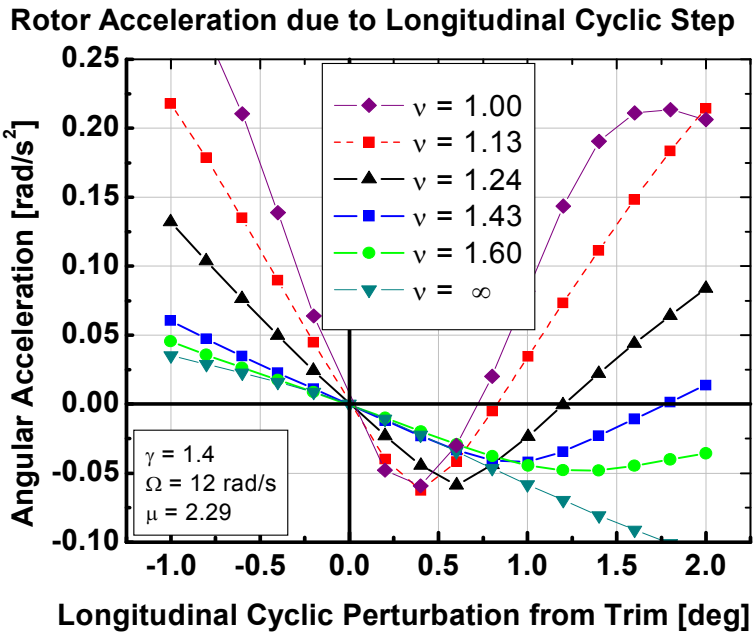

Figure 77: Rotor Acceleration Sensitivity to Rotor Flapping Stiffness

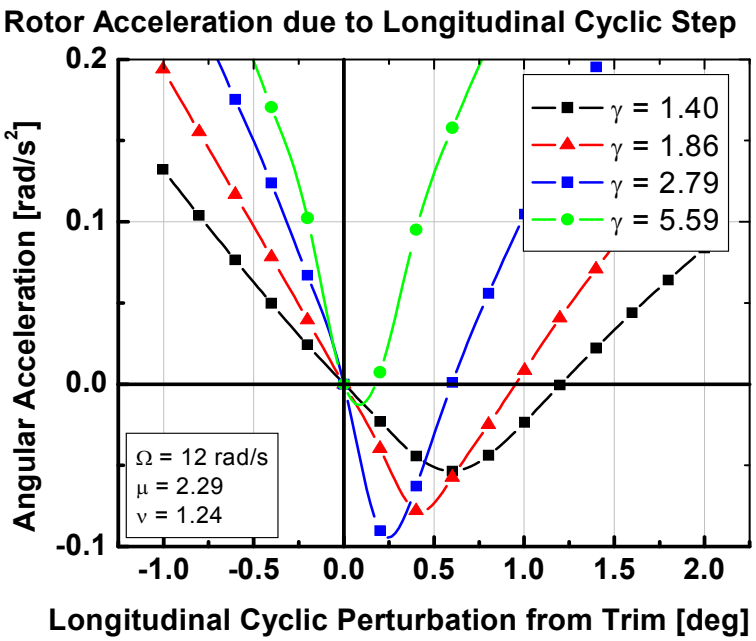

Figure 78: Rotor Acceleration Sensitivity to Lock Number

Since the rotor models use a flap hinge located at the center of rotation, the contribution to the rotor torque of a single blade can be easily used to identify which regions of the rotor azimuth tends to add torque to the rotor and which regions consume torque by examination of the blade root torque moment and its components. This was accomplished by performing an accounting of the torque moment at the root of one blade along with the effects that contribute to the torque moment over one rotor revolution.

Figure 79 shows the total blade root torque moment, and the contribution from aerodynamics, gravity, and the Coriolis effect due to the flapping motion in the rotating hub frame for the baseline rotor trimmed in autorotation at $\mu \sim 2.29$. The gravity moment results from the aft tilt of the shaft and the Coriolis moment results from the flapping angle and flapping rate. These two effects average to zero around the azimuth for each blade and for all blades combined. They do not affect the average torque on

the rotor that tends to change the rotor speed, but they are included only to provide an accounting of the total blade root torque moment around the azimuth.

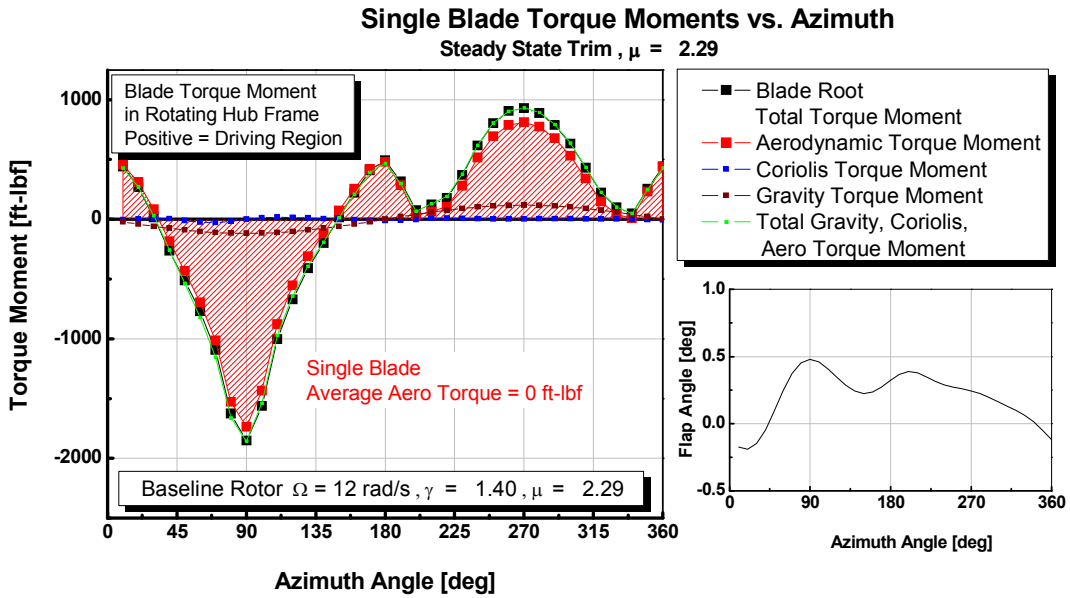

Figure 79: Blade Root Torque vs. Azimuth

The contribution to the torque from the aerodynamics shows the advancing side of the rotor provides a negative moment, meaning rotor power is consumed (driven region), while the retreating side provides a positive moment, meaning power is added to the rotor (driven region). This is the steady-state environment of an individual blade as it passes around the azimuth, and since the rotor is trimmed to zero torque, the average around the azimuth is zero. This plot is the summed effect of all of the blade element sections at each azimuth position, whereas Figure 25 is a polar contour plot accounting for the variation of the aerodynamic in-plane force along the blade span. The blade flapping angle, shown in the inset of Figure 80, remains small, and is on the order of ½ degree. When the rotor is perturbed from trim and run to a new steady state, the total

torque moments no longer average to zero. The result for a one degree longitudinal cyclic step is shown in Figure 80. The new steady state results in a higher value of cyclic flapping, on the order of three degrees, and the contribution from the aerodynamics now averages to a negative value, tending to slow the rotor. The peak magnitude of the Coriolis moment has increased due to the increase in flapping motion, but the average remains zero, making no net contribution to the average torque.

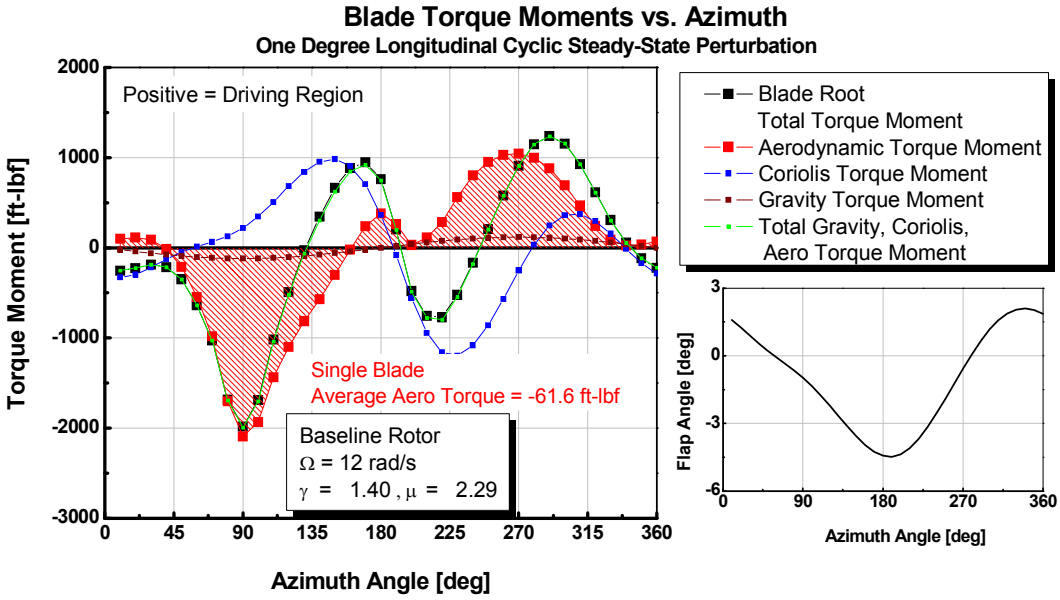

Figure 80: Individual Blade Torque Moment for 1° Steady State Cyclic Perturbation

Figure 81 shows the contributions to the torque for a two degree longitudinal cyclic perturbation from trim. In this case, the cyclic flapping has increased even further, in excess of five degrees. The magnitude of the Coriolis moment has an even larger peak to peak magnitude, but continues to average to zero, again contributing nothing to the average torque on the rotor. The aerodynamic loads, however now average to a

positive value, tending to accelerate the rotor. The azimuth region near $\psi \sim 180^o$ shows a larger contribution to the accelerating torque than the trim case with the blade experiencing large flap angle magnitude in this region as well. When the combined effect of all four blades is considered in the rotating hub frame, each blade experiences the same effect, but phased due to the blade spacing around the azimuth. The summed effect on the torque of all four blades as they are spaced around the azimuth is shown in Figure 82. The result for the trim and perturbed cases is the clear presence of a 4/rev response as expected for a four bladed rotor. The gravity and Coriolis moments continue to average to zero, making no contribution to the average torque, with the torque effect on the rotor speed due entirely to the change in aerodynamic environment. The results presented are steady-state values so that the change in aerodynamic environment includes the fact that the blade motion has been forced to consist of higher flapping rates, which affects the angle of attack in the blade element model.

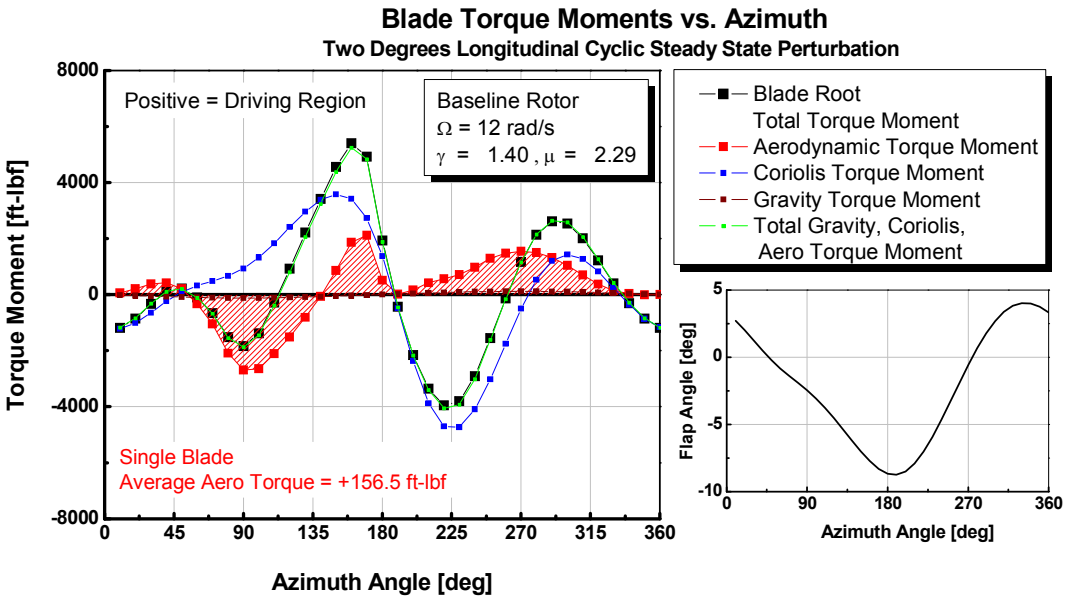

Figure 81: Individual Blade Torque Moment for 2° Steady State Cyclic Perturbation

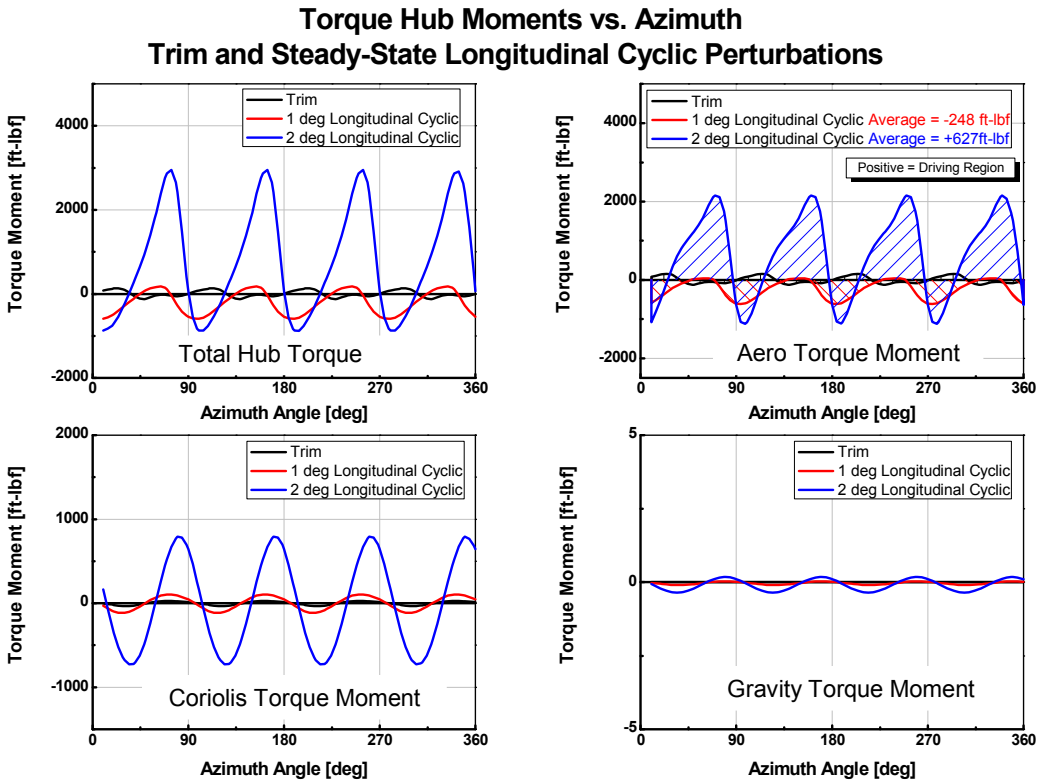

Figure 82: Steady-State and Perturbed Torque Moments from all Four Blades

3.9 Preferred Rotor Operating Point Selection Criteria

The performance plots indicate that multiple trim solutions exist at a particular flight condition and rotor speed. Several factors were considered to suggest the preferred operating point(s) for the rotor. Trim points that produce a negative lift were not considered for further analysis since negative lift would represent a performance penalty similar to added weight that the airframe must carry. The performance data shows the point of maximum rotor lift at cruise to be just less than one degree of incidence to the free stream. The maximum lift however is not necessarily desirable since the vehicle concept is to unload the rotor for greater vehicle aerodynamic efficiency. The control sensitivities suggest that the rotor should be operated at a slightly higher incidence

angle, ~ 2 to 3 degrees (0 degree collective pitch) in order to operate such that the controls have the largest range of linear variation and the largest range of travel without encountering sign reversals. The steady-state blade motion is also considered since cyclic variation of the flapping angle result in blade structural loads and manifests as vibration transmitted to the airframe. The inset of Figure 79 showed the blade flap angle versus azimuth position for trim in the cruise condition. The average pitching and rolling moments were trimmed to zero, but the blade still experienced a change in flap angle around the azimuth such that trimming to zero moments did not results in zero cyclic flapping. In terms of the motion of all of the blades, multi-blade coordinates can be used to describe the motion of the rotor as a whole in the non-rotating frame. The non-rotating degrees of freedom are derived from the Fourier coordinate transform by Johnson [50] as:

$$\beta_0 = \frac{1}{N}\sum_{m=1}^{N}\beta^{(m)}$$

$$\beta_{nc} = \frac{2}{N}\sum_{m=1}^{N}\beta^{(m)}\cos n\psi_m$$

$$\beta_{ns} = \frac{2}{N}\sum_{m=1}^{N}\beta^{(m)}\sin n\psi_m$$

$$\beta_{N/2} = \frac{1}{N}\sum_{m=1}^{N}\beta^{(m)}(-1)^m$$

The coning and first harmonic non-rotating degrees of freedom are shown in Figure 83 for the baseline rotor, trimmed at the cruise condition. The higher harmonic terms β_{2c}, β_{2s} and the reactionless mode $\beta_{N/2}$ (not shown) are necessary for the recreation of

the individual blade motion, and result from asymmetric flow pattern of the rotor due largely to the reverse flow region [61].

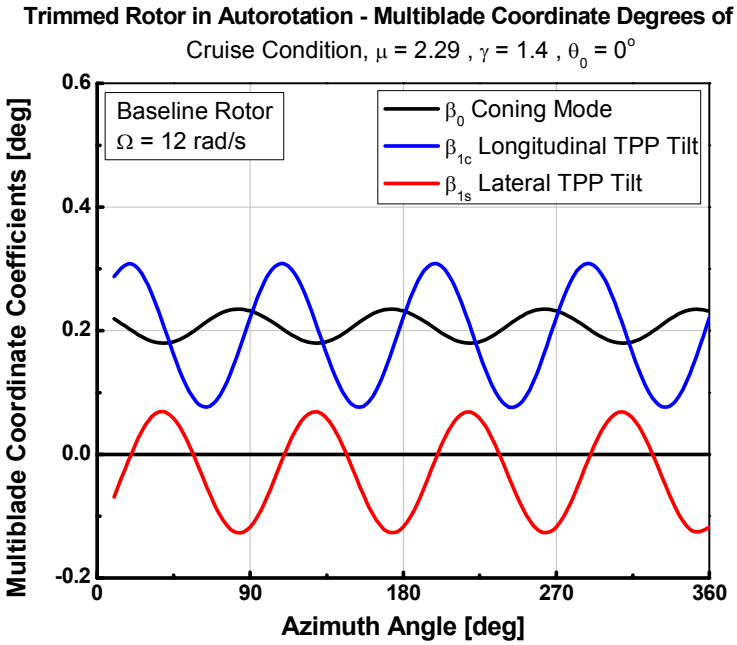

Figure 83: Rotor Non-Rotating Degrees of Freedom in Trim at Cruise Condition

The presence of this tilt of the tip path plane when the average hub pitching and rolling moments are zero can be explained by considering the equation for the hub pitching moment for a single blade as described by Bramwell [60]. The moment is determined by the inertial, centrifugal, weight, hub spring restraint, and aerodynamic forces on the blades. When the aerodynamic forces vary around the azimuth, the blade will be forced so that the other effects provide flapping moments to keep the blade in dynamic equilibrium. Figure 84 shows the sum of the aerodynamic forces for an individual blade normal to the hub plane (thrust). This aerodynamic load forces the blade such that the equilibrium condition with zero average hub moments is established when the flapping

moments created by the aerodynamics are balanced by the inertia couples resulting from a tilt of the plane of the rotor relative to the shaft.

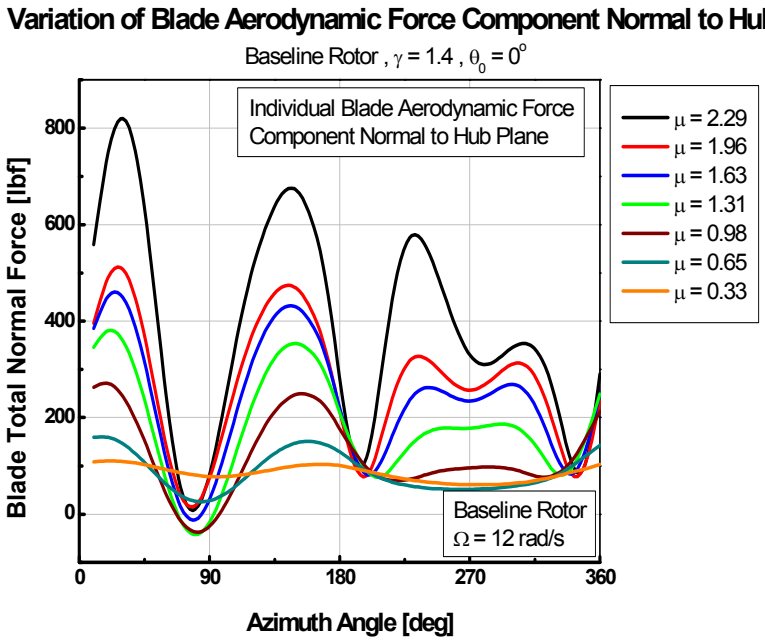

Figure 84: Advance Ratio Effect on Azimuth Thrust Distribution in Trim

The variation of the aerodynamic environment at high advance ratio will result in complex blade motion, which also depends on the particular trim solution on the trim contour. Figure 85 shows the absolute value of the maximum blade flapping angle at each steady-state trim point at the cruise condition. The minimum cyclic flapping is seen to occur at a collective pitch near zero degrees, with other points on the trim contour resulting in larger cyclic flapping. Since large cyclic flapping increases vibration and structural loads, the collective pitch of zero degrees is also a preferred operating point from this viewpoint.

The concept of the trim contour and the preferred operating conditions of the rotor are discussed further in Chapter 4. Other flight conditions are considered in the discussion of rotor control strategies and the interactions of the rotor and airframe. From the non-linear results presented in Figure 73 and Figure 75, rotor speed control using the collective and cyclic controls will require more complex control strategies that accommodate these non-linearities, and will results in rotor operation with higher cyclic flapping.

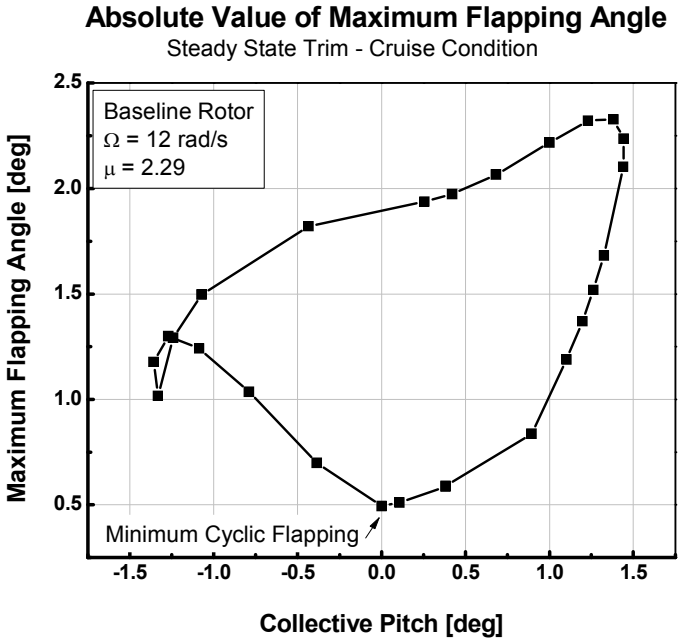

Figure 85: Maximum Cyclic Flapping Angle in Trim – Cruise Condition

3.10 Effect of Blade Twist at the Cruise Condition

The effect of blade twist was investigated from the perspective of the impact on the cruise condition trim contour and the preferred rotor operating condition. The baseline

model was modified to include a linear twist variation of negative ten degrees, where the zero collective pitch setting occurred at the 75% radius location such that the stations inboard of the 75% location were twisted leading-edge up, and the outboard stations were twisted leading-edge down. Figure 86 shows the section in-plane forces and the angle of attack contours. The contours are similar to the untwisted case, Figure 25, with the driving region shifted to include the inboard portion of the advancing blade. The magnitude of the in-plane forces shows larger forces on a smaller portion of the advancing side with lower driving forces spread over a larger portion of the retreating side when compared with the untwisted blade results.

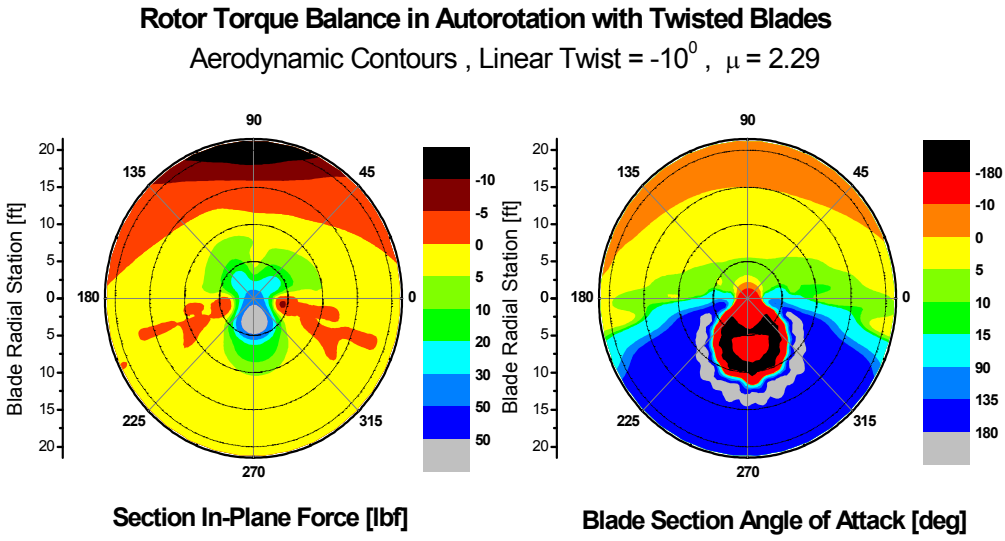

Figure 86: Aerodynamic Contours in Autorotation with Blade Twist

The cruise condition trim contour for the rotor with blade twist is shown in Figure 87, with the maximum steady-state flapping angle on the contour shown in Figure 88. The primary effects of the blade twist are to expand the lift contour to higher values (improve

the performance) and to shift the collective pitch setting for minimum flapping. For this baseline rotor with negative ten degrees of twist, the preferred collective setting has shifted to $\theta_0 \sim -0.9^\circ$, with a magnitude similar to the untwisted case with $\max|\beta_{ss}| \sim 0.5^\circ$.

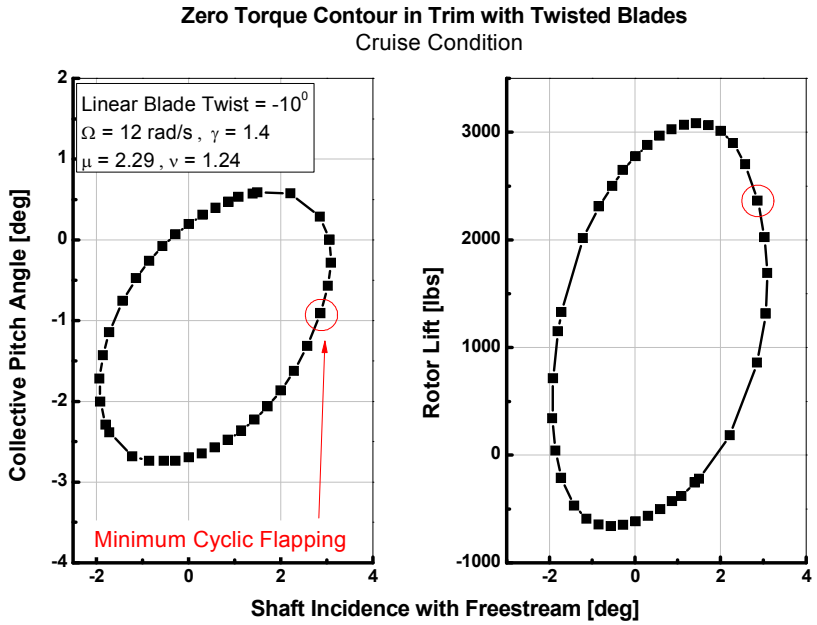

Figure 87: Cruise Condition Trim Contour with Twisted Blades

The contours for the twisted blades suggest that the effect of moderate blade twist does not fundamental alter the trends associated with the rotor, but merely shifting the various curves. Instead of repeating all of the previous analysis for the twisted blades as a sensitivity parameter, the concepts of the preferred operating point and the trim contour will be retained such that it is assumed that small variations in blade properties will have incremental effects on the trim contour and the condition for minimum cyclic flapping.

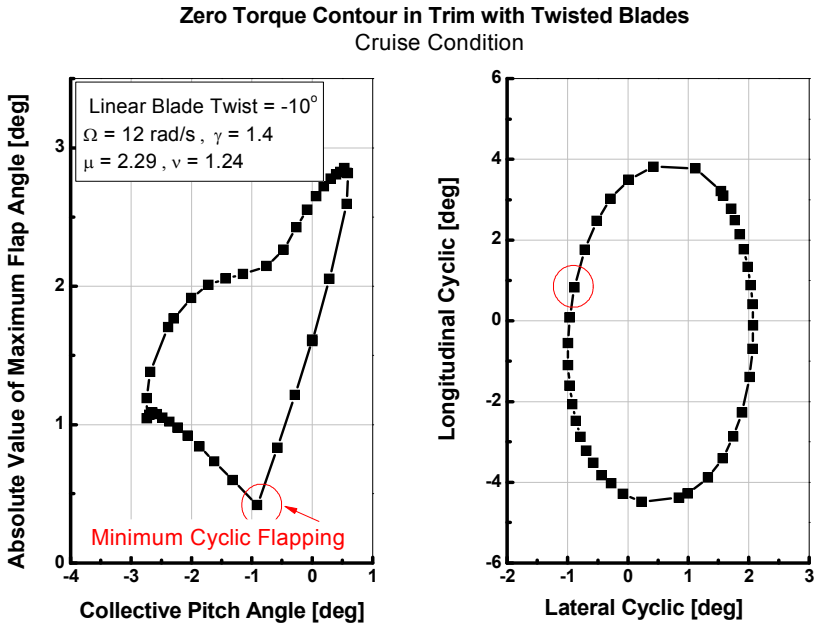

Figure 88: Blade Flapping on Trim Contour with Blade Twist

3.11 Rotor Performance Out of Moment Trim

Performance trends for trimmed rotors were shown in section 3.1. If the rotor is trimmed for autorotation using the shaft incidence angle and the hub pitching and rolling moment constraint is not imposed, a residual hub moment results. This moment would be reacted in the airframe and the control surfaces would be required to overcome these moments for trim and maneuvering. The effect of maintaining the cyclic controls fixed at zero degrees is shown for the baseline rotor in Figure 89 and Figure 90. In the out-of-trim condition higher thrust coefficient and lift to drag ratios are predicted throughout the range of advance ratio. The rotor shaft incidence to the free stream velocity for the out-of-trim case shows a lower incidence is required to sustain autorotation.

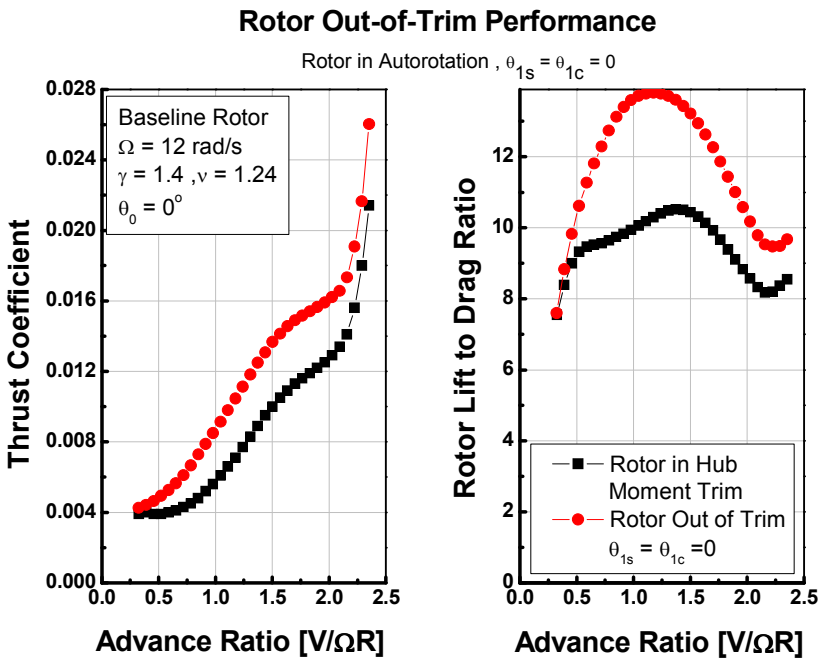

Figure 89: Baseline Rotor Performance Out of Moment Trim

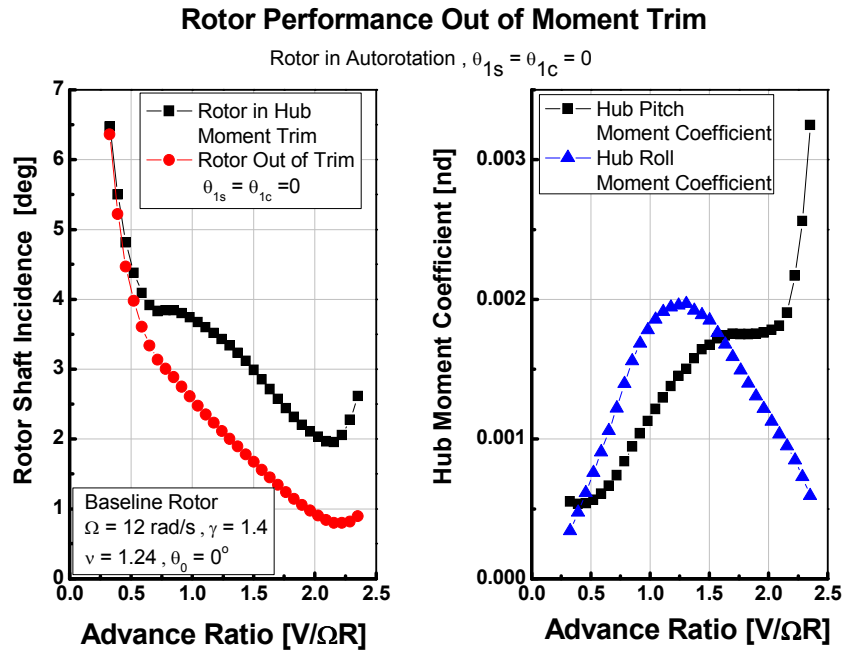

Figure 90: Baseline Rotor Out of Trim Hub Moment Coefficients

The residual hub moments are presented in coefficient form, with the pitching moment increasing with advance ratio. In dimensional terms for the baseline rotor, the residual pitching moment at the high speed condition is $M_y \approx 5{,}500$ ft-lbf. The residual rolling moment for the baseline rotor peaks near $\mu \sim 1.2$, then decreasing with further increase in advance ratio.

Operating the rotor in the out-of-trim condition represents a trade-off in the conceptual design. Gains in rotor performance and the simplifications in rotor control would be traded against the impact of the residual moments: increased structural loads and increased authority required of the airframe controls to overcome the residual hub moments.

3.12 Chapter Summary

Trim, stability, and control results related to the isolated rotor have been presented in this chapter through simulated wind tunnel experiments. The fundamental relationships between the free stream velocity, rotor speed, and shaft incidence were presented, along with the sensitivity to collective pitch setting and the rotor parameters. Rotor stability was predicted using Floquet analysis and the trends leading to a reduction in stability were discussed including the coupling of the rotor speed degree of freedom and lead-lag motion. Rotor response to swashplate control inputs was presented to highlight the dependence of control cross-coupling on advance ratio, and the non-linear behavior in the rotor speed response. Transient rotor response for slowly rotating, low Lock number blades was show to occur over a relatively long time scale which could couple with the airframe modes. Finally, multiple trim conditions suggested preferred steady-

state operating conditions that reduced cyclic flapping, and the inclusion of a -10^{o} blade twist case was shown to shift the trend curves without altering the fundamental trends.

CHAPTER 4

COUPLED ROTOR-AIRFRAME ANALYSIS

In this chapter a baseline airframe with conventional control surfaces is used to investigate the potential rotor control strategies and the concept vehicle intrinsic flight dynamics characteristics. The fundamental rotor control issue is the specification and regulation of the rotor speed. Multiple trim solutions have been shown to exist, and the isolated rotor analysis has been presented using the incidence of the rotor shaft to the free stream as a control variable. When coupled with the airframe model, the orientation of the shaft and the potential ability to control the shaft orientation represents a design choice, adding an additional degree of freedom, also adding cost and complexity. Two quasi-steady maneuvers are considered for investigation of rotor control: a rotor speed transition maneuver, and a flight path transition maneuver. The rotor speed transition maneuver results from the requirement to slow the rotor quickly in order to pass through a rotor resonance frequency, transitioning from one rotor speed to another. Analysis of this maneuver represents a commanded change in rotor speed. Commanded changes in vehicle attitude at constant rotor speed are investigated with the flight path transition maneuver.

Intrinsic flight dynamics characteristics of the concept vehicle are investigated by comparison of linear models that explicitly include the rotor states and transfer functions identified using system ID extracted from surrogate flight test data using the non-linear simulation. Together, these analyses address the research questions related to the rotor-speed control strategy and the rotor-airframe interactions.

4.1 Rotor Control in Quasi-Steady Maneuvers

4.1.1 Commanded Rotor Speed Transition Maneuver

An inherent feature of the concept vehicle is the slowing of the rotor with increasing flight speed while maintaining autorotation. At some rotor speeds, the blade natural frequencies may coincide with the rotor angular velocity causing a resonance condition, which is undesirable. In this case the rotor speed should be transitioned quickly to avoid vibration and high structural loads. An example case is considered where the vehicle has reached a flight speed of 300 kts at 30,000 ft and the rotor has already been slowed to 16 rad/s, denoted as the *transition condition*. At this point the advancing tip Mach number limit has been reached, and the rotor must be slowed further to increase the flight speed.

In this section, various means to accomplish the transition maneuver are discussed in terms of rotor control strategies and the associated trade-offs. Rotor operation out-of-moment trim was discussed in section 3.12. With the cyclic controls held at zero, residual hub moments that the airframe would be required to overcome for vehicle trim in steady-level flight persist. The choice to operate in this manner represents a design decision, simplifying the control scheme at a cost of increased loads, vibration, etc. The autorotation contours at the transition condition for out-of-moment trim are shown in Figure 91.

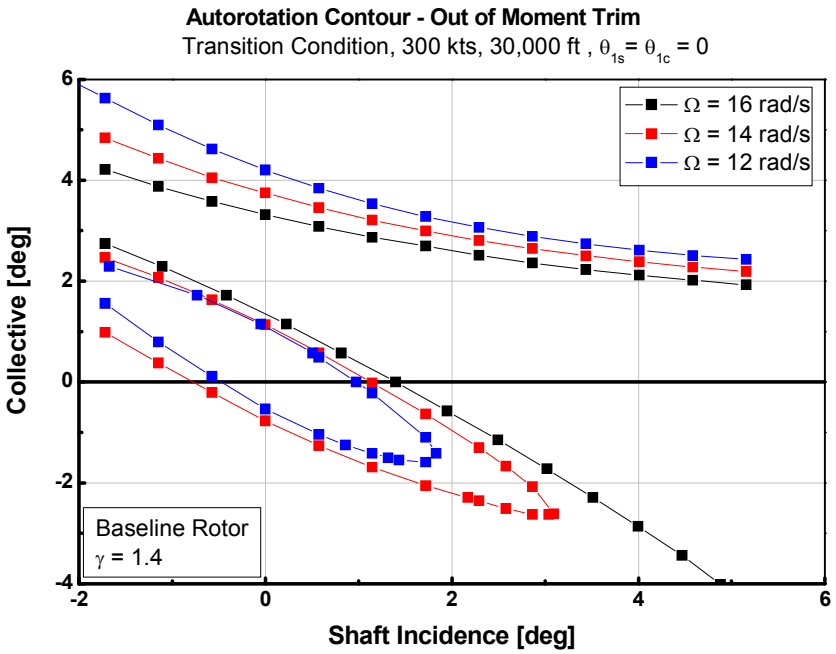

Figure 91: Transition Condition Autorotation Contour – Out of Moment Trim

Considering first the case where the rotor shaft has a fixed orientation in the airframe, the contour of Figure 91 shows that the collective control can be used to achieve autorotation. The shaft incidence will be determined by the airframe angle of attack such that the total lift equals the weight for steady-level flight. To execute the transition maneuver the collective control can be lowered to slow the rotor. Figure 92 shows the collective pitch trajectories and the rotor lift for the transition maneuver out-of-moment trim. The collective control input used to reduce the rotor speed also results in a decrease in rotor lift. The airframe would be required to provide additional lift in this case which could be accomplished with flaps, etc. or simply an increase in wing angle of attack. With the rotor shaft fixed in the airframe, an increase in angle of attack would require a further decrease in collective to control the rotor speed. Figure 91 and Figure 92 show that at an increased shaft incidence the collective control becomes ineffective at reducing the rotor speed further so that it may not be possible to execute the transition

maneuver as a steady-level maneuver without flaps or high lift devices for airframe attitude-independent lift control.

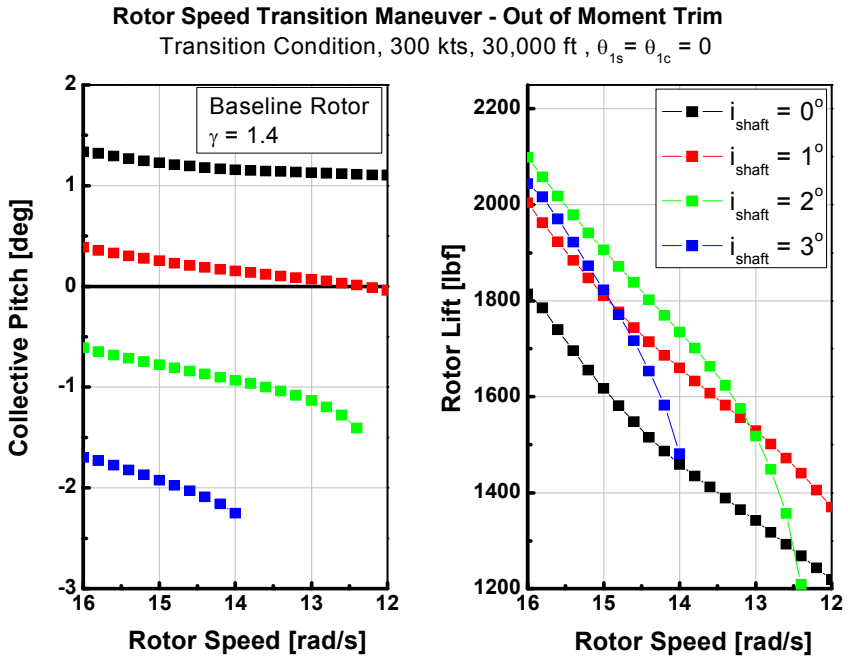

Figure 92: Transition Maneuver Out of Moment Trim

Figure 93 shows the residual hub moments and the maximum blade flapping angle in steady-state. The shaft incidence angles which allow for the rotor speed to reach 12 rad/s also result in the largest residual hub moments and blade flapping. Beyond just the vertical force balance, other configuration dependent issues exist for trim of the entire vehicle using this rotor control strategy, such as sufficient control surface authority to provide zero vehicle angular accelerations. Independent control of the shaft incidence to the free stream velocity does allow for the full range of rotor speed necessary to reach the slowed rotor speed, but with the associated rotor loads and flapping (Figure 93) in this out-of-trim condition.

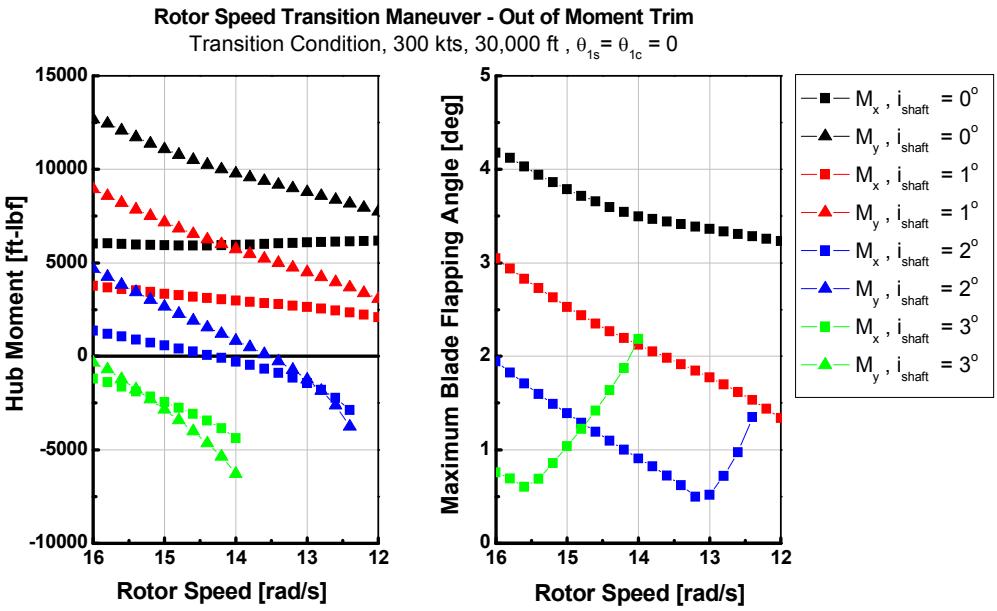

Figure 93: Residual Hub Moments and Blade Flapping – Transition Maneuver

When the hub pitching and rolling moment constraints are imposed, the autorotation contours at the trim condition are as shown in Figure 94. The transition maneuver at constant flight speed requires the rotor operating state to moves from some point on the 16 rad/s contour to some point on the 12 rad/s contour when the trim conditions are imposed. The most desirable operating points are at positive (aft) shaft incidence and collective pitch near zero degrees, or slightly negative. These points provide positive lift, minimal flapping, and the largest region of linear response to swashplate control inputs as discussed in Chapter 3. In the case of the rotor shaft orientation fixed in the airframe, rotor speed transition would then be accomplished by raising the collective pitch while adjusting the cyclic controls to maintain zero hub moments. Due to the thrust increment sign reversal effect discussed in section 3.1, a reduction in rotor thrust results. Similar to the out-of-trim operation, additional airframe lift would be required to maintain steady-level flight. When airframe attitude is used to provide the additional lift, the slowed rotor condition again may not be achievable in

steady-state. Even with the hub moment constraints applied, rotor speed transition as a steady-level maneuver may not be possible without airframe attitude-independent lift control.

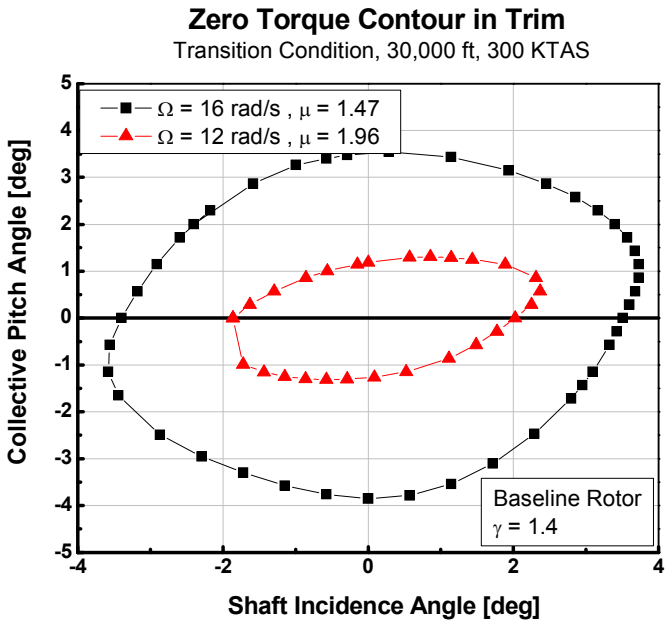

Figure 94: Transition Condition Trim Contours

Figure 95 shows the maximum flapping angle that is encountered on the trim contour in steady state. The minimum flapping angle occurs when the collective pitch is just below zero for the baseline rotor and the shaft is tilted aft. This trim condition represents a desirable operating point for the rotor since higher cyclic flapping will result in higher vibration and structural loads. The rotor is in moment balance for all of the points on the contour, but some points result in cyclic flapping in excess of one degree while in steady state trim.

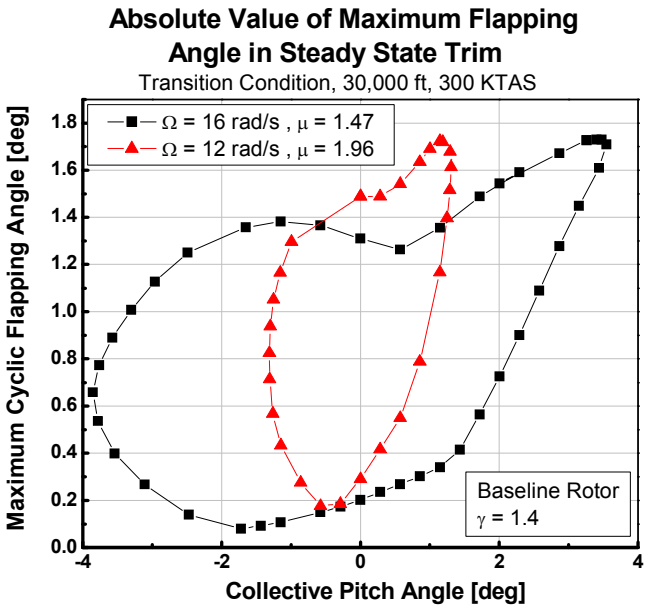

Figure 95: Maximum Flapping Angle in Trim at Transition Condition

Finally, consider a rotor control strategy that includes the ability to adjust the shaft incidence. A series of quasi-steady trim results are presented that represent intermediate trim points at rotor speeds from 16 rad/s to 12 rad/s for the coupled rotor and airframe. The quasi-steady results presented as a series of trim conditions are informative because they represent the magnitude and direction of the movement of the controls required to execute the rotor speed transition maneuver, and assume that the maneuver can be executed without exciting the vehicle dynamic modes, as might be accomplished with pilot intervention or an automated system to suppress the motion using the airframe controls.

The transition maneuver can be accomplished using a variety of piloting strategies. For the present work, a constant-throttle strategy is used so airspeed replaces the throttle as a trim variable, the collective pitch is held fixed at zero degrees, and a level flight path constraint is imposed. Trim results at decreasing rotor speeds are used to determine the quasi-steady control and attitude trajectories with decreasing rotor

speed. Figure 96 shows the trajectories for the airframe coupled with the baseline rotor at the transition condition, with the flight speed allowed to vary due to the constant throttle. In order to reduce the rotor speed in this manner the rotor shaft incidence to the freestream is reduced by moving the shaft forward, while at the same time the longitudinal cyclic is moved aft to keep the pitching moment on the rotor in trim. Only small adjustment of the lateral cyclic is required for the baseline rotor since the isolated rotor phase angle response data showed a small amount of lateral response at this condition. The inset to Figure 96 shows that the flight speed increases to about 310 kts due to a reduction in total drag. The other controls and the roll attitude show only small changes such that shaft incidence and longitudinal cyclic are the primary controls in this case. Figure 97 shows the rotor lift and the fraction of the gross weight for the quasi-steady transition. The rotor is unloaded to less than ten percent of the gross weight, and the maximum flapping angle shows that the rotor operates with low cyclic flapping with the collective at zero degrees and the shaft tilt angle adjusted for trim.

The ability to control the rotor shaft angle allows for the rotor speed to be controlled while the rotor operates with minimum cyclic flapping. During the transition maneuver, as the rotor is unloaded, the loss of rotor lift can be compensated for by the airframe to maintain steady-level flight. The rotor control strategy demonstrated in Figure 96 can be summarized as using: rotor shaft incidence to control rotor speed, cyclic to suppress hub pitching and rolling moments, and collective to minimize cyclic flapping. In the absence of airframe attitude-independent lift control, this strategy provides a means to specify the rotor speed and allow the rotor to operate at a preferred condition considering the practical constraints of structural loads and vibration, etc.

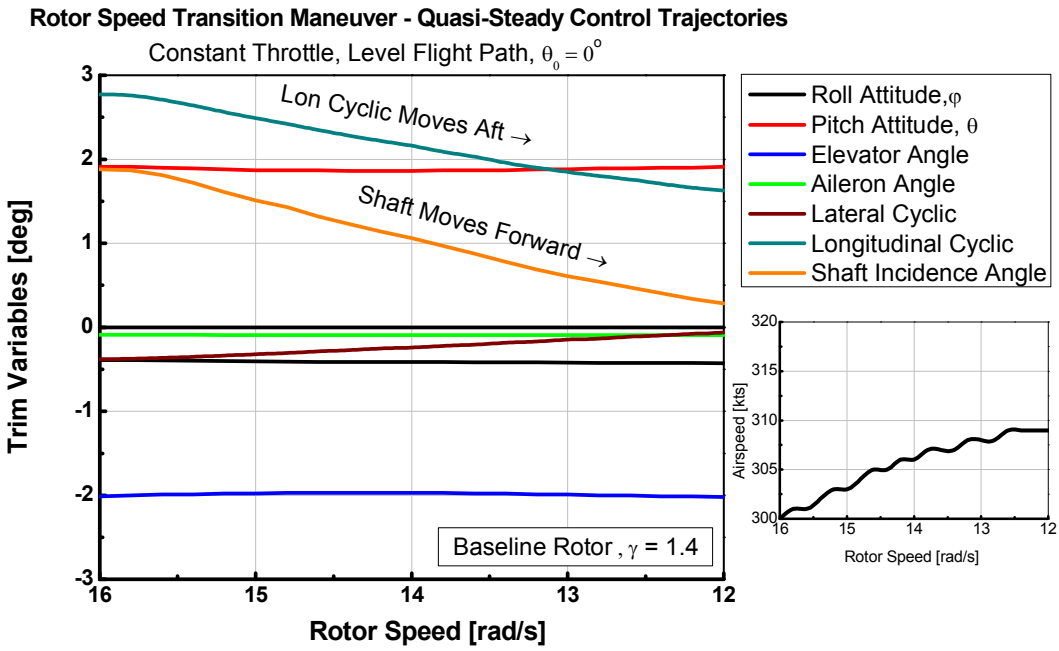

Figure 96: Quasi-Steady Control Trajectories for Rotor Speed Transition Maneuver

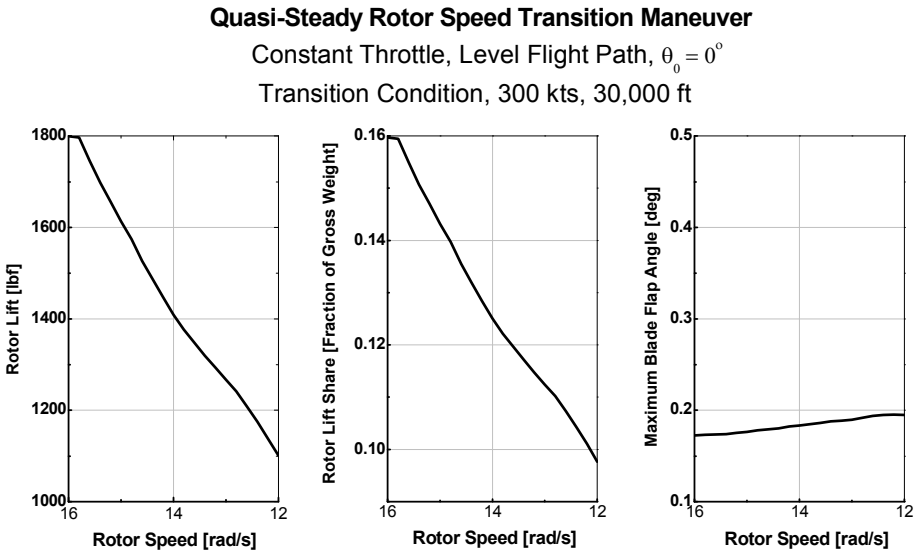

Figure 97: Constant Throttle Transition Maneuver- Rotor Lift

4.1.2 Flight Path Transition Maneuver

The flight path transition maneuver simulates the control and attitude trajectories to trim the vehicle in climb and descent at constant rotor speed. The coupled rotor and airframe was trimmed at the cruise condition for flight path angles from negative three degree to three degrees, which corresponds to climb rates up to +/- 1800 ft/min. The quasi-steady control trajectories, using the rotor control strategy described in section 4.1.1, are shown in Figure 98. To execute the maneuver at constant speed, the primary controls were the throttle and the pitch attitude, with the angle of attack, rotor lift, and cyclic flapping remaining essentially constant as shown in Figure 99.

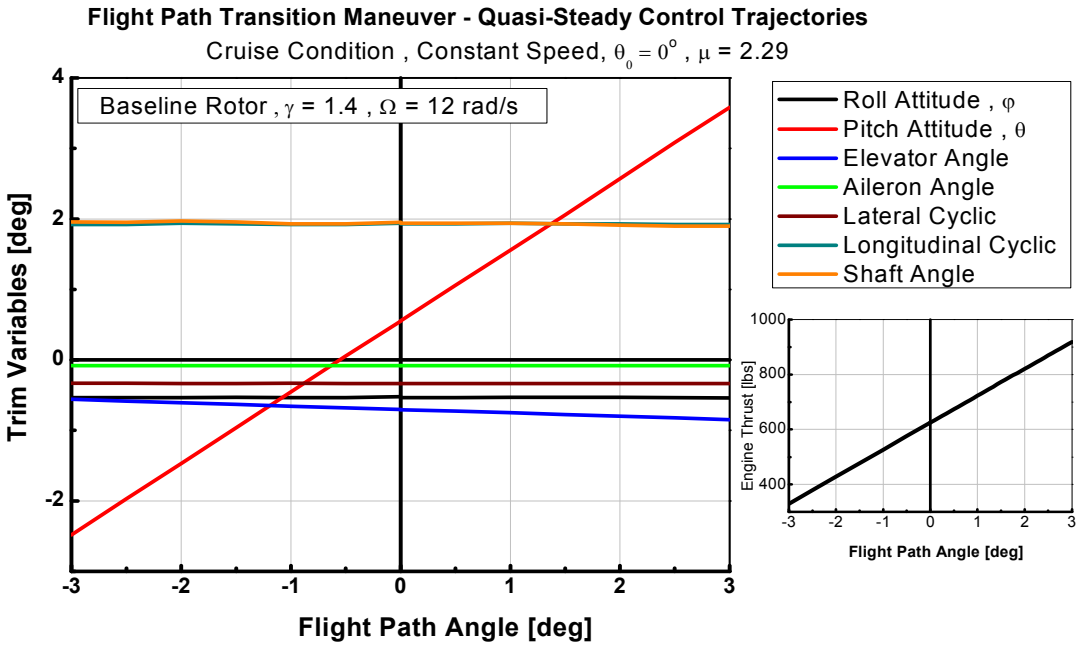

Figure 98: Flight Path Transition Maneuver Control Trajectories

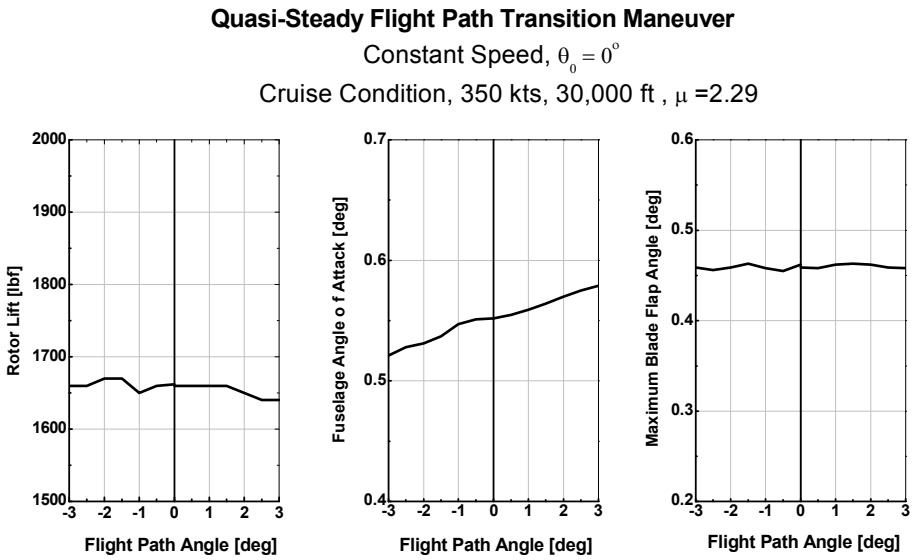

Figure 99: Flight Path Transition Maneuver Rotor Load and Blade Flapping

The small changes to the rotor shaft incidence, even with the relatively large change in pitch attitude, results because the angle of attack remains nearly constant. These results reiterate the inherent relationship presented for the isolated rotor between the rotor speed, free stream velocity, and the rotor shaft incidence to the free stream. Even though the shaft incidence changes were small in this case, without independent control of the rotor shaft, a numerical trim solution may not always exist, and collective control inputs for rotor speed regulation will again result in operation with increased cyclic flapping.

4.3 Coupled Rotor and Airframe Flight Dynamics Characteristics

Flight dynamics characteristics of the coupled rotor and airframe were investigated by a combination of linear analysis and system identification methods. Linear state space models of the form:

$$\dot{\vec{x}} = A\vec{x} + B\vec{u}$$

were extracted from FLIGHTLAB™ using the built-in linearization routines. The models explicitly included the rotor states, expressed in multi-blade coordinates (MBC), the rotor speed mode, and the vehicle body states. This formulation is similar to the hybrid formulation described by Tischler and Remple [49], who also refer to the roll control effectiveness criteria work of Heffley, et. al.[56].

All of the linear models in this chapter were extracted from the non-linear models trimmed in the cruise condition. The linear models were obtained using the "steady perturbation" method. The FLIGHTLAB™ X-Analysis User Manual [53] indicates "the steady perturbation method obtains the linear model by perturbing the state or control, running the model to steady state, and then averaging the resulting partial derivatives over a rotor revolution." Longitudinal dynamics including the rotor states, but uncoupled from the lateral states were investigated, such that the state vector was:

$$\vec{x} = \left[\beta_0 \quad \beta_{1c} \quad \beta_{1s} \quad \beta_{N2} \quad \dot{\beta}_0 \quad \dot{\beta}_{1c} \quad \dot{\beta}_{1s} \quad \dot{\beta}_{N2} \quad u \quad w \quad q \quad \theta \quad \Omega\right]^T$$

The response of the linear model to an elevator doublet was compared to the non-linear simulation response in order to assess the predictive capability of the linear model in the time domain. Figure 100 shows a time-history comparison, and for inputs consistent with small disturbances from trim, this linear model formulation was deemed sufficient to investigate the vehicle characteristics for comparison with system ID results. This

formulation effectively ignores the rotor periodicity by averaging the rotor dynamics over a rotor revolution. The formulation allows for reasonable prediction of the vehicle motion however because the low frequency rotor mode is in a frequency range that can couple with the body motion but the periodicity occurs at a much higher frequency such that the effects can be neglected for prediction of the relatively low frequency vehicle motion. Table 5 shows the eigenvalues of the stability matrix for the baseline rotor and airframe at the high speed cruise condition. The four rotor flapping modes were identified by the proximity of the frequencies to the values expected from the analytical hover solution. The real portions of the rotor eigenvalues are also seen to be similar to the transformed values reported in the Floquet analysis. The vehicle modes appear as classic aircraft longitudinal modes: short period and phugoid. The rotor speed mode appears as a single real negative root with small magnitude as was presented in the isolated rotor analysis.

Table 5: Eigenvalues from 13-State Linear Model – Longitudinal Modes

Cruise Condition, Baseline Rotor and Airframe Ω = 12 rad/s, μ = 2.29, γ = 1.40	
Eigenvalue	Mode Description
-1.9437 +/- 27.1112i	Advancing Flap
-2.1441 +/- 15.2790i	Reactionless Flap
-2.5461 +/- 14.4864i	Coning
-2.1272 +/- 1.2618i	Short Period
-2.1869 +/- 8.1163i	Regressing Flap
-0.0109 +/- 0.0905i	Phugoid
-0.0336	Rotor Speed

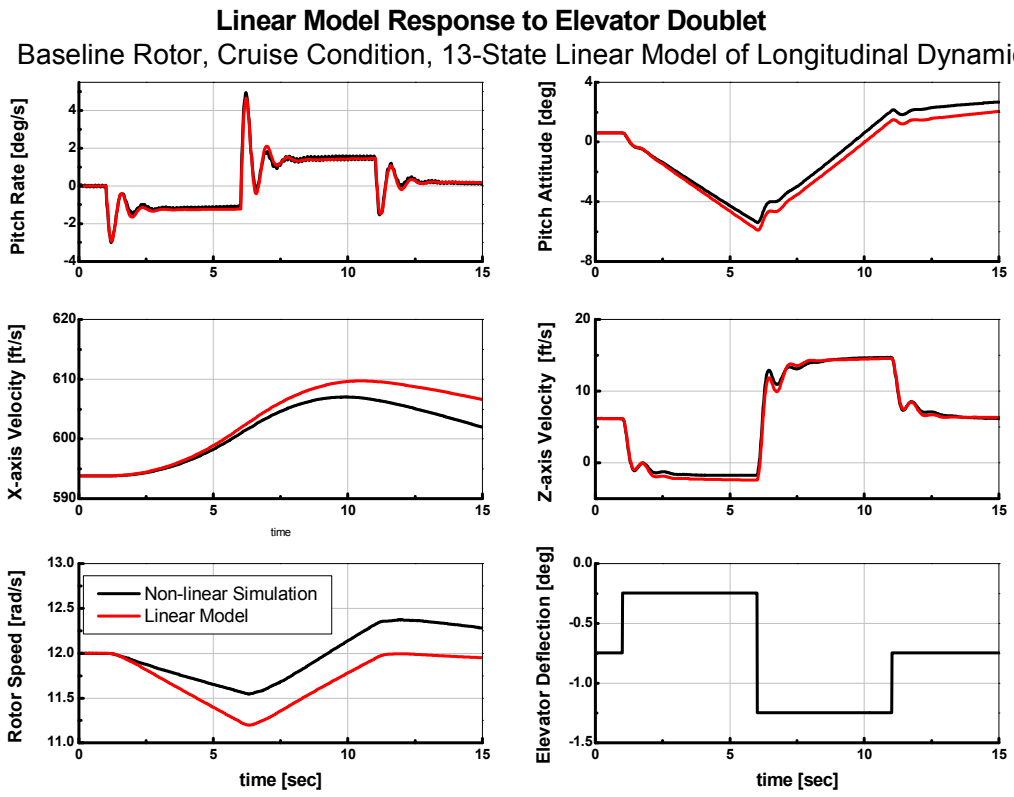

Figure 100: Linear Model and Non-linear Simulation Doublet Response

For comparison, system ID analysis was used to identify the transfer function for the pitch rate due to elevator inputs. Pitching moments on the airframe due to changes in angle of attack and pitch rate will be augmented by the rotor effects, and these effects can be seen in the frequency responses. Figure 101 shows the identified frequency responses for a range of flapping stiffness values. The responses were identified from ½ degree elevator sine sweeps, and transfer function coefficient data was identified using the CIFER® component NAVFIT. For these responses it was found that a proper fourth order transfer function fit the data extremely well as indicated by a low cost function $J \leq 6.5$ when fit to the data in the frequency range $1.0 \leq \omega \leq 30.0$.

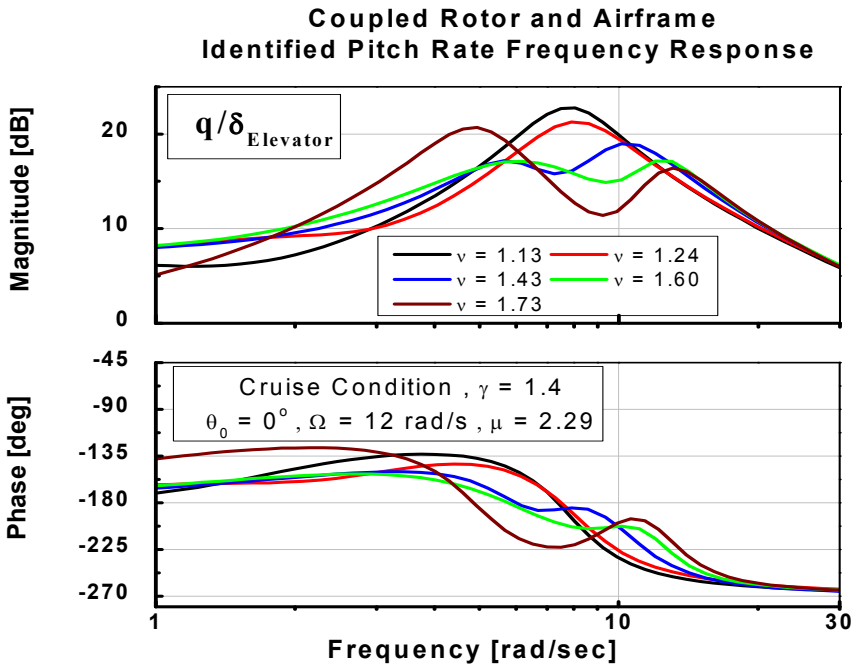

Figure 101: Identified Pitch Rate Frequency Response from Elevator Input

A comparison of the short period and regressing flap mode eigenvalues for the range of stiffness values is shown in Table 6. For the low flapping stiffness case the short period mode is predicted to be non-oscillatory (two real roots) by both analysis methods, and in the frequency response plot the result is a single amplitude peak at the frequency identified as the regressing flap mode. For higher flap stiffness values the short period mode is predicted as an oscillatory pair and the values predicted by the linear model agree well with the values identified from the system ID analysis (Table 6).

In the highest flapping stiffness cases of Figure 101, the amplitude peaks associated with both modes are clearly visible indicating the coupling of the modes contained in the pitch rate frequency response and their close proximity. Based on the two modes observed in the pitch rate response, the linear model formulation was used to obtain root locus plots based on the sensitivity to rotor Lock number and flapping stiffness.

Table 6: System ID and Linear Analysis Results – Coupled Pitch Motion

Non-dimensional Flapping Frequency, v	Transfer Function Poles $q(s)/\delta_e(s)$ From System Identification		Eigenvalues From 13-State Linear Models	
Cruise Condition , Ω = 12 rad/s , μ = 2.29 , γ = 1.40				
	Regressing Flap	Short Period	Regressing Flap	Short Period
1.13	-1.99 +/- 7.55i	-1.12 , -16.53	-2.03 +/- 7.64i	-0.98 , -3.67
1.24	-2.34 +/- 7.69i	-1.75 +/- 1.25i	-2.19 +/- 8.12i	-2.13 +/- 1.26i
1.43	-2.68 +/- 9.87i	-1.57 +/- 5.82i	-2.42 +/- 9.33i	-1.87 +/- 3.33i
1.60	-2.32 +/- 11.97i	-2.87 +/- 5.70i	-2.51 +/- 10.84i	-1.73 +/- 4.42i
1.76	-2.62 +/- 12.32i	-1.34 +/- 4.76i	-2.53 +/- 12.48i	-1.70 +/- 5.01i

Figure 102 shows the root locus for the regressing flap mode eigenvalues from the coupled linear models. For the low flapping stiffness values, all of the results tend to converge to an oscillatory pair.

The short period mode, which independently depends on the airframe parameters and the dynamic pressure, is predicted by the coupled rotor and airframe analysis to also depend on the rotor parameters. Figure 103 shows the root locus of the coupled short period mode at the cruise condition as predicted by the linear analysis. Increases in frequency of the regressing flap mode and the coupling of the two modes increases the frequency of the coupled short period mode as can also be seen in the frequency response in Figure 101. Also visible in Figure 103 at high Lock number and low stiffness is an small oscillatory mode which is a coupling of the short period mode and the rotor speed mode due to the movement of the real root toward the real axis.

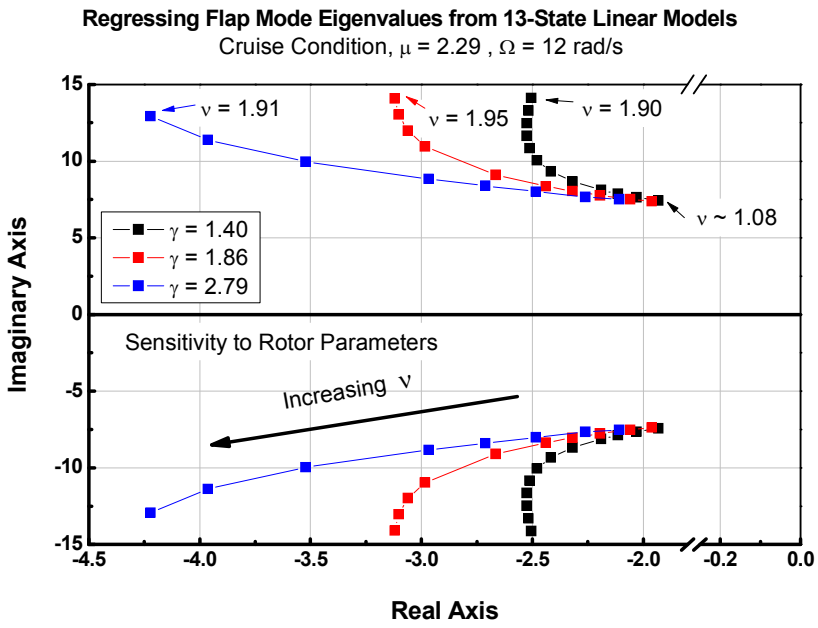

Figure 102: Coupled Regressing Flap Mode Root Locus – Longitudinal Models

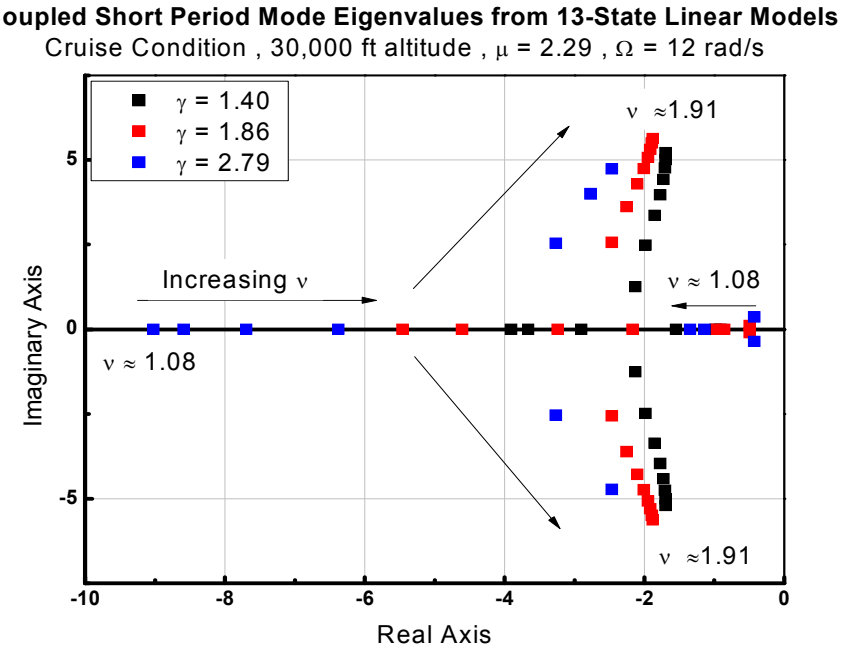

Figure 103: Coupled Short Period Mode Root Locus – Longitudinal Models

Coupling of the rotor and the lateral motion was investigated in a similar manner to the longitudinal motion. Linear models were extracted for the lateral directional vehicle modes coupled with the rotor modes, such that the state vector was:

$$\vec{x} = \left[\beta_0 \quad \beta_{1c} \quad \beta_{1s} \quad \beta_{N2} \quad \dot{\beta}_0 \quad \dot{\beta}_{1c} \quad \dot{\beta}_{1s} \quad \dot{\beta}_{N2} \quad v \quad p \quad r \quad \phi \quad \Omega\right]^T$$

Eigenvalues from the lateral-directional linear mode at the cruise condition are shown in Table 7.

Table 7: Eigenvalues from 13-State Linear Model – Lateral / Directional Modes

Eigenvalue	Mode Description
-1.9314 +/- 26.9832i	Advancing Flap
-2.2785 +/- 15.3150i	Reactionless Flap
-2.5483 +/- 14.5684i	Coning
-2.6912 +/- 4.8111i	Regressing Flap
-1.6392 +/- 8.6874i	Dutch Roll
-1.9644	Roll
0.0002	Spiral
-0.0897	Rotor Speed

Frequency response of the roll motion due to aileron inputs was used to identify the nature of the roll motion and the influence of the rotor. Figure 104 shows the identified frequency response. A proper third order transfer function was found to provide an excellent fit to the data with a very low cost function, J~1.0.

Table 8 shows a comparison of the linear and system ID results for a range of flapping stiffness values. The results show a close agreement between the linear analysis and system ID results for the prediction of the coupled modes in the roll motion. Figure 105 shows the root locus from the linear analysis for the coupled regressing flap mode from the lateral models.

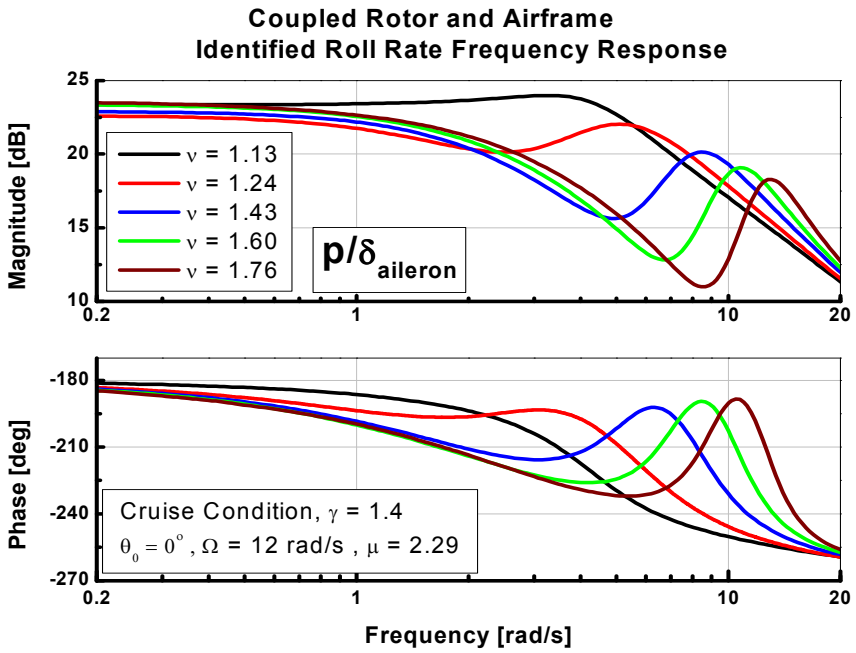

Figure 104. Roll Rate from Aileron Identified Frequency Response

Table 8: System ID and Linear Analysis Results – Coupled Roll Motion

Blade 4 Non-dimensional Flapping Frequency, v	Transfer Function Poles $p(s)/\delta_a(s)$ From System ID		Eigenvalues From 13-State Linear Models	
Cruise Condition , Ω = 12 rad/s , μ = 2.29 , γ = 1.40				
	Regressing Flap	Roll	Regressing Flap	Roll
1.13	-3.21 +/- 2.81i	-37.7	-2.93 +/- 2.94i	-1.55
1.24	-2.66 +/- 4.27i	-2.22	-2.69 +/- 4.81i	-1.96
1.43	-2.59 +/- 7.54i	-2.61	-2.22 +/- 7.65i	-2.35
1.60	-2.55 +/- 9.95i	-2.56	-2.47 +/- 10.47i	-2.55
1.76	-2.44+/- 12.22i	-2.74	-2.42 +/- 12.49i	-2.67

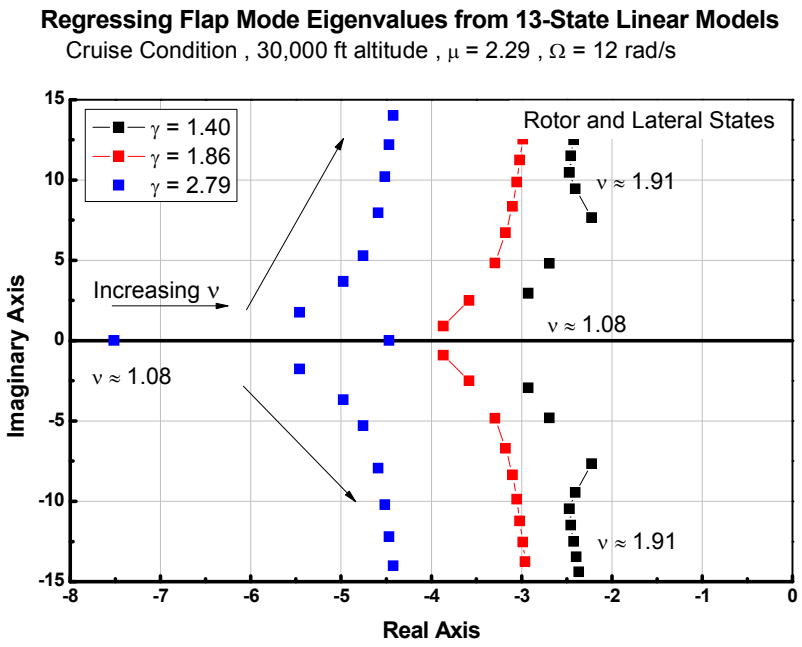

Figure 105: Regressing Flap Mode Root Locus from Lateral Linear Modes

4.4 Rotor Speed and Longitudinal Mode Coupling

The slow rotor speed changes were shown to have a minimal effect on the hub moments generated in the short time scale motion. The rotor speed was however shown to be sensitive to control inputs at high advance ratio, and possess a non-linear behavior. To further characterize the behavior of the rotor speed, a qualitative assessment was made using the non-linear simulation. An elevator frequency sweep was used to excite the longitudinal dynamics for rotor speed fixed and rotor speed free cases. The results for the baseline rotor, shown in Figure 106, indicate that the rotor speed changes have little effect of the vehicle motion, but the rotor speed shows short period and long period response. This one-way coupling for the rotor speed response indicates that rotor speed excursion for the uncontrolled rotor will result from speed and attitude changes.

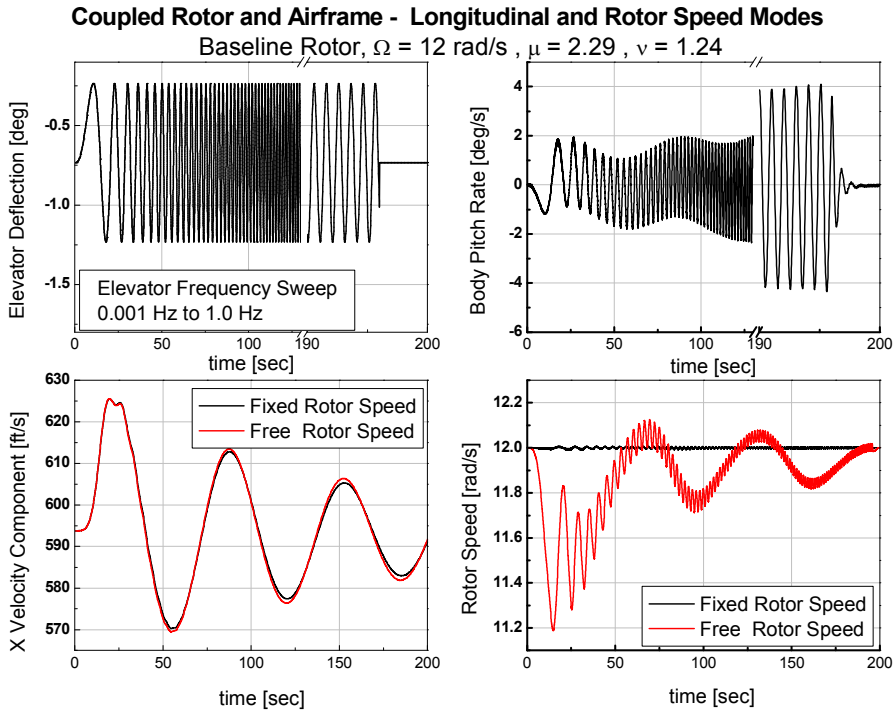

Figure 106: Rotor Speed Coupling with Longitudinal Modes

The conclusions from the coupled analysis indicate the close proximity of the body modes and the low frequency rotor modes results in a coupling of these modes. The regressing flap mode seen in the longitudinal models resulted in a higher frequency than was seen for the isolated rotor alone, and the resulting body pitch motion was seen to depend on the rotor parameters. The hybrid linear model including the rotor dynamics was seen to predict modes that were in close agreement with the modes obtained from the system ID analysis obtained from the non-linear simulation data. The rotor speed for the baseline rotor was shown qualitatively to be sensitive to flight speed and attitude changes in the non-linear simulation.

4.5 Chapter Summary

Rotor and airframe interactions were discussed in this chapter. Control trajectories for two quasi-steady maneuvers were presented. One maneuver was a commanded rotor speed change; the other was a commanded vehicle attitude change at constant rotor speed. Cases for fixed rotor shaft incidence angle and a controllable rotor shaft angle were discussed. In cases with a fixed rotor shaft orientation, intermediate steady-state trim solutions were not obtained for either the hub moment in-trim, or out-of-trim cases, indicating the maneuvers would occur as a transient maneuver and the goal of specifying the rotor speed was not certain. For cases with controllable rotor shaft incidence the maneuvers were shown as a series of quasi-steady trim cases such that the rotor speed was specified at each intermediate point and the cyclic flapping was minimized. The effect of the slowed rotor dynamics on the vehicle pitch and roll motion was shown by comparison of hybrid linear models and system ID results. System ID results identified transfer functions for airframe control to body angular rates. Transfer function poles were seen to agree well with the modes predicted by the linear models, and indicated that body rate responses were influenced by the airframe and the rotor regressing flap mode as a coupled response. Rotor speed was shown to couple with long and short period motion as the torque balance was sensitive to vehicle speed and attitude changes.

CHAPTER 5

CONCLUSIONS AND RECOMMENDATIONS

5.1 Conclusions

In this dissertation the concept vehicle has been model and analyzed. The inherent features of unloading the rotor, operating at high advance ratio, autorotation, slowed rotor dynamics, and the rotor speed degree of freedom have been considered collectively. Issues investigated relate specifically to the conceptual design of the control system and the intrinsic flight dynamics characteristics of the concept vehicle. Trends related to rotor operating conditions were identified, as well as sensitivity to rotor blade mass and stiffness properties. First simulated wind tunnel experiments were conducted using isolated rotor models, and then a baseline airframe model was incorporated for atmospheric flight analysis.

Specific findings from the studies are summarized as follows:

1. The trimmed rotor performance could be summarized non-dimensionally such that the thrust coefficient, lift over drag ratio, and shaft incidence to the freestream velocity curves versus advance ratio were coincident except as the advancing tip Mach number approached the imposed limit.
2. The effect of advance ratio was to increase the rotor thrust in autorotation, so that a reduction in rotor speed was necessary to unload the rotor for a fixed collective pitch setting.
3. Rotor shaft incidence to the freestream velocity decreased with increasing advance ratio to maintain autorotation at a specified rotor speed.
4. The thrust-increment sign reversal for the trimmed rotor was predicted at an advance ratio $\mu \sim 0.86$ which is in close agreement with experimental data,

namely the value reported in the RVR report ($\mu \sim 0.9$) [11], the value reported in the NAS 2-5419 report, ($\mu \sim 0.79$) [12], and NASA TN D-2628 [9], reported as $\mu \sim 1.0$.

5. Rotor thrust coefficient and lift to drag ratio was more sensitive to collective pitch setting beyond the thrust increment sign reversal advance ratio, with higher collective pitch settings resulting in lower thrust coefficient and lower lift to drag ratios.

6. Rotor performance predictions were essentially insensitive to flapping stiffness and weakly influenced by Lock number, primarily above advance ratio $\mu \sim 1.0$.

7. The contour plots of the in-plane aerodynamic forces indicated that the advancing side of the rotor consumes power (driven region), while the retreating side of the rotor extracts power from the air stream (driving region) both at low and high advance ratio autorotation, with an increase in the magnitude of the in-plane forces with advance ratio.

8. Flapping stability as predicted by Floquet analysis shows an increase in damping with advance ratio for the baseline rotor at constant rotor speed, with the effect of reducing rotor speed being a reduction in damping. Slowing the rotor by maintaining the maximum Mach number at the advancing blade tip indicated a minimum damping value occurred near $\mu \sim 1.0$. Sensitivity to the rotor parameters showed that higher Lock number blades had a higher damping value as predicted by the hover analytical solution, but tended to become frequency-locked at a lower advance ratio, such that further increase in advance ratio resulted a reduction in damping. Sensitivity to flapping stiffness results indicated that lower flapping stiffness resulted in roots becoming frequency-locked at a

lower advance ratio, with a reduction in damping with increased advance ratio compared to higher flapping stiffness blades.

9. Analysis of the rotor-speed mode in the absence of lead-lag motion showed a stable real mode with small magnitude over the range of advance ratio considered. The primary factors affecting the magnitude were the rotor speed and the Lock number, with higher Lock numbers and higher rotor speed resulting in larger stability. At the reduced rotor speeds, a minimum stability condition was observed near $\mu \sim 0.78$, suggesting a critical stability condition. Beyond $\mu \sim 0.78$, stability increased gradually with advance ratio, then experienced a rapid increase in damping as the advancing tip Mach number approached the imposed limit.

10. Inclusion of the lead-lag motion added lightly damped modes largely insensitive to advance ratio. Primary factors affecting the damping were shown to be the Lock number and the lead-lag damping coefficient parameter, with increases in both resulting in increased damping. A potential instability was predicted as the rotor speed mode coupling with the lead-lag motion in simulation, resulting in the selection of the lead-lag damping parameter sufficient for stability.

11. Rotor speed changes were seen to occur on a time scale much longer than the rotor hub moment transient response, justifying the hub moment sensitivity data presentation at constant rotor speed.

12. Hub moment sensitivity to swashplate control inputs were presented in terms of the steady-state on-axis, off-axis, and phase response. The effect of advance ratio was to increase the steady-state, on-axis moment sensitivity for longitudinal and lateral cyclic inputs. Hub moment phase angle response decreased with reduced rotor speed due to the associated increase in flapping frequency, while

the effect of advance ratio was to increase the phase angle response. Longitudinal and lateral cyclic inputs produced different phase angle responses at the same advance ratio, complicating the control or piloting strategy. Primary factors affecting the control sensitivities were the rotor speed and the advance ratio, with the lateral cyclic responses being less sensitive to advance ratio. Pitching and rolling moment sensitivity from collective pitch inputs increased with advance ratio with larger pitching moment magnitude compared to rolling moments. Rotor parameter sensitivity showed and increase in phase angle response with reduced flapping stiffness and increased Lock number. Gust sensitivity analysis showed an increase in sensitivity to angle of attack changes with advance ratio, and dihedral effect was destabilizing for low rotor speed and low advance ratio combinations when low rotor thrust resulted in primarily negative flapping angles.

13. System identification methods applied to identify transfer functions for hub moment response to shaft incidence angle disturbances captured the low frequency rotor mode response and the magnitude increase with advance ratio, shown in the control sensitivity study, could also be seen in the frequency response plots. For the baseline rotor, the effect of advance ratio was to reduce the low frequency oscillatory behavior in the step response, while the 4/rev high frequency content due to the large variation in aerodynamic forces around the azimuth increased in peak-to-peak magnitude indicating increased vibration. The effect of increased rotor stiffness was seen to increase the low frequency oscillatory behavior at the high advance ratio condition, and increase the peak overshoot. Increased Lock number resulted in increased peak-to-peak 4/rev excitations.

14. Multiple trim solutions were predicted for a given rotor speed and free stream velocity. Cruise condition and transition cases were presented as a contour of possible trim conditions. On this contour, rotor lift, control positions, shaft incidence angle, and steady-state flapping behavior was presented and preferred operating conditions were discussed. Minimization of cyclic flapping was suggested as a criterion for selection of a preferred operating condition.

15. Rotor speed response to swashplate inputs was shown to depend on the magnitude of the input and the trim condition. This non-linear behavior was predicted at high advance ratio, with longitudinal cyclic and collective pitch inputs from trim resulting in rotor speed excursions that changed sign with the magnitude of the input for the baseline rotor. Lateral cyclic inputs resulted in nearly linear behavior with input magnitude, but with rotor accelerations an order of magnitude lower than the collective and longitudinal cyclic responses. A study was conducted to investigate the source of the non-linear behavior. An accounting of the effects contributing to the torque moments on the rotor revealed the change in aerodynamic forces on the blades from trim with small and large inputs accounted for the sign reversal. The combined torque of all four blades showed the gravity and Coriolis effects made no net contribution to the rotor torque, but contributed to the peak-to-peak magnitude of the torque moment around the azimuth.

16. The effect of blade twist was presented in the context of the impact on the trim contour at the cruise condition. The trim contour was shifted in relation to the untwisted blade such that the collective pitch setting for minimum cyclic flapping was at a different collective pitch setting than the untwisted blade. Otherwise the twisted blade retained the fundamental characteristics of the untwisted blade, with a shift in the data.

17. Trim results for the coupled rotor and airframe models showed that steady-state trim solutions may not exist when rotor speed is prescribed and the rotor shaft incidence is fixed in the vehicle because the vehicle attitude required to produce lift from the wing and rotor combination may require a collective pitch setting that does not lie on the trim contour, thus resulting in a rotor speed different from the prescribed value. Inclusion of independent rotor attitude control allows the rotor speed to be prescribed and the collective pitch to be set to minimize the cyclic flapping, thereby reducing structural loads and vibration. With the flight speed and rotor speed prescribed, the resulting rotor lift is therefore known. The remainder of the vehicle lift must be produced by the airframe, and with independent rotor and airframe attitude control the flight envelope can be expanded in terms of the combinations of flight speed and rotor speed at which steady-state trim solutions exist. Independent rotor attitude control (shaft tilt) therefore appears as a desirable feature in order to specify the rotor speed, otherwise the ability to specify the rotor speed is limited to the collective pitch points on the contour that correspond to the shaft incidence resulting from the vertical force balance. These points will in general not be at the point of minimum cyclic flapping and could result in shaft incidence angles such that prescribing the rotor speed is not possible.

18. Rotor control strategies were discussed, including the effect of out-of-hub-moment trim operation. The minimum cyclic flapping in steady-state was shown to occur at a particular collective pitch setting, and higher flapping resulted when other solutions were imposed. The transition maneuver was used to demonstrate that the rotor speed and hub moments could be controlled over a range of target rotor speeds using the shaft incidence angle and the cyclic controls with the collective control fixed. Otherwise, using the collective and the

cyclic controls implied that at some conditions larger cyclic flapping was required to maintain trim, and no full vehicle trim solution at a specified rotor speed is guaranteed without independent control of the rotor lift and airframe lift. Therefore a control strategy using rotor attitude control for rotor speed control, with cyclic control to suppress the hub moments, and collective pitch to minimize the cyclic flapping resulted in control trajectories for quasi-steady maneuvers that satisfied the requirement to regulate the rotor speed while simultaneously controlling the hub moments and minimizing the cyclic flapping.

19. Pitch rate and roll rate frequency response to airframe control inputs shows the close proximity of low frequency rotor mode to the airframe modes due to the low Lock number and rotor speed, resulting in a coupled response. The hybrid linear model formulation and the system ID results show reasonable agreement, and the linear model captures the response trends of the non-linear simulation well because of the relatively high frequency of the periodicity compared to the large magnitude, low frequency hub moments.

20. The rotor speed mode couples with the other modes in a one-way fashion in that the torque balance on the rotor is sensitive to flight speed and attitude changes, but the vehicle longitudinal motion is weakly affected by small rotor speed excursions.

5.2 Recommendations for Future Work

Recommendations for future work are listed as follows:

1. In the present work, rigid rotor blades with uniform mass distribution were assumed. Typically helicopter blades will have a non-uniform mass distribution,

with higher mass concentration at structural attachment points or high stress regions. Further, the concept vehicle is expected to utilize a reaction drive system which can result in substantial weight associated with the combustion unit concentrated near the blade tip. The range of Lock numbers considered provides insight into the blade flapping motion for uniform, rigid blades, however similarity to rigid blades with equivalent Lock numbers but mass concentrated at the tip has not been established. Elastic blade models can also provide an increase in fidelity if sufficient blade properties are known. It is recommended that more detailed blade properties and elastic blade models be used for analysis beyond the conceptual design phase.

2. Quasi-steady, two dimensional rotor air loads were assumed for establishing trends. A study of aerodynamic force and moment models for comparison with available experiment data is recommended, as well as modification of the FLIGHTLAB^{TM} blade element model to include three dimensional lift and drag effects.
3. Dynamic inflow was selected as a computationally efficient inflow model for the present work. The literature review yielded no particular conclusive evidence regarding the applicability of dynamic inflow in autorotation at high advance ratio. In the study of the rotor speed response to swashplate inputs, the sensitivity to the inflow model was shown to have only a weak effect compared to uniform inflow, however both inflow models represent a significant simplification. It is recommended that CFD and experimental data be used to assess the importance of the inflow model for predictions of rotor behavior beyond the conceptual design phase.
4. Rotor speed changes were predicted to occur over a much longer time scale than the hub moment transient response. It is recommended that CFD and

experimental work be used to validate this result so that feedback control gains for the suppression of hub moments can be established for discrete operating points.

5. Shaft tilt was shown as an integral part of the rotor control strategy in the full vehicle trim and the investigation of the quasi-steady maneuvers. The relationship between the rotor speed changes and the speed of shaft tilt actuation has not been investigated, and speed with which the rotor shaft can be actuated may be a practical limiting factor in the control system design. It is recommended that further non-linear simulation work be conducted to establish the shaft tilt rate and rate of rotor speed change to establish this limit.
6. The articulated rotor model utilized flap, pitch and lag hinges as described in section 2.1. The sensitivity to the order of the hinges and the physical spacing dimensions should be investigated, as well as the effects of kinematic feedback such as delta-3 because it may be possible to stabilize the rotor speed instability and eliminate the need for the lead-lag dampers, which would highly desirable in a practical application.

APPENDIX

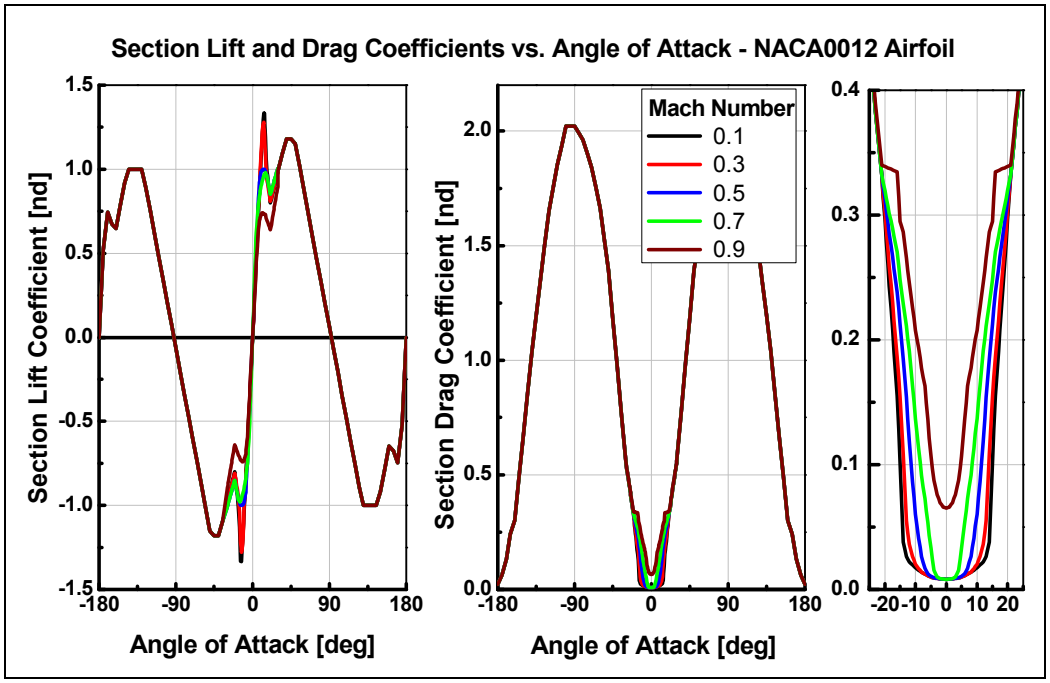

Figure 107. Rotor Blade Airfoil Lift and Drag Coefficient Data

REFERENCES

[1] Floros, Mathew W., Wayne Johnson, “Stability and Control Analysis of the Slowed-Rotor Compound Helicopter Configuration”, Journal of the American Helicopter Society, July 2007.

[2] DARPA Tactical Technology Office Website, September 19, 2008, http://www.darpa.mil/TTO/programs/Heliplane.htm.

[3] Carter Aviation Technologies Company Website, September 19, 2008, http://www.cartercopters.com/cctd_flight_data.html.

[4] Hislop, G.S., *The Fairey Rotodyne*, The Fairey Aviation Company, Presented to The Helicopter Association of Great Britain and The Royal Aeronautical Society, November 1958.

[5] Harris, Franklin D., “An Overview of Autogyros and the McDonnell XV–1 Convertiplane.” NASA Contractor Report–2003–212799, October 2003.

[6] Hohenemser, K., “A Type of Lifting Rotor with Inherent Stability”, McDonnell Aircraft Corporation, Presented at the Rotating Wing Aircraft Session, 18th Annual Meeting, I.A.S. New York, January 1950.

[7] Hickey, David A., *Full-Scale Wind-Tunnel Tests of the Longitudinal Stability and Control Characteristics of the XV-1 Convertiplane in the Autorotating Flight Range*, NACA RM A55K21a, May 1956.

[8] Jenkins, J. L., Jr.; Sweet, G. E., *Wind-Tunnel Measurements on a Lifting Rotor at High Thrust Coefficients and High Tip-Speed Ratios*, NASA, Langley Research Center, TN D-2462, September 1964.

[9] Jenkins, Julian L. Jr., *Wind Tunnel Investigation of a Lifting Rotor Operating at Tip Speed Ratios from 0.65 to 1.45*, Langley Research Center, NASA TN D-2628, February 1965.

[10] Mc Cloud, John L. III, James C. Biggers, Robert H. Stroub, *An Investigation of Full-scale Helicopter Rotors at High Advance Ratios and Advancing Tip Mach Numbers*, Ames Research Center, NASA-TN-D-4632, 68N28268.

[11] Ewans, J.R., F.J. McHugh, *Further Model Wind Tunnel Tests of a Reverse Velocity Rotor System*, Fairchild Republic Company, Department of the Navy, Air Systems Command HC171R1089, July 1975.

[12] Kuczynski, W. A., Sissingh, G. J.,” *Research program to determine rotor response characteristics at high advance ratios Final report*”, LR-24122; NASA-CR-114290, NASA, Feb 1, 1971.

[13] Sissingh, G.J., “*Dynamics of Rotors operating at High Advance Ratio*s”, Lockheed-California Company, Rotary Wing New Design Division, Presented at AGARD Specialists’ Meeting, Goettingen, September, 1967.

[14] Bramwell, A.R.S., E. Wilde, R. Summerscales, “The Flapping Behaviour of a Helicopter Rotor at high Tip-Speed Ratios”, Aeronautical Research Council, Ministry of Aviation, London, 1966.

[15] Perisho, Clarence H., “Analysis of the Stability of a Flexible Rotor Blade at High Advance Ratio”, McDonnell Aircraft Corp., Journal of the American Helicopter Society April 1959, Vol. 4, No. 2.

[16] Peters, David A., Kurt H. Hohenemser, “Application of the Floquet Transition Matrix to Problems of Lifting Rotor Stability”, American Helicopter Society 26th Annual National Forum, June 1970.

[17] Floros, Mathew W., Wayne Johnson, “Stability Analysis of the Slowed Rotor Compound Helicopter Configuration”, American Helicopter Society 60th Annual Forum, Baltimore, MD, June 2004.

[18] Floros, Mathew W., Wayne Johnson, “Performance Analysis of the Slowed-Rotor Compound Helicopter Configuration”, American Helicopter Society 4th Decennial Specialists’ Conference on Aeromechanics, San Francisco, California, 2004.

[19] Bergquist, R.R., Tanner, W.H., , New York, NY 1964, "Some Problems of Design and Operation of a 250 knot Compound Helicopter Rotor”, American Inst. of Aeronautics and Astronautics, AIAA Paper 1964-195.

[20] Ashby, Dale, William Eadie, Guy Juan Montoro, “An Investigation of the Reverse Velocity Rotor Concept and its Application to High Speed Rotorcraft”, Sikorsky Aircraft Corporation, presented at 2002 Biennial International Powered Lift Conference, Nov. 2002.

[21] Schank, Troy C., Optimal Aeroelastic Trim for Rotorcraft with Contrained, Non-unique Trim Solutions, PhD Thesis, School of Aerospace Engineering, Georgia Institute of Technology, April 2008.

[22] Glauert, H., “A General Theory of the Autogyro”, R. & M. No 1111, British A.R.C., 1926.

[23] Lock, C.N.H., “Further Development of Autogyro Theory –Parts I and II”, R. & M. No. 1127, British A.R.C., 1928.

[24] Bailey, F.J. Jr., *A Study of the Torque Equilibrium of an Autogiro Rotor*, Langley Memorial Aeronautical Laboratory, NACA Report No. 623, 1938.

[25] Bailey, F.J. Jr., F. B. Gustafson, *Observations in Flight of the Region of Stalled Flow Over the Blades of an Autogiro Rotor*, Langley Memorial Aeronautical Laboratory, NACA Report No. 741, 1939.

[26] Bailey, F.J. Jr., *Flight Investigation of Control-Stick Vibration of the YG-1B Autogiro*, Langley Memorial Aeronautical Laboratory, NACA Report No.764.

[27] Wheatley, John B., *The Aerodynamic Analysis of the Gyroplane Rotating-Wing System*, Langley Memorial Aeronautical Laboratory, NACA technical Note 492, 1934.

[28] Wheatley, John B., *An Aerodynamic Analysis of the Autogiro Rotor with a Comparison Between Calculated and Experimental Results*, Langley Memorial Aeronautical Laboratory, NACA Report No. 487, 1934.

[29] Wheatley, John B., Manley J. Hood, *Full-Scale Wind-Tunnel Tests of a PCA-2 Autogiro Rotor*, Langley Memorial Aeronautical Laboratory, NACA Report No. 515, 1935.

[30] Wheatley, John B., *The Influence of Wing Setting of the Wing load and Rotor Speed of a PCA-2 Autogiro as Determined in Flight*, Langley Memorial Aeronautical Laboratory, NACA Report No. 523, 1934.

[31] Wheatley, John B., Carlton Bioletti, *Wind-Tunnel Tests of a 10-Foot-Diameter Gyroplane Rotor*, Langley Memorial Aeronautical Laboratory, NACA Report No. 536, 1934.

[32] Wheatley, John B., *An Analytical and Experimental Study of the Effect of Periodic Blade Twist on the Thrust, Torque, and Flapping Motion of an Autogiro Rotor*, Langley Memorial Aeronautical Laboratory, NACA Report No. 591, 1937.

[33] Schrenk, M., *Static Longitudinal Stability and Longitudinal Control of Autogiro Rotors*, NACA Report No. 879, 1938.

[34] Hohenemser, K., *Performance of Rotating-Wing Aircraf*t, NACA TM 871, December 1937.

[35] Bennett, J.A.J., *The Flight of an Autogiro at High Speed*, NACA Technical Memorandum No. 729, 1933.

[36] Breguet, Louis, *The Gyroplane – Its Principles and its Possibilities*, NACA Technical Memorandum No. 816, 1936.

[37] Houston, S.S., "*Rotor-Wake Modeling for Simulation of Helicopter Flight Mechanics in* Autorotation", Journal of Aircraft, Sep/Oct 2003 Vol. 40, Issue5, p938.

[38] Houston, S.S., "Modeling and Analysis of Helicopter Flight Mechanics in Autorotation", Journal of Aircraft, Jul/Aug, Vol. 40, Issue 4, p675, Aug, 2003.

[39] Houston, S.S., "Identification of Autogyro Longitudinal Stability and Control Characteristics", *Journal of Guidance, Control, and Dynamics* Vol. 21, No. 3, May-June 1998.

[40] Houston, S.S., "Identification of Gyroplane Lateral/Directional Stability and Control Characteristics from Flight Test", Proc. Inst. Mech. Engrs, Part G, Vol. 212 No. G4, pp. 271-285 (1998).

[41] Deal, P.L., Jenkins, J.L.,J.R., National Aeronautics and Space Administration. Langley Research Center, Hampton, VA 1970, *Investigation of level-flight and maneuvering characteristics of a hingeless-rotor compound helicopter*, WASHINGTON. NASA-TN-D-5602; L-6661.

[42] Deal, P.L., Jenkins, J.L.,J.R. *Flight investigation of the wing-rotor lift-sharing characteristics of a hingeless rotor compound helicopter*, National Aeronautics and Space Administration. Langley Research Center, Hampton, VA 1968.

[43] Van Wyckhouse, J.F., *High-Performance UH-1 Compound Helicopter Maneuver Flight Test Program Final Report,* Bell Helicopter Co., Fort Worth, TX, 1966, BHC-533-099-025; USAAVLABS-TR-66-17.

[44] Blackburn, W.E., Rita, A.D., *Flight Research Program to Evaluate Methods of Improving Compound Helicopter Maneuver Capability Final Report,* Kaman Aircraft Corp., Bloomfield, CT, R-622A; USAAVLABS-TR-67-59.

[45] Orchard, M, S Newman, "The Fundamental Configuration and Design of the Compound Helicopter*", Proceedings of the Institution of Mechanical Engineers, Part G: Journal of Aerospace Engineering,* vol. 217, no 6, 2003.

[46] Leishman, J. Gordon, "Development of the Autogiro: A Technical Perspective", Journal of Aircraft, Vol. 41, No. 4, July-August 2004.

[47] Hohenemser, K., *Hingeless Rotorcraft Flight Dynamics*, AGARD No. 174, September 1974.

[48] Bielawa, Richard L., *Rotary Wing Structural Dynamics and Aeroelasticity,* AIAA Educational Series, Washington, DC, 1992.

[49] Tischler, Mark B., Robert K. Remple, *Aircraft and Rotorcraft System Identification*, American Institute of Aeronautics and Astronautics Education Series, Reston, VA, 2006.

[50] Johnson, Wayne, *Helicopter Theory*, Dover Publications, New York, 1980.

[51] Leishman, J. Gordon, *Principles of Helicopter Aerodynamics*, Cambridge university Press, New York, NY, 2000.

[52] Padfield, Gareth D., *Helicopter Flight Dynamics: The Theory and Application of Flying Qualities and Simulation Modeling*, AIAA Educational Series, Washington, DC, 1996.

[53] Advanced Rotorcraft Technology, Inc., 1330 Charleston Road, Mountain View, CA, 94043.

[54] US Army Materiel Command, Engineering Design Handbook: Helicopter Engineering, Part Two, Detail Design, AMC Pamphlet AMCP 706-202, January 1976.

[55] Manumala, Binoy, Daniel Walker, Gareth Padfield, “Rotorcraft Simulation Modelling and Validation for Control Design and Load Prediction”, 31st European Rotorcraft Forum, Florence, Italy, September 13-15, 2005.

[56] Heffley, Robert K., Simon M. Bourne, Howard C. Curtiss, Jr., William Hindson, Ronald A. Hess, *Study of Helicopter Roll Control Effectiveness Criteria*, NASA Contract Report 177404, April 1986.

[57] Kuczynski, W.A., G. J. Sissingh, “Characteristics of Hingeless Rotors with Hub Moment Feedback Controls Including Experimental Frequency Response”, Lockheed-California Company, Burbank, California, Contract NAS 2-5419, Accession Number 72N18024, January 1972.

[58] CIFER® Software Program, Aeroflightdynamics Directorate, U.S. Army Aviation and Troop Command, Ames Research Center, Moffett Field, CA.

[59] Rigsby, James, J.V. R. Prasad, “Stability and Control Issues Associated with Light Loaded Rotors, Autorotating at High Advance Ratio”, Presented at the 64th Annual Forum of the American Helicopter Society, Montreal, Canada, May 2008.

[60] Bramwell, A.R.S., George Done, David Balmford, *Bramwell’s Helicopter Dynamics*, American Institute of Aeronautics and Astronautics, Reston, VA, 2001.

[61] Gessow, Alfred, Garry C. Meyers, Jr., *Aerodynamics of the Helicopter*, Frederick Ungar Publishing Co., New York, New York, 1952.